TURUN
YLIOPISTO
UNIVERSITY
OF TURKU

POSITRON EMISSION TOMOGRAPHY IMAGING OF DISEASE ACTIVITY IN ATHEROSCLEROSIS

Jenni Virta

TURUN YLIOPISTON JULKAISUJA – ANNALES UNIVERSITATIS TURKUENSIS
SARJA – SER. D OSA – TOM. 1804 | MEDICA – ODONTOLOGICA | TURKU 2024

TURUN
YLIOPISTO
UNIVERSITY
OF TURKU

POSITRON EMISSION TOMOGRAPHY IMAGING OF DISEASE ACTIVITY IN ATHEROSCLEROSIS

Jenni Virta

TURUN YLIOPISTON JULKAISUJA – ANNALES UNIVERSITATIS TURKUENSIS
SARJA – SER. D OSA – TOM. 1804 | MEDICA – ODONTOLOGICA | TURKU 2024

University of Turku

Faculty of Medicine
Department of Clinical Medicine
Clinical Physiology and Nuclear Medicine
Drug Research Doctoral Programme
Turku PET Centre

Supervised by

Professor Anne Roivainen, PhD
Turku PET Centre and
Turku Center for Disease Modeling
University of Turku
Turku, Finland

Professor Antti Saraste, MD, PhD
Turku PET Centre and Heart Center
University of Turku and
Turku University Hospital
Turku, Finland

Reviewed by

Associate professor Kirsten Bouchelouche, MD, DMSc
Aarhus University
Aarhus University Hospital
Aarhus, Denmark

Docent Katariina Öörni, PhD
Wihuri Research Institute
Helsinki, Finland

Opponent

Professor Sohvi Hörkkö, MD, PhD
Research Unit of Biomedicine and Internal Medicine
Faculty of Medicine
University of Oulu
Oulu, Finland

ISBN 978-951-29-9783-1 (PRINT)
ISBN 978-951-29-9784-8 (PDF)
ISSN 0355-9483 (Print)
ISSN 2343-3213 (Online)
Painosalama, Turku, Finland 2024

To my family

UNIVERSITY OF TURKU
Faculty of Medicine
Department of Clinical Medicine
Department of Clinical Physiology and Nuclear Medicine
JENNI VIRTA: Positron emission tomography imaging of disease activity in atherosclerosis
Doctoral Dissertation, 181 pp.
Drug Research Doctoral Programme (DRDP)
June 2024

ABSTRACT

Atherosclerosis is a progressive inflammatory disease characterized by the accumulation of lipids and fibrotic elements in the arterial wall. Incidence of type 2 diabetes mellitus (T2DM) has risen globally throughout the years and is known to accelerate the progression of atherosclerosis. Macrophages have a key role in regulating atherosclerotic disease activity and can either prevent or provoke disease progression. Positron emission tomography (PET) is an imaging technique used to image biological processes *in vivo* and it may provide tools for non-invasive evaluation of atherosclerotic disease activity.

The aim of this thesis was to evaluate the applicability of three novel PET tracers ^{68}Ga-NODAGA-exendin-4, (2S, 4R)-4-[^{18}F]fluoroglutamine (^{18}F-FGln) and ^{18}F-AlF-NOTA-folate (^{18}F-FOL) for the imaging of atherosclerotic disease activity and to study the effects of a T2DM treatment, dipeptidyl peptidase-4 (DPP-4) inhibitor linagliptin, using an established PET tracer. The studies were conducted using two mouse models and a rabbit model of atherosclerosis, with or without diabetes. Tracer uptake was assessed by *in vivo* PET imaging and the uptake was confirmed by analyses of *ex vivo* biodistribution and *ex vivo* and *in vitro* autoradiography of atherosclerotic vessels. Immunohistolochemical staining was used to confirm the precense of the tracer target in the tissues and blocking experiments were performed to ensure the specifity of the tracers. The effects of linagliptin intervention on atherosclerotic plaque formation and inflammation and hepatic steatosis and inflammation was evaluated from histology and by utilizing 2-deoxy-2-[^{18}F]fluoro-D-glucose (^{18}F-FDG).

The results demonstrated that ^{68}Ga-NODAGA-exendin-4, ^{18}F-FGln and ^{18}F-FOL all detected atherosclerotic lesions *in vivo*. Linagliptin treatment showed no effect on atherosclerotic plaque formation or inflammation or hepatic steatosis. However it did sigificantly enhance glucose tolerance of the mice and decrease hepatic inflammation. In conclusion, all three studied PET tracers showed potential for the imaging of atherosclerotic disease activity. We did not find evidence of reduced inflammatory activity in atherosclerotic lesions by linagliptin treatment in this model.

KEYWORDS: Atherosclerosis, type 2 diabetes mellitus (T2DM), inflammation, positron emiossion tomography (PET) imaging

TURUN YLIOPISTO
Lääketieteellinen tiedekunta
Kliininen lääketiede
Kliininen fysiologia ja isotooppilääketiede
JENNI VIRTA: Ateroskleroosin tautiaktiivisuuden positroniemissio-tomografia kuvantaminen
Väitöskirja, 181 s.
Lääketutkimuksen tohtoriohjelma
Kesäkuu 2024

TIIVISTELMÄ

Ateroskleroosi on etenevä tulehduksellinen sairaus, jossa rasvaa ja sidekudosta kertyy verisuonten seinämiin. Tyypin 2 diabeteksen (T2DM) esiintyvyys on vuosien aikana noussut maailmanlaajuisesti ja sen tiedetään kiihdyttävän ateroskleroosin etenemistä. Makrofageilla eli syöjäsoluilla on tärkeä rooli ateroskleroosin tauti-aktiivisuuden säätelyssä ja ne voivat joko estää tai edistää sairauden etenemistä. Positroniemissiotomografia (PET) on kuvantamismenetelmä, jolla voidaan kuvata biologisia toimintoja *in vivo* ja se voi mahdollistaa ateroskleroosin tautiaktiivisuuden ei-invasiivisen arvioinnin.

Tämän väitöskirjatyön tarkoituksena oli tutkia kolmen uuden PET merkkiaineen ^{68}Ga-NODAGA-exendin-4, (2S, 4R)-4-[^{18}F]fluoroglutamiini (^{18}F-FGln) ja ^{18}F-AlF-NOTA-folaatti (^{18}F-FOL) soveltuvuutta ateroskleroosin tautiaktiivisuuden kuvantamiseen ja diabeteslääkkeenä käytettävän dipeptidyylipeptidaasi-4 (DPP-4) inhibiittorin linagliptiinin vaikutuksia hyödyntämällä tunnettua merkkiainetta. Tutkimukset suoritettiin kahdella ateroskleroosin hiirimallilla sekä kanimallilla, osalla hiiristä oli lisäksi diabetes. Merkkiaineiden kertymistä tutkittiin i*n vivo* PET kuvantamisella ja kertymä varmistettiin analysoimalla *ex vivo* kudosjakautuminen sekä ateroskleroottisten verisuonten *ex vivo* ja *in vitro* autoradiografia. Kudosvärjäysten avulla varmistettiin, että merkkiaineen kohdetta on kudoksissa ja merkkiaineiden spesifinen sitoutuminen varmistettiin merkkiaineen sitoutumista estävillä kokeilla. Linagliptiinin vaikutuksia ateroskleroottisten plakkien muodostumiseen ja tulehdukseen sekä maksan rasvoittumiseen ja tulehdukseen tutkittiin histologisen arvioinnin ja 2-deoksi-2-[^{18}F]fluoro-D-glukoosin (^{18}F-FDG) avulla.

Tulokset osoittivat, että ^{68}Ga-NODAGA-exendin-4, ^{18}F-FGln ja ^{18}F-FOL kertymä ateroskleroottisiin plakkeihin voitiin havaita *in vivo*. Linagliptiini-hoidolla ei ollut vaikutusta ateroskleroosiin tai maksan rasvoittumiseen. Se kuitenkin merkittävästi paransi hiirten sokerinsietokykyä ja vähensi maksan tulehdusta. Yhteenvetona voidaan todeta, että kaikki tutkitut merkkiaineet voivat soveltua ateroskleroosin tautiaktiivisuuden kuvantamiseen. Linagliptiinihoidolla ei ollut havaittavaa vaikutusta ateroskleroottisten plakkien tulehduksen aktiivisuuteen tutkitulla kokeellisella mallilla.

AVAINSANAT: Ateroskleroosi, tyypin 2 diabetes mellitus (T2DM), tulehdus, positroniemissiotomografia (PET)- kuvantaminen

Table of Contents

Abbreviations **8**

List of Original Publications **11**

1 Introduction **12**

2 Review of the literature **14**
2.1 Atherosclerosis 14
2.1.1 Pathophysiology of atherosclerosis 14
2.1.2 Inflammation in atherosclerosis 16
2.1.2.1 The role of macrophages in the pathogenesis of atherosclerosis 18
2.1.2.2 Other inflammatory cells in atherosclerosis 20
2.1.3 Animal models of atherosclerosis 22
2.1.3.1 Mouse models of atherosclerosis 22
2.1.3.2 Mechanically induced mouse models of vascular injury 27
2.1.3.3 Other animal models of atherosclerosis 27
2.2 Type 2 diabetes 28
2.2.1 Atherosclerosis and type 2 diabetes 28
2.2.2 Glucagon-like peptide-1 32
2.2.3 GLP-1 therapy 33
2.3 Imaging of atherosclerosis 34
2.3.1 Anatomical imaging 35
2.3.2 Positron emission tomography imaging 36
2.3.2.1 ^{18}F-FDG 36
2.3.2.2 GLP-1R targeting tracers 37
2.3.2.3 Glutamine metabolism targeting tracers 38
2.3.2.4 Folate receptor targeting tracers 39
2.3.2.5 Other tracers targeting macrophages 39

3 Aims **42**

4 Materials and Methods **43**
4.1 Experimental animals 43
4.1.1 Mouse models (I–IV) 43
4.1.2 Rabbit model (IV) 43
4.2 Study design 44
4.2.1 Intervention study (I) 45
4.2.2 Oral glucose tolerance test (I, II) 45

4.2.3 Imaging studies (II, III, IV) ... 45
4.3 Tracer radiosynthesis ... 46
4.3.1 ^{68}Ga-NODAGA-exendin-4 ... 46
4.3.2 (2*S*, 4*R*)-4-[^{18}F]fluoroglutamine ... 46
4.3.3 ^{18}F-AlF-NOTA-folate ... 47
4.4 PET/CT imaging ... 47
4.5 Ex vivo biodistribution ... 49
4.6 Autoradiography studies ... 50
4.7 Specificity of tracer binding (II, IV) ... 52
4.7.1 *In vitro* binding (IV) ... 52
4.8 *In vivo* tracer stability (III, IV) ... 53
4.9 Histology and immunohistochemistry ... 54
4.10 Measurement of plasma biomarkers (I, II) ... 55
4.11 Statistical analyses ... 56

5 Results ... 57
5.1 Study animal characteristics ... 57
5.1.1 Histology and immunohistochemistry ... 57
5.1.2 Plasma biomarkers ... 58
5.1.3 Glucose tolerance tests ... 59
5.2 Specificity of tracer binding (II, IV) ... 60
5.2.1 *In vitro* binding (IV) ... 60
5.3 *In vivo* tracer stability (III, IV) ... 60
5.4 PET/CT imaging ... 60
5.5 *Ex vivo* biodistribution ... 62
5.6 Autoradiography ... 63

6 Discussion ... 65
6.1 Imaging in different animal models of atherosclerosis ... 65
6.1.1 Plaque characterization ... 66
6.2 GLP-1 therapy ... 67
6.2.1 Effects of linagliptin therapy ... 68
6.2.2 SGLT2 therapy ... 69
6.3 Evaluation of the PET tracers for imaging atherosclerotic disease activity ... 70
6.3.1 ^{68}Ga-NODAGA-exendin-4 ... 70
6.3.2 ^{18}F-FGln ... 71
6.3.3 ^{18}F-AlF-NOTA-folate ... 73
6.4 Future aspects of PET imaging of atherosclerosis ... 74

7 Summary and Conclusions ... 75

Acknowledgements ... 76

References ... 79

Original Publications ... 105

Abbreviations

^{18}F-FDG	2-deoxy-2-[^{18}F]fluoro-D-glucose
^{18}F-Gln	(2*S*, 4*R*)-4-[^{18}F]fluoroglutamine
α-SMA	Alpha smooth muscle actin
ABCA1	ATP-binding cassette subfamily A 1 protein
ABCG1	ATP-binding cassette subfamily G 1 protein
AGE	Advanced glycation end product
ANOVA	One-way analysis of variance
APC	Antigen presenting cell
ApoB100	Apolipoprotein B 100
ApoB48	Apolipoprotein B 48
APOBEC-1	ApoB mRNA editing catalytic polypeptide-1
APOC1	Apolipoprotein C1
ApoE	Apolipoprotein E
ARG	Autoradiography
AUC	Area under the curve
CCL19	CC-chemokine ligand 19
CE	Cholesteryl ester
CETP	Cholesteryl ester transfer protein
CT	Computed tomography
CV	Cardiovascular
CVD	Cardiovascular disease
DAP	3.3′-diaminobenzidine tetrahydrochloride hydrate
DC	Dendritic cell
DPP-4	Dipeptidyl peptidase-4
EC	Endothelial cell
eNOS	Endothelial NO synthase
ET-1	Endothelin-1
Fbn1	Fibrillin-1
FFA	Free fatty acid
FH	Familial hypercholesterolemia
FKN	Fractalkine (also known as CX3CL1)

FR	Folate receptor
GIP	Gastric inhibitory polypeptide
GLP-1	Glucagon-like peptide-1
GPL-1R	GLP-1 receptor
GLP-1RA	GLP-1R agonist
GLUT	Glucose transporter
Hb	Hemoglobin
HE	Hematoxylin and eosin
HFD	High-fat diet
HDL	High-density lipoprotein
HIF-1α	Hypoxia-inducible factor 1 α
HO-1	Heme oxygenase 1
HPLC	High-performance liquid chromatography
hsCRP	High sensitivity C-reactive protein
HSL	Hormone sensitive lipase
ICAM-1	Intercellular adhesion molecule-1
Ig	Immunoglobulin
IGF	Insulin-like growth factor
IGF-II	Insulin-like growth factor II
IL	Interleukin
IMT	Intima-media thickness
INF-γ	Interferon gamma
iNOS	Inducible nitric oxide synthase
i.p.	Intraperitoneal
ipGTT	Intraperitoneal glucose tolerance test
i.v.	Intravenous
LDL	Low-density lipoprotein
LDLR	LDL receptor
LOX-1	ox-LDL receptor-1
LPL	Lipoprotein lipase
LPS	Lipopolysaccharide
Ly6C	Lymphocyte antigen 6 complex
MACS	Magnetic-activated cell sorting
MCP-1	Monocyte chemoattractant protein-1 (also known as CCL2)
M-CSF	Macrophage colony-stimulating factor
M(Hb)	Hemoglobin stimulated macrophage
MI	Myocardial infarction
MMP	Matrix metalloproteinase
MRC-1	Mannose receptor C-type 1
MRI	Magnetic resonance imaging

mRNA	Messenger RNA
NADPH	Nicotinamide adenine dinucleotide phosphate
NAFLD	Non-alcoholic fatty liver disease
NAS	NAFLD scoring
NASH	Non-alcoholic steatohepatitis
NF-κB	Nuclear factor kappa B
NO	Nitric oxide
Nrf2	Nuclear factor erythroid 2–related factor 2
oGTT	Oral glucose tolerance test
oxLDL	Oxidized LDL
PBS	Phosphate-buffered saline
PCSK9	Subtilisin/kexin type 9
PET	Positron emission tomography
PSL/mm^2	Photostimulated luminescence per square millimeter
rAAV	Recombinant adeno-associated virus
RAGE	AGE receptor
RANTES	Regulated on activated normal T-cell expressed and secreted (also known as CCL-5)
ROS	Reactive oxygen species
SD	standard deviation
SGLT2	Sodium-glucose co-transporter-2
SUV	Standardized uptake value
TBR	Target-to-background ratio
T2DM	Type 2 diabetes mellitus
TG	Triglyceride
TGF-β	Transforming growth factor beta
T_H	T helper cell
Th-1	Type 1 T helper cell
Th-2	Type 2 T helper cell
TNF-α	Tumor necrosis factor alpha
T_{reg}	Regulatory T-cells
TSPO	Translocator protein
VCAM-1	Vascular cell adhesion molecule-1
VEGF	Vascular endothelial growth factor
VLDL	Very low-density lipoprotein
VSMC	Vascular smooth muscle cell

List of Original Publications

The thesis is based on the following original publications, which are referred to in the text by their Roman numerals: I‑IV.

I. Jenni Virta, Sanna Hellberg, Heidi Liljenbäck, Mia Ståhle, Johanna MU Silvola, Jenni Huusko, Mirva Söderström, Juhani Knuuti, Pirjo Nuutila, Seppo Ylä-Herttuala, Maria F. Gomez, Anne Roivainen, Antti Saraste. Effects of dipeptidyl peptidase 4 inhibition on inflammation in atherosclerosis: A ^{18}F-fluorodeoxyglucose study of a mouse model of atherosclerosis and type 2 diabetes. Atherosclerosis. 2020; 305: 64–72.

II. Mia Ståhle, Sanna Hellberg, Jenni Virta, Heidi Liljenbäck, Olli Metsälä, Xiang-Guo Li, Matti Jauhiainen, Pekka Saukko, Seppo Ylä-Herttuala, Pirjo Nuutila, Juhani Knuuti, Antti Saraste, Anne Roivainen. Evaluation of glucagon-like peptide-1 receptor expression in nondiabetic and diabetic atherosclerotic mice using PET tracer ^{68}Ga-NODAGA-exendin-4. American Journal of Physiology- Endocrinology and Metabolism 2021; 320(5): E989–E998.

III. Senthil Palani, Maxwell W.G. Miner, Jenni Virta, Heidi Liljenbäck, Olli Eskola, Tiit Örd, Aarthi Ravindran, Minna U. Kaikkonen, Juhani Knuuti, Xiang-Guo Li, Antti Saraste, Anne Roivainen. Exploiting Glutamine Consumption in Atherosclerotic Lesions by Positron Emission Tomography Tracer (2*S*,4*R*)-4-^{18}F-Fluoroglutamine. Frontiers of Immunology 2022; 13: 821423.

IV. Johanna M.U. Silvola, Xiang-Guo Li, Jenni Virta, Päivi Marjamäki, Heidi Liljenbäck, Jarkko P. Hytönen, Miikka Tarkia, Virva Saunavaara, Saija Hurme, Senthil Palani, Harri Hakovirta, Seppo Ylä-Herttuala, Pekka Saukko, Qingshou Chen, Philip S. Low, Juhani Knuuti, Antti Saraste, Anne Roivainen. Aluminum fluoride-18 labeled folate enables in vivo detection of atherosclerotic plaque inflammation by positron emission tomography. Scientific Reports 2018; 8(1): 9720.

1 Introduction

Atherosclerosis is characterized by the accumulation of lipids and fibrous elements in the arterial wall resulting in lesion formation. It is the major cause of death globally and it is estimated that 31% of all deaths are caused by cardiovascular disease. Atherosclerosis is pronounced in low- to moderate-income countries where known risk factors such as obesity, unhealthy diet and physical inactivity are common. The main clinical manifestations of atherosclerosis are heart disease (commonly due to coronary atherosclerosis), and stroke, which are still the leading causes of death worldwide, even though there has been an overall decline in both cases. (Libby et al. 2019)

Development of atherosclerosis is triggered when the level of circulating low-density lipoproteins is increased and they start to accumulate in the vessel wall. In type 2 diabetes mellitus (T2DM), dyslipidemia, most often hypertriglyceridemia, is related to insulin resistance and can precede the development of overt diabetes. The lipoproteins are modified causing an inflammatory response and recruitment of monocytes from the circulation to the lesion site. The monocytes traverse into the vessel intima where they differentiate into macrophages, which ingest the modified lipoproteins, resulting in the formation of foam cells. Macrophages can either promote or prevent the progression of atherosclerosis by secreting several different cytokines. Proinflammatory macrophages can decrease collagen synthesis and secrete proteolytic enzymes that in later stages of the disease can lead to plaque erosion or rupture. (Wu et al. 2017.) T2DM affects more than 370 million people worldwide as a result of increased obesity. Diabetes is known to accelerate the development of atherosclerosis due to dyslipidemia, oxidative stress, hyperglycemia, and increased inflammation. (Poznyak et al. 2020.) As diabetes and atherosclerosis are tightly connected, a lot of research has been focusing on the cardiovascular effects of glucagon-like peptide-1 (GLP-1) targeting therapies that are used to treat T2DM (Ma et al. 2022; Gallego-Colon et al. 2018).

Positron emission tomography (PET) imaging can be utilized to assess atherosclerotic disease activity. 2-deoxy-2-[18F]fluoro-D-glucose (^{18}F-FDG), is the most well-known tracer which shows binding in macrophage-rich atherosclerotic lesions (Rudd 2002; Johnsrud et al. 2019; Toner et al. 2022). ^{18}F-FDG-PET imaging

has been used to monitor therapy responses as well as identifying active plaques (Tawakol et al. 2013; Kim et al. 2020; Jarr et al. 2020). However, there are some limitations to ^{18}F-FDG-PET imaging, raising the need for more specific tracers to evaluate atherosclerotic disease activity. This thesis evaluates three novel PET tracers for imaging atherosclerotic disease activity in mouse and rabbit models of atherosclerosis. In addition, the effects of dipeptidyl peptidase-4 (DPP-4) inhibitor linagliptin on atherosclerotic plaque formation and inflammation and hepatic inflammation and steatosis are studied in a mouse model of atherosclerosis and T2DM.

2 Review of the literature

2.1 Atherosclerosis

2.1.1 Pathophysiology of atherosclerosis

Atherosclerosis is a progressive arterial disease involving both the innate and adaptive immune system and is characterized by chronic low-grade inflammation of the arterial wall, lipoprotein retention, and accumulation of fibrous elements leading to plaque formation (Benzon et al. 2014). Shear stress is vital for the homeostasis of vascular endothelial cells (EC). Atherosclerotic plaques commonly build up in areas with low shear stress in regions such as vessel curvatures and bifurcations, causing endothelial dysfunction, making these areas more prone to atherosclerosis. (Heo et al. 2014.) In addition to endothelial dysfunction, intimal thickening is one of the main characteristics of predilection sites where atherosclerotic plaques start to form. When the production of nitric oxide (NO) by ECs is impaired, permeability of the vessel wall is increased. It is accompanied by the accumulation of circulating low-density lipoprotein (LDL) particles into the vessel intima where they undergo modification including oxidation, having proinflammatory effects. Modified LDLs induce endothelial and vascular smooth muscle cells (VSMC) to express adhesion molecules, chemoattractants and growth factors, which help attract and differentiate circulating monocytes. Monocytes are internalized into the intima, where they differentiate into macrophages. Macrophages ingest the modified lipoproteins and form foam cells, which is a hallmark of the early fatty streak lesions. (Falk 2006; Bentzon et al. 2014; Gimbrone et al. 2016.)

Proliferation of VSMCs and synthesis of extracellular matrix components leads to the development of fibroatheromas where a fibrous cap is covering a necrotic core consisting of lipids, oxidized lipoproteins, cholesterol crystals, and cellular debris. The necrotic core forms when foam cells and VSMCs go through apoptosis or secondary necrosis and the removal of apoptotic remnants, efferocytosis, is impaired. (Bentzon et al. 2014.) The fibrous cap may lose thickness over time and fibroatheromas where the cap thickness is < 65 μm are considered as thin-cap fibroatheromas. Cap thickness and infiltration of macrophages correlate with plaque vulnerability. (Virmani et al. 2003.) Calcification is frequently observed in plaques,

and they can vary in size from early microcalcifications (≥ 0.5 to < 15 μm) that can further coalesce into larger calcified sheets and even whole plaque calcifications. Calcification is more advanced in men and the presence of diabetes accelerates the calcification process. (Otsuka et al. 2014.) Several studies have reported that coronary artery calcification correlates with adverse cardiac events, however it is unclear whether these events originate from highly calcified or mildly calcified plaques or from other lesions with no calcification. All in all, the presence of small calcifications like micro- or fragmented calcifications are thought to serve as predictors of unstable plaques, whereas large calcifications like sheet calcifications and fibrocalcific plaques (plaques characterized by a thick fibrous cap and extensive calcification) are predictors of more stable plaques. (Jinnouchi et al. 2020a.)

Growing fibroatheromas often have areas that are hypoxic, promoting neovascularization. Neovessels are often fragile having an incomplete mural cell coverage and compromised structural integrity and provide new entry pathways for monocytes (Sluimer et al. 2009; Moore & Tabas 2011). Erythrocytes leaking from neovessels into the plaques, increase the size of necrotic cores and further stimulate inflammation, potentially increasing the risk of plaque destabilization (Kolodgie et al. 2003). Plaques with these features are weaker and more vulnerable to rupture and erosion. The weakest part is usually located in the junction between the plaque and adjacent less-diseased vessel wall, the so-called shoulder region. Plaque ruptures can be caused by degradation of the fibrous cap and physical stressors such as increased heart rate and blood pressure. In plaque erosion, the endothelium is typically absent exposing the underlying plaque to circulating blood, triggering thrombosis. Plaque rupture can be asymptomatic, where the plaque heals and grows larger. However clinical manifestations can occur. (Falk et al. 1995; Virmani et al. 2000; Bentzon et al. 2014.) Figure 1. summarizes the main mechanisms underlying the pathogenesis of atherosclerosis.

The main clinical manifestations of atherosclerosis are ischemic heart disease (IHD), stroke, and peripheral artery disease. In IHD, one or several coronary arteries become obstructed by atherosclerotic plaque, inhibiting normal blood flow to the myocardium, and inducing myocardial ischemia. Ischemia can also be caused by plaque erosion or rupture that causes an acute thrombus formation and can lead to a total blockage of an artery and subsequent myocardial infarction (MI). (Virmani et al. 2000; Severino et al. 2020.) Similarly, as in MI, during stroke blood flow to the brain is obstructed, causing ischemia and cell death. Peripheral artery disease affects the peripheral arteries, mainly the arteries in the lower limbs and kidneys, but also in the mesentery and the vicinity of the abdominal aorta. Blockage of a peripheral artery affects the patient's mobility and can lead to amputation of the affected limb. (Herrington et al. 2016.)

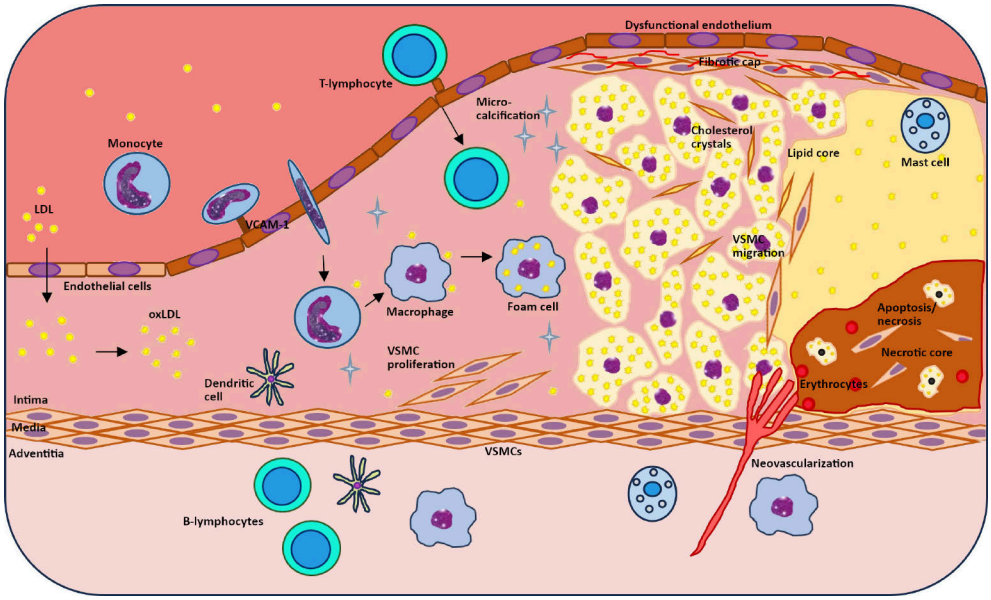

Figure 1. Pathogenesis of atherosclerosis. Summary of the main mechanisms underlying the development of atherosclerotic lesions. Endothelial dysfunction increases the vessel wall permeability and it is accompanied by the accumulation of LDL in the intima where it is oxidized into oxLDL. Ly6C^{hi} monocytes attach to VCAM-1s and transmigrate to the intima where they differentiate into macrophages, which ingest oxLDL, transforming into foam cells. VSMC proliferation and migration, and synthesis of extracellular matrix components leads to the formation of a fibrous cap that covers a lipid core (fibroatheroma). Dendritic cells as well as T-lymphocytes can be both pro- or antiatherogenic depending on their subpopulation, whereas B-lymphocytes are concidered more atheroprotective. Hypoxia inside the growing fibroatheroma causes the formation of a necrotic core consisting of apoptotic foam cells and VSMCs, promoting neovascularizarion. Fragile neovessels leak causing intraplaque hemorrhage which further increases plaque size and inflammation. Mast cells can destablizise the fibrotic cap, rendering the plaque prone to rupture. LDL= low-densitity lipoprotein, oxLDL= oxidized LDL, VCAM-1= vascular cell adhesion molecule 1, VSMC= vascular smooth muscle cell.

2.1.2 Inflammation in atherosclerosis

Originally, atherosclerosis was mostly considered to be a lipid storage disease but over the years it became evident that inflammation is an integral part of atherogenesis when signs of inflammation were detected in several different animal models of atherosclerosis. Inflammation mediates disease progression in atherosclerosis and elevated levels of inflammatory biomarkers such as high sensitivity C-reactive protein (hsCRP) and different cytokines correlate with adverse prognosis. They can however also serve as implications for prevention. (Libby et al. 2002.)

The inflammatory process in atherosclerosis is triggered by the formation and accumulation of minimally oxidized LDL (oxLDL). Circulating LDL is bound to apolipoprotein B 100 (ApoB100) and crosses the endothelium by both passive

filtration and active transcytosis involving different cell surface receptors. (Borén et al. 2020.) Once in the intima, ApoB-100 binds to proteoglycans resulting in the retention of LDL (Borén & Williams 2016). LDL undergoes modifications including glycation and oxidation after which it induces monocyte trafficking to the arterial wall and mediates proinflammatory responses (van der Valk et al. 2016; Borén et al. 2020; Poznyak et al. 2023).

Cytokines have an essential role in atherogenesis, but also in the regression of atherosclerosis. Cytokines are small signaling molecules that affect leukocyte extravasation and their differentiation and polarization. Chemokines are small chemotactic cytokines that signal through G-protein coupled transmembrane receptors and attract cells to enter tissues (chemotaxis) (Haribabu et al. 1999). Cytokines can be proinflammatory (interleukins IL-1β, IL-6, IL-12, IL-15, IL-18, tumor necrosis factor alpha, TNF-α and interferon gamma INF-γ) or anti-inflammatory (IL-4, IL-10, IL-13 and transforming growth factor beta, TGF-β) (Hansson & Libby 2006; Tedqui & Mallat 2006).

Active proinflammatory cytokine, IL-1β, is produced mainly in monocytes, macrophages, and dendritic cells (DC). It increases the expression of cell adhesion molecules, attracts mononuclear phagocytes, and induces chemokine, monocyte chemoattractant protein-1 (MCP-1/CCL2). (Dinarello 2009; Libby 2017.) IL-6 secretion from macrophages, monocytes, and other cell types typically follows IL-1 stimulation and further increases expression of cell adhesion molecules as well as potentiates vascular permeability (Ridker & Rane 2021). Together with IL-12, these two cytokines also control the production of hsCRP, which is associated with an increased risk of cardiovascular complications and non-alcoholic fatty liver disease (NAFLD) (Mani et al. 2019; Henein et al. 2022; Zhao et al. 2023).

Anti-inflammatory cytokine IL-10 has a key role in preventing atherosclerotic plaque development and modulates cellular and collagen plaque composition (Potteaux et al. 2004). TGF-β has an important role in plaque development and composition and lack of TGF-β signaling has been shown to result in an unstable plaque phenotype (Mallat et al. 2001).

There are three main chemokines in atherogenesis. MCP-1/CCL2 attracts monocytes to transmigrate into the intima, regulated on activated normal T-cell expressed and secreted (RANTES/CCL5) attracts T cells, neutrophils, and monocytes and fractalkine (FKN/CX3CL1) mediates the arrest and migration of monocytes into the intima. (von Hundelshausen et al. 2001; Ancuta et al. 2003; Veillard et al. 2004; Blin et al. 2019; Georgakis et al. 2022.) Proinflammatory cytokines induce vascular ECs to express adhesion molecules for white blood cells on sites with low shear stress. The cells recognize adhesion molecules with their surface antigens, attach and transmigrate into the intima. The most important adhesion molecules are vascular cell adhesion molecule-1 (VCAM-1), intercellular

adhesion molecule-1 (ICAM-1) and P-selectin. (Nagel et al. 1994; Sakai et al. 1997; Nakashima et al. 1998; Cybulsky et al. 2001; Ye et al. 2019.)

2.1.2.1 The role of macrophages in the pathogenesis of atherosclerosis

Macrophages have a central role in innate immunity, and they are involved in all stages of atherogenesis from initiation to complications. Atherogenesis is initiated when the circulating levels of LDL are increased and start to accumulate in the intima through the dysfunctional endothelium. ECs secrete chemokines that attract monocytes into the intima where they differentiate into macrophages. In mice, the monocytes that are involved in atherogenesis are mostly from the proinflammatory subset $Ly6C^{hi}$ ($CD14^{high}CD16^{-}$ in humans) which infiltrate into the plaque and differentiate into M1 macrophages. Anti-inflammatory subset of monocytes, $Ly6C^{lo}$ ($CD14^{low}CD16^{+}$ in humans), are mostly involved in the resolution of inflammation and are considered to be the precursors of M2 macrophages (Moore & Tabas 2011; Yang et al. 2014; Kang et al. 2021.)

Macrophage polarization

The differentiation of monocytes into macrophages is driven by cytokines like macrophage colony-stimulating factor (M-CSF) (Moore & Tabas 2011). Macrophages are stimulated by several different signals to polarize into a variety of subclasses that all have specific functions in atherosclerosis. The polarization process is constantly ongoing since macrophages keep adapting to the changing microenvironment. Macrophages can also modulate the phenotype of other macrophages and thus affect plaque development. The subclasses express a unique set of surface molecules and secrete different cytokines and other soluble mediators that affect the course of atherosclerosis. There are currently six subclasses of macrophages identified in atherosclerotic plaques: M1, M2, Mox, hemoglobin stimulated macrophages (M (Hb)), Mhem, and M4. (Wu et al. 2023.)

The proinflammatory M1 macrophages are activated by several different factors, including INF-γ and the toll-like receptor 4 ligand lipopolysaccharide (LPS). M1 macrophages produce and secrete proinflammatory cytokines including TNF-α, IL-6 and IL-1β. M1 (analogous to type 1 T helper cells (Th-1)) macrophages also produce chemokines like MCP-1/CCL2 and also inducible nitric oxide synthase (iNOS) and reactive oxygen species (ROS) by activating the nicotinamide adenine dinucleotide phosphate (NADPH) oxidase complex. The production of ROS can increase oxidative stress in the plaques and promote oxidation of LDL particles. Expression of chemokine receptor ligands on M1 macrophages promotes further recruitment of inflammatory cells Th-1 T cells and natural killer cells. The

accumulation and death of M1 macrophages causes the formation and expansion of the necrotic core in atherosclerotic plaques. (Tabas & Bornfeldt 2016; Jinnouchi et al. 2020b; Wu et al. 2023.)

In contrast to M1 macrophages, M2 (analogous to type 2 T helper cells (Th-2)) macrophages are considered to be anti-inflammatory by nature and they are involved in clearing up cell debris and apoptotic cells and also contribute to tissue remodeling and repair. M2 macrophages are activated by IL-4 and IL-13 produced by Th-2 T cells, and secrete IL-10 and TGF-β, thereby promoting tissue repair. M2 macrophages can be further divided into four subtypes: M2a, M2b, M2c, and M2d. Subtype M2a is induced by cytokines IL-4 and IL-13 and express high levels of glucocorticoid receptor mannose receptor. They secrete pro-fibrotic factors like fibronectin, insulin-like growth factor (IGF), and TGF-β, thereby contributing to tissue repair which is the reason these macrophages are often referred to as wound healing macrophages. M2b macrophages are induced by immune complexes, TLR agonists, and IL-1R ligands and produce both anti-inflammatory cytokine IL-10 and proinflammatory cytokines IL-1, IL-6 and TNF-α. M2c macrophages on the other hand, are induced by glucocorticoids and IL-10 and release large amounts of IL-10 and TGF-β causing a strong anti-inflammatory reaction against apoptotic cells. M2b and M2c macrophages are commonly referred to as regulatory macrophages. M2d has a proinflammatory effect, because it decreases phagocytosis, but its main action is anti-inflammatory. It inhibits secretion of pro-inflammatory cytokines IL-12 and TNF-α and induces secretion of anti-inflammatory cytokine IL-10 and vascular endothelial growth factor (VEGF). M2d macrophages lack the expression of CD206, which distinguishes them from the other three M2 subtypes. (Jinnouchi et al. 2020b; Xie et al. 2022; Wu et al. 2023.)

Oxidized LDL induces M1 and M2 macrophages to switch their polarization into Mox macrophages, mediated by transcription factor nuclear factor erythroid 2–related factor 2 (Nrf2) which upregulates a cluster of redox regulated genes including heme oxygenase 1 (HO-1). This change in gene expression is thought to protect the cells from cell death caused by oxidative stress. However, Mox macrophages also show upregulation of proinflammatory genes IL-1β and cyclooxygenase 2, making their role in atherosclerosis rather controversial. Mox macrophages are characterized by a reduced chemotactic and phagocytic capacity, which can contribute to tissue damage and the formation of a necrotic core. In LDL receptor knock out mice, Mox macrophages can comprise up to 30 % of all macrophages in advanced lesions. (Kadl et al. 2010.)

Intraplaque hemorrhage releases hemoglobin (Hb), which binds to haptoglobin (Hp) forming Hb:Hp complexes. Hb:Hp complexes induce macrophages to polarize into M(Hb) macrophages that express MR and a scavenger receptor CD163 that bind Hb:Hp complexes and mediate their endocytosis. (Chinetti-Gbaguidi et al. 2015.) Hb:Hp complexes induce secretion of anti-inflammatory cytokine IL-10, which upregulates the expression of CD163 thus amplifying the scavenging of Hb:Hp

complexes. IL-10 also increases intracellular production of HO-1 via an autocrine mechanism. (Philippidis et al. 2004.) Expression of scavenger receptors responsible for the uptake of oxLDL is downregulated in M(Hb) macrophages, but on the other hand, liver X receptor α activity is increased and expression of ATP-binding cassette subfamily A 1 and G1 proteins (ABCA1 and ABCG1) which are responsible for the efflux of cholesterol is upregulated, making M(Hb) cells resistant to foam cell formation (Habib & Finn 2014). Expression of the iron transporter ferroportin is upregulated in M(Hb) macrophages, leading to increased cellular export of iron, and thus decreased production of ROS, lowering oxidative stress. (Finn et al. 2012.) The endocytosed Hb:Hp complexes and erythrocytes release heme, which can induce macrophages to polarize into Mhem macrophages. Heme induces upregulation of HO-1 and transcription factor liver X receptor beta by activating transcription factor 1. This leads to the upregulation of liver X receptor α and ABCA1 expression thereby enhancing cholesterol efflux and preventing foam cell formation and oxidative stress. (Boyle et al. 2012.) There are several similarities between M(Hb) and Mhem macrophages since they are both found in bleeding sites and unstable plaques and both have a role in iron handling and cholesterol efflux, providing protective effects against atherosclerosis (Wu et al. 2023).

M4 macrophages are considered proinflammatory and proatherogenic and are induced by platelet factor 4 chemokine. They express several proinflammatory cytokines including IL-6 and TNF-α and expression of CD163 is down-regulated, making them prone to foam cell formation. They also overexpress 7 (MMP-7) which is an enzyme capable of degrading extracellular matrix and calcium-binding protein S100A8, which is a biomarker for cardiovascular events. (Erbel et al. 2015; Domschke & Gleissner 2019.)

2.1.2.2 Other inflammatory cells in atherosclerosis

Lymphocytes

Lymphocytes can be divided into T-cells, which are located in atherosclerotic lesion sites and B-cells, which are located in the adventitia. Lymphocytes are less abundant in atherosclerotic lesions than macrophages, but they still have an important role in atherogenesis. (Weber et al. 2008.) B-cells develop from hematopoietic precursors in the bone marrow and upon activation maturate into antibody-secreting plasma cells in the spleen. They can be divided into subgroups according to their effects: B1, follicular, marginal zone, regulatory B-cells, and innate response activator B-cells. B-cells express membrane-bound immunoglobulins called B-cell receptors that bind both autoantigens and foreign antigens and secrete antibodies including immunoglobulin M (IgM), E (IgE) and G (IgG). B-cells are generally considered to

have an atheroprotective role and IgM antibodies show a substantial protective effect by binding to and neutralizing oxidation-specific epitopes such as phosphorylcholine containing oxLDL and its degradation product malondialdehyde both of which are increased in atherosclerosis. (Sage et al. 2019.)

Naïve T-cells originate from the thymus and migrate to atherosclerotic lesion sites via the circulation. Macrophages secrete TNF-α which attracts more T-cells and B-cells to the developing lesions. In the lesions, T-cells are activated by antigen presenting cells (APC), usually macrophages or DCs which present epitopes of oxLDL and heatshock protein 60/65 (hsp60/65). All T-cell subsets ($CD4^+$, $CD8^+$, $TCR\gamma\delta^+$ and NK cells can be found in atherosclerotic lesions, but there is a preponderance of $CD4^+$ T-cells. (Tse et al. 2013.) $CD4^+$ T-cells can differentiate into T helper cells (T_H) or regulatory T-cells (T_{reg}) though T_H1 is the most common type found in developing lesions. T_H1 cells secrete INF-γ and other pro-inflammatory cytokines that can activate macrophages which is why they are commonly considered proatherogenic but the role of other T_H subsets in the development of atherosclerosis is still unclear. T_{reg} cells secrete IL-10 and TGF-β both of which have atheroprotective effects. They also have the ability to suppress effector T-cell proliferation providing further protective effects. Mature $CD8^+$ T-cells (cytotoxic T-cells) are most common in advanced plaques, more specifically in the fibrous cap area, outnumbering even $CD4^+$ T-cells. $CD8^+$ T-cells can have both pro- and antiatherogenic effects depending on where their cytotoxic effects are directed to. (Saigusa et al. 2020.)

Dendritic cells

DCs differentiate from monocytes and are commonly found in the intima of healthy individuals, but their amount increases in atherosclerosis. They act in both innate and adaptive immunity and are able to activate both naïve and memory T cells. The role of DCs in atherosclerosis depends on the subpopulation. Mature DCs lose their efferocytosis ability and accumulate in sites of lesion progression. They attract T-cells by secreting chemokines such as CC-chemokine ligand 19 (CCL19) and activate autologous T_H1 cells, which produce proinflammatory cytokines and IFN-γ, thus perpetuating lesion progression. Immature DCs can delete responsive T-cells and induce production of atheroprotective T_{reg} cells. However, immature DCs are able to ingest lipids via efferocytosis and have a foam cell-like appearance, which suggests that they might also mediate early lipid accumulation in atherosclerotic lesions. Plasmacytoid DCs comprise only a small portion of all DCs. They possess proatherogenic properties by secreting IFN-α and IFN-β, but deletion of plasmacytoid DCs in experimental models has led to aggravation of atherosclerosis so their role in atherosclerosis is not yet clear. (Weber et al. 2008; Subramanian & Tabas 2014.)

Mast cells

Mast cells are highly potent immune cells that originate from hematopoietic stem cells in the bone marrow and derived from circulating myeloid progenitor cells. Mast cells can be found both in adventitia and intimal areas and their numbers are significantly increased in ruptured plaques. Indeed, the number of mast cells increases in adventitia upon plaque progression and advanced plaque fibrous cap region, where secretion of tryptase can affect the fibrous-cap stability. Mast cells are also associated with intraplaque hemorrhage and colocalize with small fragile neovessels prone to leakage, providing further evidence that they are actively involved in destabilization of atherosclerotic plaques. (Hermans et al. 2019.)

2.1.3 Animal models of atherosclerosis

Animal models are essential in atherosclerosis research, providing insight into the molecular mechanisms behind atherosclerotic plaque formation and progression of the disease. Furthermore, animal models enable the initial assessment of novel treatments and diagnostic methods. Animal models of atherosclerosis are typically genetically modified to induce plaque formation due to changes in cholesterol metabolism leading to hypercholesterolemia. Plaque formation can be accelerated by feeding the animals a high-fat diet (HFD) rich in cholesterol, typically known as Western diet. The atherosclerotic phenotype may be accompanied by additional risk factors such as type 2 diabetes mellitus (T2DM).

2.1.3.1 Mouse models of atherosclerosis

Mice are the most frequently used species in atherosclerosis research for many reasons. Mice have rapid reproduction, a relatively short lifespan and are easy to genetically manipulate. It is also relatively inexpensive to breed and maintain mice. However, normal, healthy mice are generally resistant to atherosclerosis due to their different lipid profile compared to humans, making genetic modification mandatory in order to accelerate atherosclerosis. Most of the cholesterol in mice is packed in high-density lipoprotein (HDL) particles, whereas they have only small amounts of LDL and very high-density lipoprotein (VLDL). They also lack cholesteryl ester transfer protein (CETP) that facilitates the transport of cholesteryl esters (CE) and triglycerides (TG) between different lipoproteins contributing to atherogenic lipid profile. (Emini et al. 2017; Lee et al. 2017.) Most of the current atherosclerotic mouse models have been developed from C57BL/6J mice, which were found to be more susceptible to atherosclerotic lesion formation than other mouse strains (Paigen et al. 1985). Mouse models of spontaneous atherosclerosis are summarized in Table 1.

Apolipoprotein E deficient ($ApoE^{-/-}$) mouse model was developed in the early 90's by inactivating the endogenous apolipoprotein E (*apoE*) gene by homologous recombination in mouse embryonic stem cells (Piedrahita et al. 1992; Plump et al. 1992). ApoE is a structural component of lipoprotein particles, especially in chylomicrons that are synthesized in the intestine and takes part in hepatic lipoprotein clearance by binding to LDL receptors. $ApoE^{-/-}$ mice exhibit hypercholesterolemia even on a low-fat diet due to the severely impaired plasma lipoprotein clearance. The elevated cholesterol levels are mostly comprised of increased amount of VLDL particles, although also intermediate density lipoproteins and LDL levels are elevated. (Plump & Breslow 1995.) Already at 10 weeks of age the mice start developing atherosclerotic lesions throughout the arterial tree with predilection for aortic root, lesser curvature of the aortic arch, the principal branches of the aorta and in the pulmonary and carotid arteries. Feeding a HFD is often used to accelerate the disease progression. (Plump et al. 1992; Nakashima et al. 1994.)

ApoE3-Leiden mutation was initially found in a large family study and is associated with a dominantly inherited form of familial dysbetalipoproteinemia. The mutation was recreated in mice by introducing a 27 kb DNA fragment containing the *ApoE3-Leiden* gene, apolipoprotein C1 (*APOC1*) gene and a liver-positive element. ApoE3-Leiden mice display hyperlipoproteinemia which is exacerbated by feeding the mice a HFD. The mice develop atherosclerotic plaques in the aorta and large vessels only on HFD and exhibit all lesion types except type VI lesions with plaque rupture, thrombus formation, and hemorrhage. (van den Maagdenberg et al. 1993; Lutgens et al. 1999.) To make the ApoE3-Leiden mice more comparable to humans, they were crossbred with a mouse strain that expresses human CETP. CETP mediates the exchange of CEs and TGs between ApoB containing lipid particles and HDL in plasma. CETP-ApoE3-Leiden mice have lowered HDL and increased LDL and VLDL levels and develop much more advanced atherosclerotic lesions than ApoE3-Leiden mice alone. (Westerterp et al. 2006.)

LDL-receptor deficient ($LDLR^{-/-}$) mice were created in 1993 using homologous recombination technique on mouse embryonic stem cells. The mice lack functional LDL receptors. On a chow diet $LDLR^{-/-}$ mice exhibit mild elevation of plasma cholesterol levels and usually no or slow atherosclerotic lesion formation. HFD induces severe hypercholesterolemia and development of atherosclerotic lesions that resembles familial hypercholesterolemia (FH) in humans both in the lipid profile and lesion formation. The mice develop lesions in the aorta, coronary ostia, and the aortic root. Prolonged feeding of a HFD can also cause the mice to develop xanthomas where cholesterol-loaded macrophages accumulate in the skin and subcutaneous tissue. (Ishibashi et al. 1993; 1994.) Soon after the introduction of the $ApoE^{-/-}$ and $LDLR^{-/-}$ mice, the ApoE/LDLR double knockout mouse strain was generated, exhibiting a more severe hyperlipidemia and atherosclerosis than its predecessors. On a chow diet, these mice develop marked

intima-media thickening of the ascending aorta. Their plasma cholesterol, TG and vitamin E levels also increase with age. (Bonthu et al. 1997; Witting et al. 1999.)

The LDLR$^{-/-}$ strain has been used in combination with other genetic modifications, creating models that more closely resemble human atherosclerosis. In humans, lipoproteins mostly contain apolipoprotein B100 (ApoB100) but in mice the lipoproteins contain a truncated version, apolipoprotein B48 (ApoB48), which is produced in the liver due to ApoB messenger RNA (mRNA) editing, mediated by ApoB mRNA editing catalytic polypeptide-1 (APOBEC-1). A model that combines LDLR$^{-/-}$ mice with a mouse strain expressing only ApoB100 (LDLR$^{-/-}$ ApoB$^{100/100}$) can be generated by targeted genetic mutation of the ApoB gene (Powell-Braxton et al. 1998) or by disrupting the *APOBEC-1* gene resulting in abolished ApoB editing (Hirano et al. 1996). The reason why these mice develop hypercholesterolemia, lies in the lipoprotein clearance mechanism. LDL related protein has an important role in the clearing of ApoB48 and LDLR's are responsible for the clearance of ApoB100 containing lipoproteins (Véniant et al. 1998). Since LDLR$^{-/-}$ ApoB$^{100/100}$ mice only express ApoB100 and lack LDLR's, their cellular uptake of cholesterol is severely impaired, explaining why these mice develop hypercholesterolemia even on chow diet. The hypercholesterolemia leads to the development of spontaneous and severe atherosclerosis throughout the aorta of these mice and male mice develop more extensive lesions than females. In addition, a great advantage of this model is that it closely resembles familial hypercholesterolemia in humans because of the unique lipid profile. (Powell-Braxton et al. 1998; Véniant et al. 1998.)

The need to study combined effects of risk factors for atherosclerotic cardiovascular disease led to the development of a mouse strain where hypercholesterolemic and atherosclerotic LDLR$^{-/-}$ ApoB$^{100/100}$ mice were cross-bred with a mouse strain that overexpresses insulin-like growth factor II in pancreatic beta cells (IGF-II/LDLR$^{-/-}$ ApoB$^{100/100}$), giving the mice also characteristics of T2DM. These mice develop insulin resistance, hyperglycemia, and mild hyperinsulinemia, but have a similar lipid profile as LDLR$^{-/-}$ ApoB$^{100/100}$ mice. The mice develop atherosclerotic lesions throughout the aorta regardless of the diet but on HFD the lesions are more advanced and show increased calcification. (Heinonen et al. 2007.)

The above-mentioned mouse models were developed through germline genetic engineering but generating a model of atherosclerosis can also be achieved with different methods. Proprotein convertase subtilisin/kexin type 9 (PCSK9) is highly expressed in the liver where it binds LDLRs and directs them into lysosomes for degradation, thus reducing uptake of LDL from the circulation. By injecting recombinant adeno-associated virus (rAAV) encoding gain-of-function mutant form of PCSK9 intravenously into mice, they start to overexpress PCSK9 resulting in significant hypercholesterolemia when the mice are fed a HFD and the development of atherosclerotic lesions. The PCSK9-AAV model can also be induced in other

species making it a very convenient tool for atherosclerosis research. (Bjørklund et al. 2014; Roche-Molina et al. 2015.)

While these mouse models of atherosclerosis are of great use in atherosclerosis research, they are still lacking some characteristics that are common in human atherosclerosis, mainly vulnerable or ruptured plaques. Atherosclerotic lesions also predominantly form in the aorta, whereas in humans the carotid arteries are a common site for lesion development. (Bentzon & Falk 2010.) For this reason, $ApoE^{-/-}$ mice were crossbred with mice that have a heterozygous mutation (C1039G+/2) in the *fibrillin-1* (*Fbn1*) gene ($ApoE^{-/-}Fbn1^{C1039G+/-}$). When fed a HFD, $ApoE^{-/-}Fbn1^{C1039G+/-}$ mice develop extensive atherosclerotic lesions with increased size of the necrotic core, augmented T-cell infiltration and significant decrease in collagen and elastin content resulting in a thinner fibrous cap. There is also increased expression of inflammatory markers and matrix degrading enzymes in the lesions and neovascularization and intraplaque hemorrhage in the common carotid arteries and brachiocephalic artery. These mice exhibit plaque ruptures followed by signs of stroke, MI, and sudden death, making them a very useful model for human end-stage atherosclerosis. (Van Herck et al. 2009; Van der Donckt et al. 2015.) One of the more recent mouse models combines Nrf2 deficient mice with $LDLR^{-/-}ApoB^{100/100}$ mice ($Nrf2^{-/-}LDLR^{-/-}ApoB^{100/100}$). In this model, the phenotype differs between males and females as the female mice exhibit reduced lesion formation during ageing, whereas the males do not. Even though the lesion size is reduced, the size of the necrotic core is significantly increased at the age of 6 months and at 12 months, the lesions have extensive calcification. Fibrous cap thickness is also reduced, which further increases plaque instability. In male $Nrf2^{-/-}LDLR^{-/-}ApoB^{100/100}$ mice, plasma total cholesterol is lower than in $LDLR^{-/-}ApoB^{100/100}$ mice, whereas the females do not differ in this regard. However, Nrf2 deficient females have reduced plasma TG levels. Unlike other mouse models of atherosclerosis, this model develops atherosclerotic lesions in the coronary arteries, which can lead to MI and sudden death. (Ruotsalainen et al. 2019.)

There are a few novel mouse models that combine the atherosclerotic phenotype with either hypertension or the metabolic syndrome. A model that has atherosclerosis and hypertension was generated by combining the atherosclerotic $ApoE^{-/-}$ mouse model with the hypertensive NOS3 knockout mouse model ($ApoE^{-/-}NOS3^{-/-}$). The mice have higher total cholesterol and LDL levels than $ApoE^{-/-}$ mice on both chow and HFD and develop severe atherosclerotic lesions regardless of the diet. The mice also develop hypertension and hypertensive complications such as nephropathy and retinopathy. (Liu et al. 2022.) The model combines atherosclerosis, and the metabolic syndrome was generated by crossbreeding $ApoE^{-/-}$ mice with hypertensive BPH/2J Schlager mice (designated as BPHx). The mice develop hypertension regardless of the diet. When fed a HFD, the mice developed dyslipidemia characterized by elevated total cholesterol and TG levels and gained significantly more weight than $ApoE^{-/-}$ mice.

The mice become hyperglycemic with impaired glucose tolerance and insulin resistance and have increased plasma insulin levels. In addition, the mice exhibit an altered metabolic profile, which in part accounts for the increased weight gain. Atherosclerotic plaques develop in aortic sinuses with an increased amount of lipids and macrophages and a reduced amount of collagen, suggesting the plaques in this mouse model have a more unstable phenotype. (Dragoljevic et al. 2021.)

Table 1. Mouse models of spontaneous atherosclerosis.

Strain	Model	Characteristics	References
ApoE$^{-/-}$	Disruption of the *apoE* gene	Hypercholesterolemia, atherosclerotic lesion formation on chow diet	Piedrahita et al. 1992 Plump et al. 1992 Nakashima et al. 1994
ApoE3-Leiden	ApoE3-Leiden mutation via DNA fragment (ApoE3-Leiden, APOC1, liver-positive element)	Resembles familial dysbetalipoproteinemia, hyperlipoproteinemia, atherosclerotic lesion formation on HFD	van den Maagdenberg et al. 1993 Lutgens et al. 1999
CETP-ApoE3-Leiden	ApoE3-Leiden mutation, human CETP expression	Hypercholesterolemia with humanized lipoprotein profile, atherosclerotic lesion formation on HFD	Westerterp et al. 2006
LDLR$^{-/-}$	Disruption of the *ldlr* gene	Resembles FH, atherosclerotic lesion formation on HFD	Ishibashi et al. 1993; 1994
ApoE$^{-/-}$ LDLR$^{-/-}$	Disruption of the *apoE* and *ldlr* genes	More severe hypercholesterolemia and atherosclerotic lesion formation than its predecessors, intima-media thickening on chow diet	Bonthu et al. 1997 Witting et al. 1999
LDLR$^{-/-}$ ApoB$^{100/100}$	Disruption of the *ldlr* gene, expression of ApoB^{100} only	Resembles FH, atherosclerotic lesion formation on chow diet	Powell-Braxton et al. 1998 Hirano et al. 1996 Véniant et al. 1998
IGF-II/LDLR$^{-/-}$ ApoB$^{100/100}$	Expression of ApoB^{100} only, disruption of the *ldlr* gene, IGF-II overexpression	Resembles FH, atherosclerotic lesion formation on chow diet, insulin resistance, hyperglycemia, mild hyperinsulinemia	Heinonen et al. 2007
PCSK9-AAV	Recombinant adeno-associated virus-mediated gain-of-function mutation of *PCSK9* gene	Hypercholesterolemia, atherosclerotic lesion formation on HFD	Bjørklund et al. 2014 Roche-Molina et al. 2015
ApoE$^{-/-}$ Fbn1^{C1039G}	Disruption of the *apoE* gene, C1039G mutation in the *fibrillin-1* gene	Hypercholesterolemia, atherosclerotic lesion formation on HFD, spontaneous plaque rupture, intraplaque neovascularization and hemorrhage	Van Herck et al. 2009 Van der Donckt et al. 2015
Nrf2$^{-/-}$ LDLR$^{-/-}$ ApoB$^{100/100}$	Disruption of the *ldlr* and *Nrf2* genes	Resembles FH, female mice exhibit unstable lesions, coronary artery lesion formation, spontaneous MIs	Ruotsalainen et al. 2019
ApoE$^{-/-}$ NOS3$^{-/-}$	Disruption of the apoE and NOS3 genes	Hypercholesterolemia, hypertension, atherosclerotic lesion formation on chow diet	Liu et al. 2022
BPHx	Disruption of the *apoE* gene, BPH/2 (hypertensive strain developed by selective breeding)	Metabolic disorder, hypertension, dyslipidemia, and unstable atherosclerotic lesion formation on HFD	Dragoljevic et al. 2021

2.1.3.2 Mechanically induced mouse models of vascular injury

In addition to spontaneous mouse models of atherosclerosis there are also mechanically induced models that are utilized to study vascular injury resulting from post-angioplasty complications. A mouse model that resembles balloon-angioplasty is generated by inserting a straight spring wire into the femoral vein for 1 min causing denudation and dilatation of the artery. This results in medial cell apoptosis and neointimal hyperplasia composed of VSMCs. (Sata et al. 2000.) Another similar mouse model was produced by passing a 0.25 mm angioplasty guidewire 1-3 times in the femoral artery causing endoluminal injury which led to substantial intimal hyperplasia consisting mostly of VSMCs. The injury also resulted in the expression of adhesion molecules P-selectin, ICAM-1 and VCAM-1 on the luminal surface and rapid accumulation of neutrophils which were later replaced by macrophages. (Roque et al. 2000.) A more recent model of intensive vascular injury was produced by inserting a guide wire into the femoral artery, where it was left for 1 min and then retracted by twisting it to expand and damage the endothelium. The insertion and retraction were repeated ten more times causing breakdown of elastic lamina and neointimal hyperplasia consisting of α-SMA-positive cells, ECs, and adventitia lineage cells. (Nomura-Kitabayashi & Kovacic 2018.)

Photochemically and laser induced vascular injuries can also be used to cause hemostasis and thrombosis. Photochemically induced injuries involve the use of a specific photosensitizer such as hematoporphyrin or Evan's blue in conjunction with a low-powered laser. The laser stimulation of the dyes induces production of free radicals, which cause oxidative damage to the vascular endothelium. Laser induced injury is performed by using a high-powered laser which is focused on a small specific area of the vessel. The laser rapidly heats the tissue resulting in rupture of cells and tissue structures which can lead to a platelet and coagulation response. The extent of the injuries can vary from endothelial denudation to perforating injury to the vessel wall followed by bleeding, depending on the laser as well as biological parameters. (Stalker 2020.)

2.1.3.3 Other animal models of atherosclerosis

Even though mice are convenient in atherosclerosis research, larger animals like rabbits, pigs and non-human primates are better for *in vivo* imaging. Producing and maintaining these larger animal models is costly and time consuming and the disease course is much slower than in mice. The models can be both genetically engineered or mechanically induced by causing physical damage to the vessel or blocking it for example by balloon denudation or cuffing or using bottleneck stents (Abarbanell et al. 2010).

The Watanabe-heritable hyperlipidemic rabbits have a defect in the LDLR, which causes them to spontaneously develop hypercholesterolemia, atherosclerosis and tendon xanthoma, all resembling human familial hypercholesterolemia. Watanabe rabbits exhibit a wide range of atherosclerotic lesions from fatty streaks to advanced lesions and can also develop coronary atherosclerosis and MI. (Fan et al. 2015.) Other rabbit models of atherosclerosis include the cholesterol fed New Zealand White rabbit and ApoE knockout rabbits (Emini et al. 2017).

2.2 Type 2 diabetes

T2DM affects millions of people, and its prevalence has increased rapidly throughout the years. T2DM accounts for ∼90% of diabetes worldwide and is characterized by insulin resistance and hyperinsulinemia, which lead to impaired metabolism of glucose, lipids and proteins and is often accompanied by obesity and metabolic syndrome. Worryingly, the occurrence in children and adolescents is rising, and depending on the population, T2DM can account for 8–45% of all new cases of diabetes. T2DM can be found incidentally, but it is often undiagnosed until development of complications. (Baynest 2015; Bhori et al. 2022.) T2DM patients have a 2–4-fold increased risk of coronary artery disease and the most common cause of death among T2DM patients is cardiovascular complications (Beckman et al. 2002). A recent study reported an association between early onset of T2DM and shorter life expectancy, highlighting the importance of prevention or delaying the onset of the disease (Emerging Risk Factors Collaboration 2023). While T2DM is strongly associated with obesity and lack of physical activity, there are also several genes that have been found to predispose to T2DM and one of the most studied is polymorphism in the gene coding for leptin receptors, which has shown strong association with T2DM (Su et al. 2016; Yang. et al. 2016; Bhori et al. 2022; Zeng et al. 2022).

2.2.1 Atherosclerosis and type 2 diabetes

Endothelial dysfunction and development of atherosclerosis

The altered metabolic state in T2DM including hyperglycemia, dyslipidemia and insulin resistance cause arterial dysfunction and render arteries susceptible to the development of atherosclerosis. A single layer of endothelial cells that line the inner surface of blood vessels plays an important role in regulation of blood vessel structure, and function. Prolonged periods of hyperglycemia can trigger endothelial dysfunction by inhibiting the production of NO thus impairing vasodilation and increasing the production of ROS causing oxidative stress. Hyperglycemia causes

vascular damage also by enhancing intracellular production of advanced glycation end products (AGEs) and their receptors, AGE receptors (RAGE), which are expressed by several different cells including monocytes and macrophages. AGEs accumulate in diabetic tissues with the help of cross-links and generate ROS. AGEs increase production of superoxide, promoting vascular inflammation, they induce decreased expression of endothelial NO synthase (eNOS), decreased NO synthesis and increased expression of endothelin-1 (ET-1), the most potent endothelial-derived vasoconstrictor that also causes hypertension and smooth muscle proliferation. (Schmidt et al. 1993; Hopfner & Gopalakrishnan 1999; Kaur et al. 2018.) Activation of RAGE can also cause inflammatory cells to release high mobility group-box 1 and S100/calgranulins, further increasing the inflammatory response (Yan et al. 2009). Endothelial dysfunction is further propagated by insulin resistance via the two major pathways involved in insulin signaling. Phosphatidylinositol-3-kinase pathway is impaired causing decreased production of NO and mitogen activated protein kinase dependent pathway is activated leading to increased production of ET-1. (Kaur et al. 2018.) Insulin resistance also stimulates proliferation of VSMCs, an excessive release of free fatty acids (FFA), which increase production of ROS through protein kinase C dependent activation of NADPH oxidase and contribute to the pro-atherogenic lipid profile and dyslipidemia. (Inoguchi et al. 2000; Beckman et al. 2002; Kaur et al. 2018.) The combined effects of decreased production of NO, increased production of ROS and activation of RAGEs increase the activation of redox-sensitive transcription factors such as nuclear factor kappa B (NF-κB) and activator protein 1 (AP-1). NF-κB and AP-1 induce transcription of several genes involved in atherogenesis including VCAM-1, pro-coagulant tissue factor and ET-1. (Rösen et al. 2001.) They've also been found to increase expression of genes involved in monocyte chemotaxis like MCP-1 and M-CSF (Schmidt & Stern 2000). Finally, the development of rupture prone atherosclerotic lesions may be promoted in diabetic conditions, caused by increased production of MMPs, especially MMP-9, which take part in collagen degradation (Uemura et al. 2001).

Dyslipidemia

Dyslipidemia in T2DM is related to insulin resistance and can occur even before overt diabetes develops. The most common changes in the lipid profile in diabetic dyslipidemia are hypertriglyceridemia, which can result from either overproduction of TGs or lack of clearance, increased amount of VLDL which is related to the levels of TG, overproduction of small dense LDL particles due to increased supply of glucose and FFAs and lowered HDL levels due to increased clearance. (De Man et al. 1996; Guérin et al. 2001; Borén et al. 2022.) Elevated fasting and postprandial plasma FFA levels have been found in individuals who are obese, insulin resistant

or have T2DM (Laws et al. 1997). Insulin is known to suppress the hormone sensitive lipase (HSL), which is responsible for lipolysis in the adipose tissue. Since FFA levels are elevated in T2DM it has been speculated that also HSL becomes resistant to the effects of insulin and thus the rate of lipolysis is increased. However, several studies have reported that activity of HSL remains unchanged in obese and T2DM individuals. One possible factor increasing the FFA levels is leptin, which increases lipolysis and is known to counteract the antilipolytic effects of insulin. As the expression of leptin is often increased in obese individuals, it might in part explain the increase in circulating FFA levels. (Duncan et al. 2007.) FFAs are used in the liver to synthesize VLDL particles, which are the predominant TG containing lipoproteins. In normal weight individuals, insulin inhibits the production of VLDLs, but in the case of obesity and insulin resistance, the inhibitory effects of insulin are lost and the production of VLDLs remains high. (Lewis et al. 1993.) Another factor affecting the levels of VLDL is lipoprotein lipase (LPL), an enzyme that catalyzes hydrolysis of TGs in the blood. Insulin is known to induce LPL and in the case of insulin resistance, the activity of LPL is reduced, resulting in decreased clearance of VLDL. (Miyashita et al 2002.) CETP transfers CEs from HDL to LDL and $VLDL_1$, which is the precursor of small dense LDLs, and the transfer rate is increased with increased plasma levels of TGs. In return, LDL and $VLDL_1$ give a TG molecule to HDL, making it less protective and increasing its clearance. (Guérin et al. 2001.) Small dense LDL is very atherogenic due to its small size which makes it easy to penetrate the endothelium and enter the intima where it binds to glycosaminoglycans and gets phagocytosed by macrophages, promoting lesion formation (Qiao et al. 2022). Elevated levels of small dense LDL have been shown to associate with the progression of intima media thickening and MI and to increase the risk and severity of cardiovascular disease (CVD). It can also be used to predict future cardiovascular events. (Ikezaki et al. 2000; Duran et al. 2020; Huang et al. 2021.) TGs and TG-rich lipoproteins and their remnants direct role in atherogenesis is debatable, but they are thought to excert proinflammatory effects as well as contribute to plaque formation and progression (Ginsberg et al. 2021).

Thrombus formation

Platelets modulate vascular function and take part in thrombus formation. When the endothelium in disrupted or an atherosclerotic plaque is ruptured, platelets activate and adhere to the damaged area. (Badimon & Vilahur 2014.) In diabetics, platelet activation is increased due to changes in their calcium regulation, and increased surface expression of glycoprotein Ib (GpIb) and GpIIb/IIIa, both of which mediate platelet aggregation (Vinik et al. 2001). Thrombus formation is further exacerbated by abnormal coagulation resulting from impaired fibrinolytic capacity, increased

expression of tissue factor and other coagulation factors such as Factor 1 (fibrinogen) and von Willebrand factor and inversely decreased expression of anticoagulant factors such as antithrombin III (ATIII) and protein C, although there are also several reports of increased ATIII levels in diabetics (Carr 2001).

Plaque calcification

As mentioned in Chapter 2.1.1, plaque calcification is a common finding in diabetic patients with atherosclerosis and they can develop both intimal and medial calcifications. Vascular calcification can be broadly divided into three types: inflammatory, metabolic, and genetic, and the types can occur separately or overlap, even at the same site. Inflammatory and metabolic calcification are common in atherosclerosis and diabetes, respectively. Inflammatory calcification forms in intimal areas through osteogenesis and chondrogenesis and the formation is mediated by oxLDL, cytokines and MMPs, all of which are found in atherosclerotic lesions. (Demer & Tintut 2014.) A recent study reported that systemic arterial inflammation is related to future systemic arterial microcalcification after a five year follow up in early T2DM patients (Reijrink et al. 2022). Later it was revealed that microcalcification is significantly increased in T2DM patients with preserved kidney function and severe albuminuria. However, in patients with severely decreased glomerular filtration rate, macrocalcification is increased. (Reijrink et al. 2023.)

Calcification causes arterial stiffness and can make the plaques more vulnerable to rupture, although it has been suggested that the reduced thickness of the fibrous cap rather than calcification is more likely to contribute to increased plaque vulnerability in T2DM patients (Milzi et al. 2017). Contrary to inflammatory calcification, metabolic calcification forms in medial areas through nucleation and osteogenesis. The calcification is mediated by several factors including elastin, AGE and RAGE, and proteases and causes arterial stiffness. Several circulating factors like lipids, phosphate and glucose can also mediate the calcification process. (Demer & Tintut 2014.) There is extensive research on how diabetes can accelerate the calcification process and what mechanisms it involves. *In vivo, in vitro,* and clinical studies have indicated that regulatory glycoproteins osteoprotegrin, receptor activator of nuclear factor kappa-B ligand and TNF-related apoptosis-inducing ligand, which are normally associated with bone remodeling, have a fundamental relevance in vascular calcification (Harper et al. 2016). In hyperglycemic conditions, decreased expression of sirtuin 1 can lead to increased DNA-damage due to insufficient activation of DNA repair, accelerating calcification (Bartoli-Leonard et al. 2021). The vascular calcifications can also translocate according to a recent study where the researchers found that macrophage galectin-3, which is a soluble β-galactoside-binding lectin that is involved in the regulation of cell proliferation,

differentiation, and homing, can regulate the migration of VSMC-derived extracellular vesicles and mediate translocation of calcifications to the intima (Sun et al. 2020).

2.2.2 Glucagon-like peptide-1

Gastric inhibitory polypeptide (GIP) and glucagon-like peptide-1 (GLP-1) are gut derived incretins that are responsible for up to 70% of the postprandial insulin secretion in healthy subjects. In T2DM patients, the incretin effect is either greatly reduced or absent, due to the loss of GIP action and decreased secretion of GLP-1. This affects the patient's ability to adjust secretion of insulin and glucagon according to need and thus contributes to the development of hyperglycemia.

GLP-1 is secreted from L-cells in the distal small intestine and large intestine, and it directly stimulates insulin secretion from pancreatic β-cells and indirectly inhibits glucagon secretion from α-cells, by binding to its G-protein coupled receptors (GLP-1R). In addition to the pancreas, GLP-1R is expressed in the lung, brain, kidney, stomach, heart, adipose tissue, and enteric and peripheral nervous system. The glucose lowering effect of GLP-1 is a combination of islet cell regulation and inhibition of gastric emptying. Its effect on the brain also increases satiety, which can lead to decreased food intake and weight loss. (Müller et al. 2019; Tan et al. 2020.) A recent study also revealed that GLP-1R is expressed in macrophages and that it can potentially regulate macrophage polarization towards M2 (Yang et al. 2021). Expression of GLP-1R protein in the heart of humans and monkeys is localized in myocytes in the sinoatrial node, although its mRNA transcripts have been detected in all four chambers of the heart (Pyke et al. 2014; Baggio et al. 2018). Activation of GLP-1Rs has also been shown to improve cardiomyocyte survival and cardiac function after MI (Noyan-Ashraf et al. 2009).

There are studies reporting expression of GLP-1R in the vasculature, but the results have been varying. Baggio et al. found no GLP-1R expression in cardiac fibroblasts, human coronary artery ECs or VSMCs (Baggio et al. 2018), whereas Koska et al. found direct effects of GLP-1R agonist (GLP-1RA) on cultured human aortic ECs (Koska et al. 2015). In preclinical studies, GLP-1R protein has been found in mouse aorta and in the arteries and arterioles of the heart, kidney, pancreas, and intestines, and also in aortas of rats, and the expression co-localizes with VSMCs (Green et al. 2008; Richards et al. 2014; Zhang et al. 2020). However, little is still known about the expression pattern of GLP-1R in the vasculature.

Native GLP-1 has a very short plasma half-life, which varies from two to three minutes depending on the species and is caused by rapid degradation by the enzyme dipeptidyl peptidase-4 (DPP-4). Due to GLP-1's short half-life, it only has limited

pharmacological availability, and it is estimated that only 10–15% of active GLP-1 ever reaches the systemic circulation. (Tan et al. 2020.)

2.2.3 GLP-1 therapy

The effect of GLP-1 on blood glucose levels is pronounced, as research has shown that exogenous administration of GLP-1 can help restore blood glucose levels close to normal in T2DM patients (Holst et al. 2009). Indeed, GLP-1 based therapies have been of great interest during the last decade and the effects on both glycemic control and atherosclerosis have been thoroughly studied.

GLP-1R agonists

Exenatide was the first approved GLP-1R agonist (GLP-1RA) for the treatment of T2DM and was administered twice a day due to its short half-life. Since then, improvements have been made to increase the half-life of GLP-1RAs, which have to be administered once daily or even once a week. Liraglutide was approved in 2009 and semaglutide in 2017 and their amino acid sequence is almost identical to mammalian GLP-1. (Nauck et al. 2021.)

GLP1-RAs have demonstrated many cardiovascular benefits in both preclinical and clinical settings. Liraglutide improved endothelial dysfunction by enhancing acetylcholine-induced vasodilation, reduced expression of ox-LDL receptor-1 (LOX-1) in the aorta and decreased circulatory levels of inflammatory and oxidative stress markers including superoxide dismutase, IL-1β and IL-6 in $LDLR^{-/-}$ mice (Ying et al. 2023). Liraglutide and semaglutide both reduced major adverse cardiovascular (CV) events in diabetic individuals (Verma et al. 2022) and attenuated lesion development in $ApoE^{-/-}$ and $LDLR^{-/-}$ mice (Rakipovski et al. 2018). Albiglutide and dulaglutide are similar to liraglutide and semaglutide and were approved in 2014 (Nauck et al. 2021). In T2DM patients, albiglutide (Hernandez et al. 2018) and dulaglutide (Gerstein et al. 2019) both reduced the risk for major adverse CV events and dulaglutide also prevented heart failure and metabolic remodeling in diabetic cardiomyopathy in T2DM mice (Xie et al. 2022). However, GLP1-RAs have shown no beneficial effects on heart failure related events in clinical studies (Pfeffer et al. 2015; Holman et al. 2017; Ferreira et al. 2020).

DPP-4 inhibitors

In addition to degrading GLP-1 and GIP, DPP-4 has a variety of other substrates including cytokines, chemokines, neuropeptides, and growth factors, and its expression and activity are altered in many pathophysiological conditions like

diabetes. Since GLP-1 has a very short half-life due to degradation by DPP-4, several different DPP-4 inhibitors have been developed, many of which have also shown positive effects on cardiovascular health. The inhibitors similarly lower blood glucose, but there are some differences in the effectiveness, half-life, and metabolism. Sitagliptin was the first approved DPP-4 inhibitor in 2006. (Bae 2016.) In T2DM patients, sitagliptin attenuated the progression of coronary (Li et al. 2020) and carotid (Mita et al. 2017) atherosclerosis. In mice it has been shown to attenuate VSMC apoptosis and reduce atherosclerotic lesion formation (Li et al. 2021). Vildagliptin and alogliptin treatment have both shown significant improvements in several cardiovascular aspects, including attenuation of endothelial dysfunction and atherogenesis in ApoE$^{-/-}$ mice (Aini et al. 2019), inhibition of VMSC proliferation and reduction of stenosis of injured carotid artery of db/db mice (Ji et al. 2019), attenuation of carotid intima-media thickness progression in T2DM individuals (Mita et al. 2016) and reduction of atherosclerotic lesion size in diabetic ApoE$^{-/-}$ mice (Ta et al. 2011). Linagliptin has also shown some positive effects on cardiovascular health. Linagliptin treatment increased acetylcholine-induced vascular relaxation of isolated arteries of Zucker diabetic rats (Takai et al. 2014) and decreased aortic pulse wave velocity (a surrogate marker for arterial stiffness and early atherosclerosis) in a randomized, double-blind, controlled trial (de Boer et al. 2017). However, studies on the effects of linagliptin treatment on endothelial dysfunction have reported varying results. In ApoE$^{-/-}$ mice, linagliptin ameliorated endothelial dysfunction and decreased the development of atherosclerotic lesions (Salim et al. 2016), whereas in a randomized, placebo-controlled, double-blind trial, linagliptin had no effect on endothelial dysfunction determined by measuring flow-mediated dilatation of the brachial artery (Tripolt et al. 2018). In Watanabe rabbits, linagliptin treatment both inhibited atherosclerotic plaque growth and stabilized the plaques (Kurosawa et al. 2021). In ApoE$^{-/-}$ mice it decreased lesion size and increased M2 macrophage polarization (Nishida et al. 2020). The cardiovascular and renal microvascular outcome study with linagliptin (CARMELINA) found no effect on the risk of hospitalization for heart failure or other heart failure-related outcomes (McGuire et al. 2019). DPP-4 inhibitors as well as GLP1-RAs have also been shown to improve lipid profiles by decreasing plasma TG, LDL, and total cholesterol and ApoB48 levels (Piccirillo et al. 2023; Ussher & Drucker 2023).

2.3 Imaging of atherosclerosis

In vivo imaging of atherosclerosis provides a way to diagnose and monitor disease progression and serves as a valuable tool in atherosclerosis research. *In vivo* imaging can be divided into two categories: anatomical imaging and molecular imaging. Anatomical imaging provides visualization of the lesions whereas molecular

imaging provides information of the biological processes in the lesions. Molecular imaging is usually conducted together with anatomical imaging to gain information on both size, location, and molecular activity of the lesions.

2.3.1 Anatomical imaging

Invasive angiography is the most used anatomical imaging technique and is thought of as the "golden standard" of anatomic atherosclerosis imaging. Angiography is based on radio-opaque iodinated contrast agent that is injected intra-arterially and visualized under x-ray fluoroscopy. It provides excellent spatial (0.1–0.2 mm) and temporal (10 ms) resolution and information of possible obstructions in the vasculature and possibility for percutaneous coronary intervention, making it a convenient and cost-effective method for assessment of atherosclerotic cardiovascular disease. However, due to its invasiveness, low diagnostic yield and radiation burden, non-invasive methods should be considered first. (Tarkin et al. 2016; Hajhosseiny et al. 2020.)

X-ray computed tomographic (CT) angiography is a non-invasive imaging method that can be used to visualize both vessel lumen and vessel wall and detect atherosclerotic plaques. It can also differentiate between calcified and non-calcified lesions and be used in assessing the amount of non-calcified and calcified atherosclerotic plaque (calcium scoring). In addition to large arteries, it has become possible to do CT angiography of coronary arteries (coronary CT angiography). CT angiography is based on a rotating x-ray source and multiple parallel detector rings from which the data can be reconstructed into multidimensional images. Intravenous iodinated contrast agent is used to visualize the vasculature in CT angiography. Its spatial resolution is about 0.5-0.6 mm, and the negative predictive value is high. CT angiography can also be combined with functional imaging techniques, such as myocardial perfusion imaging to assess myocardial blood flow. Its disadvantages are radiation burden, the need for high contrast agent volumes increasing the risk for contrast agent induced nephropathy. Furthermore, it provides limited insight on the functional significance of stenosis. (Tarkin et al. 2016; Kolossváry et al. 2017; Antoniades & West 2021.)

Unlike invasive angiography and CT angiography that utilize x-rays, magnetic resonance imaging (MRI) is based on using a strong magnetic field that aligns hydrogen atoms found in water with the magnetic field. High-frequency pulses are applied that excite the atoms, which spin and change their polarization. After the pulses, the atoms return to their original state, aligned with the magnetic field and this relaxation can be detected to form an image. MRI can be used to assess plaque size and allows detailed assessment of plaque composition including fibrosis, calcification and, intraplaque hemorrhage in the aorta, carotid, coronary and

peripheral arteries with the help of gadolinium-based contrast agents. The limitations of MR imaging include limited temporal resolution, which can hamper imaging of coronary arteries due to the rapid movement, a lack of generally accepted imaging protocols and high costs. (Corti & Fuster 2011.)

Ultrasound can also be used to image vasculature, though due to its low tissue penetration, its use is limited to superficial vessels like the carotid arteries. It's based on high frequency sound waves that are reflected when they come into contact with tissues containing different acoustic properties. Ultrasound can be used to measure intima-media thickness (IMT) of the carotid arteries, but it also gives information about plaque size and composition. Transesophageal ultrasound can be used to image atherosclerosis in the thoracic aorta. (Gallino et al. 2012.)

2.3.2 Positron emission tomography imaging

Positron emission tomography (PET) imaging utilizes intravenously injected or inhaled radiotracers that are comprised of small molecules as probes, which are labelled with short lived positron emitting radionuclides. The radioactive nuclide decays and emits a positron, which annihilates with a nearby electron and creates two 511-keV gamma photons that are emitted in opposite directions. The photons from these coincidences are simultaneously detected by the PET scanners detector rings, and an image of the radiotracer distribution can then be reconstructed. (Turkington 2001.) PET imaging has been investigated as a tool to image atherosclerosis due to the wide variety of tracers already available and good possibilities for developing new ones. The spatial resolution of PET scanners (clinical scanners ~ 3–6 mm, pre-clinical scanners ~ 1–2 mm) and their sensitivity are high (as compared to other nuclear imaging techniques), and the use of radiotracers allows imaging of specific biological processes in atherogenesis. Since PET imaging doesn't provide detailed structural or anatomical information, it is commonly used in combination with either CT or MRI with contrast enhancement, to provide anatomical reference. (Meester et al. 2019; Fan et al. 2020; Prenosil et al. 2021.)

2.3.2.1 ^{18}F-FDG

2-deoxy-2-[18F]fluoro-D-glucose (^{18}F-FDG) is a glucose analog that is the most common PET tracer for inflammation imaging. ^{18}F-FDG is readily taken up by metabolically active cells including macrophages. Cells take up ^{18}F-FDG via glucose transporters (GLUT) 1 and 3 and inside the cells it is phosphorylated by the hexokinase enzyme to produce ^{18}F-FDG-6-phosphate which cannot be further metabolized and is thus trapped inside the cells. Uptake of ^{18}F-FDG directly reflects

the rate of glucose utilization of the cells. (Sriranjan et al. 2021.) In 2002, ^{18}F-FDG was first established at PET-imaging of atherosclerosis when it was shown to accumulate in symptomatic carotid artery lesions and *ex vivo* autoradiography of excised lesions with tritiated deoxyglucose (an *in vitro* analogue of ^{18}F-FDG) showed that the accumulation co-localized with macrophages (Rudd et al. 2002). ^{18}F-FDG uptake in macrophage-rich atherosclerotic lesions has since been shown in other patient studies (Rudd et al. 2009; Johnsrud et al. 2019) and in several animal models of atherosclerosis (Hyafil et al. 2009; Wenning et al. 2014; Toner et al. 2022). It has also been shown that uptake of ^{18}F-FDG is lower in calcified lesions (Rudd et al. 2009; Masteling et al. 2011), however some nonspecific binding to calcifications has also been observed (Laitinen et al. 2006). The uptake of ^{18}F-FDG can also be influenced by several other factors than inflammatory stimuli. Hypoxia causes changes in the rate of glycolysis and expression of hypoxia-inducible factor 1 α (HIF-1α), which in turn leads to increased uptake of ^{18}F-FDG (Folco et al. 2011; Pedersen et al. 2013). The clear mechanism how glucose uptake is increased under hypoxic conditions is still unclear, however an increase in the expression of glucose transporter gene *Slc2a1* in response to chronic hypoxia has been reported (Midha et al. 2023). Another study has shown that oxLDL can lead to increased uptake of ^{18}F-FDG via NADPH oxidase 2 induced production of ROS which promotes upregulation of HIF-1α. The increased rate of glycolysis and uptake of ^{18}F-FDG are caused by upregulation of GLUT1 and hexokinase. (Lee et al. 2014.) Studies performed in oncologic patients have demonstrated that arterial ^{18}F-FDG-PET/CT can be possibly used as an indicator for future cardiovascular events (Figueroa et al. 2013; Paulmier et al. 2008). Patient and animal studies involving therapeutic interventions have shown that ^{18}F-FDG-PET/CT is useful in identifying active plaques and treatment monitoring (Kim et al. 2020; Jarr et al. 2020; Tawakol et al. 2013). There are several advantages in ^{18}F-FDG-PET/CT imaging of atherosclerosis including reproducibility and sensitivity, however it also has its limitations. ^{18}F-FDG is not specific to macrophages, but also other metabolically active cells take up ^{18}F-FDG, for example cardiac myocytes. This together with motion artifacts has limited imaging of coronary arteries. Fasting or dietary preparation, which lower glucose metabolism in the myocardium (but not macrophages) may help, but ultimately ^{18}F-FDG imaging of the coronary arteries is challenging. (Blomberg & Høilund-Carlsen 2015.)

2.3.2.2 GLP-1R targeting tracers

GLP-1R are expressed in several different organs but the level of expression and density of the receptors is quite scarce in many of the tissues. Nevertheless, GLP-1Rs have been of great interest as an imaging target. GLP-1R targeting tracers are

mostly based on exendin-4 which is a GLP-1 analog that readily binds to GLP-1R and is resistant to DPP-4 degradation. It has a plasma half-life of 2.4 h, and the plasma concentration remains high for up to 4–8 h after a subcutaneous injection. (Meier 2012.) Exendin-4 can easily be modified for tracer production and labeled with different radionuclides such as ^{68}Ga, ^{18}F and ^{64}Cu. GLP-1R targeting tracers have been of great interest because they enable *in vivo* imaging and quantification of pancreatic β-cell mass (Mikkola et al. 2013; Selvaraju et al. 2013; Bandara et al. 2016) as well as imaging malignant changes in the pancreas, such as insulinomas (Wild et al. 2011; Kiesewetter et al. 2012; Kalff et al. 2021). A major drawback of exendin-4 based tracers is high kidney uptake, but modification of the tracer, for example by adding an albumin- binding moiety has been shown to effectively decrease renal retention of the tracer (Kaeppeli et al. 2019). It is also important to note that exendin-4 can exacerbate hypoglycemia and a glucose infusion during imaging may be needed to maintain the blood glucose levels (Christ et al. 2009). Exendin-4 based imaging has not been commonly used in cardiovascular imaging but interestingly, ^{18}F-AlF-NOTA-MAL-Cys40-Exendin-4 has been successfully utilized in imaging MI and reperfusion, (Pan et al. 2019) and ^{68}Ga-NODAGA-Exendin-4 imaging the healing phase of MI (Ståhle et al. 2020) where GLP-1R expression is upregulated in the infarcted area. There is no knowledge yet on whether GLP-1R targeting tracers could be useful in imaging atherosclerotic inflammation until the studies included in this thesis.

2.3.2.3 Glutamine metabolism targeting tracers

Glutamine is an abundant and versatile amino acid, and it has a fundamental role in metabolism, interorgan nitrogen exchange and pH homeostasis and it can be utilized in many biosynthetic pathways including nucleotide synthesis. Immune cells readily use glutamine to fuel their function in catabolic conditions like during high intensity exercise and glutamine supplementation is routinely used to restore immune function. (Cruzat et al. 2018.) Glutamine-based tracers such as 4-^{18}F-fluoroglutamine (4-[^{18}F]F-GLN), ^{18}F(2 S,4 R)4-fluoroglutamine and l-[5-^{11}C]-glutamine have all proven useful in PET-imaging of different cancers since cancer cells readily use glutamine as a nutrient for cellular growth and proliferation and many aggressive cancers adapt to using glutaminolysis (a process where glutamine is converted into α-ketoglutarate) as their metabolic pathway (Schulte et al. 2017; Zhou et al. 2017; Cohen et al. 2022). Glutamine-based tracers may be especially useful in imaging brain tumors like gliomas and neuroblastomas, since uptake of glutamine is low in healthy brain and uptake in cancer cells is high, providing a good target-to-background ratio (TBR) (Venneti et al. 2015; Li et al. 2019). Glutamine-based tracers have also successfully been used to image bacterial infections caused

by Escherichia coli (E. coli) and methicillin-resistant Staphylococcus aureus (Renick et al. 2021) and invasive fungal infections (Co et al. 2022). Even though glutamine is readily used by immune cells, there is lack of information on how glutamine metabolism targeting tracers work in imaging inflammatory conditions such as atherosclerosis.

2.3.2.4 Folate receptor targeting tracers

Folic acid is essential for the biosynthesis of many compounds including nucleic acids and amino acids, and it binds to reduced folate carrier, and folate receptors (FR). After binding to FR, the complex gets internalized into the cytoplasm. There are three different types of FRs: FR-α, which is expressed in epithelial and cancer cells, FR-β, which is expressed in several different tissues, and FR-γ/γ′, which is only expressed in hematopoietic cells. A fourth type, FR-δ, has also been identified but the expression or function of the receptor has not been established. (Spiegelstein et al. 2000; Elnakat & Ratnam 2019.) FR-β is highly expressed on activated macrophages, presenting an interesting target for folate-based imaging of inflammation (Nakashima-Matsushita et al. 1999; Steintz et al. 2022). FR-β targeting tracer ^{18}F-fluoro-PEG-folate has proven useful in PET/CT imaging of rheumatoid arthritis in both preclinical (Gent et al. 2013) and clinical settings (Verweij et al. 2020), whereas folate-PEG_{12}-NOTA-Al^{18}F, ^{68}Ga and ^{64}Cu labeled NODAGA-folate have shown promising results in PET/CT imaging of tumors (Farkas et al. 2016; Chen et al. 2017). Different FR-β targeting tracers have also been developed and evaluated for imaging atherosclerosis. *In vitro* study using endarterectomized human carotid arteries showed that 3′-aza-2′-^{18}F-fluorofolic acid binds FR-β expressing macrophage-rich plaques (Müller et al. 2014). Single-photon emission computed tomography studies with different FR-β targeting tracers, have also shown specific uptake in plaques where it co-localizes with macrophages (Ayala-López et al. 2010; Jager et al. 2014; Winkel et al. 2014). However, it is not known how FR targeting tracers work in *in vivo* PET/CT-imaging and whether it would give sufficient TBR for the detection of atherosclerotic inflammation.

2.3.2.5 Other tracers targeting macrophages

Somatostatin receptor targeting tracers

Somatostatin receptors are G-protein coupled transmembrane receptors that are highly expressed in neuroendocrine tumors and activated macrophages (Sriranjan et al. 2019). Activated human macrophages express SST_1R and SST_2R so they present an interesting target for tracer development (Armani et al. 2007). ^{68}Ga-DOTATATE

uptake in atherosclerotic plaques co-localizes with macrophages expressing SST_2R in $ApoE^{-/-}$ mice (Li et al. 2013). Clinical studies have shown that ^{68}Ga-DOTATATE-PET enables detection of coronary atherosclerosis (Tarkin et al. 2017) and uptake of the tracer is associated with coronary artery calcification and other known risk factors of CVD (Li et al. 2012). Another study using ^{64}Cu-DOTATATE showed tracer accumulation in atherosclerotic lesions in asymptomatic carotid arteries and the uptake correlated with macrophage biomarkers CD68 (macrophage load) and CD163 (macrophage activation) (Pedersen et al. 2015). A comparative study with ^{68}Ga-DOTANOC, ^{18}F-FDR-NOC, and ^{68}Ga-DOTATATE demonstrated that both ^{68}Ga-DOTANOC and ^{68}Ga-DOTATATE but not ^{18}F-FDR-NOC, show tracer uptake in macrophage-rich plaque, but ^{68}Ga-DOTANOC performed better *in vivo*, showing better aortic uptake and aorta-to-blood-ratio in mice (Rinne et al. 2016).

Translocator protein targeting tracers

18-kDa translocator protein (TSPO) is a membrane-bound protein, which is primarily situated in mitochondrial membranes and has many cellular functions such as regulation of cholesterol translocation. TSPO is expressed in peripheral tissues and the expression is known to be increased in neuroinflammatory conditions, different cancers and also in Schwann cells and activated macrophages. (Scarf & Kassiou 2011.) TSPO-targeting tracers such as ^{11}C-PK11195 are commonly used in PET/CT imaging of neuroinflammatory diseases (Cagnin et al. 2002), but it has also proven useful in imaging vascular inflammation (Pugliese et al. 2010) and mitochondrial disease (van den Ameele et al. 2021). ^{11}C-PK11195 use in PET/CT imaging of atherosclerosis has also been studied in both preclinical (Laitinen et al. 2009) and clinical (Gaemperli et al. 2012) settings where it showed more uptake in inflamed plaques compared to non-inflamed plaques, however uptake of the tracer was also prominent in other parts of the vessel wall and the TBR was low. Indeed, cultured human macrophages express TSPO 20 times more than other cell types in plaques and *in vitro* incubation of endarterectomized human carotid artery sections with TSPO targeting tracers has shown clear uptake in atherosclerotic plaques, which co-localized with TSPO expressing macrophages (Bird et al. 2010). More recently, ^{18}F-labelled TSPO tracers such as ^{18}F-GE387 have been developed with the advantage of longer physical half-lives and potentially better TBR, though the genetic polymorphism in human TSPO (rs6971) can cause changes in the affinity of the tracer (Qiao et al. 2019). ^{18}F-GE-180 and ^{18}F-FEMPA have shown specific uptake in inflamed atherosclerotic plaques however the uptake of either of the tracers did not differ from the uptake in healthy vessel wall (Hellberg et al. 2016; Hellberg et al. 2017a). A preclinical study with $ApoE^{-/-}$ mice showed a 3-fold higher *in vivo* uptake of TSPO tracer ^{18}F-PBR111 in atherosclerotic aortas than healthy controls

and the uptake co-localized with monocyte-derived macrophage marker (CD11b) and TSPO positive macrophages (Kopecky et al. 2019).

Mannose receptor targeting tracers

Mannose receptor belongs to the C-type lectin family. It is mostly expressed in macrophages, immature DCs and ECs and the expression can vary depending on external stimuli such as cytokines. (van der Zande et al. 2019.) MR targeting tracers have been studied in cancer imaging and more specifically, targeting tumor-associated macrophages that are known to promote cancer growth (Blykers et al. 2015; Jiang et al. 2017; Gao et al. 2019). Research has also been carried out on MR targeting tracers for imaging atherosclerosis. 2-deoxy-2-^{18}F-fluoro-D-mannose (Tahara et al. 2014), ^{111}In-tilmanocept (Varasteh et al. 2017) and ^{68}Ga-NOTA-MSA (Kim et al. 2016) have all shown potential in preclinical studies with significant uptake of the tracer in atherosclerotic plaques rich with MR positive macrophages. A multiparametric study combined a nanobody tracer ^{68}Ga-MMR for PET imaging macrophage burden in plaques and MRI to determine plaque burden. ^{18}F-FDG and ^{18}F-sodium fluoride (^{18}F-NaF) were also used to image inflammation and microcalcifications respectively. The study provided extensive knowledge about the different processes occurring during atherosclerosis progression and shows the value of combining different imaging modalities and tracers. (Senders et al. 2019.)

3 Aims

The purpose of the study was to evaluate novel PET tracers for imaging atherosclerotic disease activity in hypercholesterolemic mice with or without type 2 diabetes. Another aim was to study effects of a drug intervention on plaque formation and inflammation by utilizing the tracer ^{18}F-FDG.

The specific aims of this study were:

1. To study the effects of DPP-4 inhibitor linagliptin on atherosclerotic plaque formation and inflammation as well as hepatic steatosis and inflammation in hypercholesterolemic and diabetic IGF-II/ApoB$^{100/100}$LDLR$^{-/-}$ mice using ^{18}F-FDG.

2. To assess GLP-1R expression in atherosclerotic lesions in hypercholesterolemic diabetic IGF-II/ApoB$^{100/100}$LDLR$^{-/-}$ mice and hypercholesterolemic non-diabetic ApoB$^{100/100}$LDLR$^{-/-}$ mice using PET tracer ^{68}Ga-NODAGA-exendin-4.

3. To investigate the uptake of ^{18}F-FGln into inflamed atherosclerotic plaques in hypercholesterolemic ApoB$^{100/100}$LDLR$^{-/-}$ mice, in comparison to ^{18}F-FDG.

4. To evaluate the feasibility of ^{18}F-FOL in detecting inflamed atherosclerotic lesions *in vivo* in rabbit and mouse models of atherosclerosis, in comparison to ^{18}F-FDG.

4 Materials and Methods

4.1 Experimental animals

The mice were bred and housed in standardized conditions in the Central Animal Laboratory of the University of Turku with a 12h/12h light/dark cycle and they had access to food and water ad libitum throughout the studies. The experiments were approved by the National Project Authorization Board in Finland (license numbers: ESAVI/2163/04.10.07/2015, ESAVI/4835/04.10.03/2011 and ESAVI/1583/04.10.03/2012) and were carried out in compliance with the EU Directive 2010/EU/63 on the protection of animals used for scientific purposes.

4.1.1 Mouse models (I–IV)

Two hypercholesterolemic mouse strains were utilized: low-density lipoprotein receptor deficient mice expressing only ApoB100 (n=40 $ApoB^{100/100}LDLR^{-/-}$, strain #003000, The Jackson Laboratory, Bar Harbor, ME, USA) (Powell-Braxton et al. 1998) and the diabetic version of the strain overexpressing insulin-like growth-factor II in pancreatic β-cells (n=44 IGF-II/$ApoB^{100/100}LDLR^{-/-}$, A. I. Virtanen Institute for Molecular Sciences, University of Eastern Finland, Kuopio, Finland) (Heinonen et al. 2007). All mice were initially fed a normal chow diet (9.1% of calories from fat, CRM [E], 801730; Special Diet Services, Essex, United Kingdom) for 2 months and then most were switched to a HFD (study I. 42% of calories from fat, 0.2% total cholesterol, TD 88137 mod; Ssniff Spezialdiäten GmbH, Soest, Germany; studies II-IV. 42% of calories from fat, 0.2% total cholesterol, TD 88137, Harlan Teklad, Harlan Laboratories, Madison, WI, USA) for additional 3–5 months to accelerate the development of atherosclerotic lesions. In addition, C57BL/6N mice (n=19, Central Animal Laboratory of the University of Turku) and C57BL/6Rj mice (n=12, Central Animal Laboratory of the University of Turku) were utilized in the studies as controls and were fed normal chow diet.

4.1.2 Rabbit model (IV)

Watanabe heritable hyperlipidemic rabbits with a mutated *LDLR* gene were utilized in study IV (males n=3, females n=1, A. I. Virtanen Institute for Molecular Sciences,

University of Eastern Finland, Kuopio, Finland) (Fan et al. 2015). At the age of 6 months the rabbits underwent balloon endothelial denudation of the abdominal aorta that was performed by a trained professional. The rabbits were anesthetized with a mixture of ketamine (15 mg/kg, Ketalar, Pfizer, New York, NY, USA) and medetomidine (0.3 mg/kg, Domitor, Orion Pharma, Espoo, Finland) after which a 3F Fogarty embolectomy balloon catheter (120403F, Edwards Lifesciences, Irvine, CA, USA) was inserted via the right femoral artery and advanced proximally for 20 cm up to the lower thoracic aorta. The catheter was inflated with 0.6 mL of air and pulled down to the level of the aortic bifurcation for endothelial denudation and the procedure was repeated three times. After removing the catheter, the femoral artery was ligated, and the wound was closed in layers with resorbable sutures. The rabbits were returned to their cages after recovery from anesthesia. The rabbits were maintained on a normal diet throughout the whole study and the imaging studies were performed when the rabbits were 45 months old.

4.2 Study design

Details of the number of animals and imaging methods used in each study are presented in Table 2.

Table 2. Number of animals and the imaging methods used in each study.

Study	Tracer	Number of animals (f/m)	PET-CT (n)	ARG (n)	Biodistribution (n)
LDLR$^{-/-}$ApoB$^{100/100}$					
II	^{68}Ga-NODAGA-exendin-4	10 (5/5)	2 + 2[b]	7	-
III	^{18}F-FDG	12 (0/12)	4	5	-
	^{18}F-FGln	12 (0/12)	4	5	5
IV	^{18}F-FDG	12 (0/12)	8	-	-
	^{18}F- FOL	12 (0/12)	9 + 2[b]	8 + 2[b]	9 + 3[b]
IGF-II/LDLR$^{-/-}$ApoB$^{100/100}$					
I	^{18}F-FDG	34 (0/34)	-	34	34
II	^{68}Ga-NODAGA-exendin-4	10 (5/5)	2 + 2[b]	8	-
C57BL/6N					
II	^{68}Ga-NODAGA-exendin-4	12 (6/6)	4	10	-
IV	^{18}F-FDG	9 (0/9)	4	-	-
	^{18}F- FOL[a]	9 (0/9)	6	6	9
C57BL/6JRj					
III	^{18}F-FDG	12 (0/12)	4	4	-
	^{18}F-FGln	12 (0/12)	4	5	5
Watanabe rabbit					
IV	^{18}F-FDG	4 (1/3)	4	-	-
	^{18}F- FOL[a]	4 (1/3)	4	4	4

[a]Same animals were imaged with ^{18}F-FDG on the previous day.

[b]Number of animals used for blocking study.

PET= positron emission tomography, CT= computed tomography, ARG= autoradiography, f/m= female/male

4.2.1 Intervention study (I)

In study I, the effects of linagliptin intervention on plaques, glucose tolerance as well as hepatic steatosis and inflammation were studied using ^{18}F-FDG. The hypercholesterolemic and type 2 diabetic IGF-II/LDLR$^{-/-}$ApoB$^{100/100}$ mice were initially fed a chow diet (9.1% of calories from fat, CRM [E], 801730; Special Diet Services, Essex, United Kingdom) for 2 months and then switched to a HFD (42% of calories from fat, 0.2% total cholesterol, TD 88137 mod; Ssniff Spezialdiäten GmbH, Soest, Germany) for another 2 months after which baseline blood samples and oral glucose tolerance test (oGTT) (see Chapter 4.2.2) was performed. The mice were then randomly allocated to either continue on the HFD (n = 14) or to receive HFD mixed with linagliptin (n = 15) (85 mg/kg of feed; Boehringer Ingelheim International GmbH, Ingelheim am Rhein, Germany) for the duration of 3 months. Five mice were fed a chow diet throughout the study period. The food consumption of the mice was measured weekly. At the end of the intervention period, blood sampling and oGTT were repeated and *ex vivo* ^{18}F-FDG biodistribution and autoradiography (ARG) was performed. The aortic root and a piece of liver were fixed in formalin for histological analyses.

4.2.2 Oral glucose tolerance test (I, II)

In study I, an oGTT was performed before and after the intervention. The mice were fasted for 5 h before performing the oGTT. All of the mice received a fixed dose of glucose (180 µl of 20% glucose) per os, and blood glucose was measured using a glucometer (Contour Next, Bayer AG, Leverkusen, Germany) from tail vein blood before (0 min) and 15, 30, 60, 90, and 120 min after glucose administration. Blood insulin concentration was measured from 11 mice from both linagliptin and HFD groups before and 15 and 120 min after glucose administration, using an enzyme-linked immunosorbent assay (Ultra-sensitive Mouse Insulin ELISA Kit; Crystal Chem, Chicago, IL, USA).

In study II, an intraperitoneal glucose tolerance test (ipGTT) was performed one week prior to imaging. The mice were fasted for 4 h and glucose was administered (1 mg/kg) by intraperitoneal injection (i.p.). Blood glucose levels were measured from the tail vein before (0 min) and 20, 40, 60 and 90 min after glucose administration using a glucometer (Contour Next, Bayer AG, Leverkusen, Germany).

4.2.3 Imaging studies (II, III, IV)

Generally, the imaging studies used a similar protocol where the tracer uptake was evaluated by *in vivo* PET/CT imaging, followed by *ex vivo* ARG after injecting the

tracer intravenously (i.v.) through a tail vein catheter. *In vivo* stability and specificity of the tracers was also studied. Histological analysis of the aorta and aortic root using different histological and immunohistochemical staining's were performed to detect features of atherosclerosis. In study II, various biomarkers were also studied from mouse plasma samples.

4.3 Tracer radiosynthesis

The PET tracers used in the studies were synthetized in the Radiopharmaceutical Chemistry Laboratory of Turku PET Centre. ^{18}F-FDG was obtained either from batches allocated for clinical use, or purchased from MAP Medical Technologies Oy (Helsinki, Finland). The radiochemical purity of all the tracers used was always > 95%.

4.3.1 ^{68}Ga-NODAGA-exendin-4

^{68}Ga was obtained from a ^{68}Ge/^{68}Ga generator (Eckert & Ziegler, Berlin, Germany). ^{68}Ga-NODAGA-exendin-4 was prepared by mixing ^{68}Ga-$GaCl_3$ eluate (0.5 ml, 184 ± 19 MBq) with sodium acetate (18 mg, Merck, Kenilworth, NJ, USA) and the pH adjusted to approximately 3.5 with HCl. After this, NODAGA-exendin-4 (5 nmol in 5 µl deionized water) was added and the reaction mixture was incubated at 95 °C for 15 min. The radiochemical purity was determined by radio-high-performance liquid chromatography (radio-HPLC) (Jupiter C_{18}, 300 Å, 150 × 4.6 mm, 5 µm column, Phenomenex, Torrance, CA, USA).

4.3.2 (2*S*, 4*R*)-4-[^{18}F]fluoroglutamine

Approximately 12 GBq of ^{18}F-F^- was put on a pre-conditioned (10 ml 3% K_2HCO_3 in H_2O followed by 20 ml of water) Waters Sep-Pak Accell Plus QMA Plus Light cartridge (WAT023525) and eluted into R2 with 2000 µl of mixture comprised of 16.5 mg of 18-Crown-6 ($C_{12}H_{24}O_6$), 3.0 mg of potassium bicarbonate ($KHCO_3$), 77 µl of H_2O, and 1923 µl of acetonitrile (CH_3CN). The vessel was then heated to 115 °C under 70 ml/min flow of nitrogen gas for 25–27 min and 2 min past any visible moisture in the vessel or the outflowing line. After cooling the eluate to 55 °C, 10 mg of the glutamine precursor (2*S*, 4*S*)-tert-butyl-2-(tert-butoxycarbonylamino-5-oxo-4-(tosyloxy)-5-(2, 4, 6- trimethoxybenzylamino) pentanoate was dissolved in 500 µl of dry acetonitrile and added to the eluate which was heated to 70 °C for 15 min. The vessel was then cooled to room temperature and mixture of 500 µl of H_2O and 300 µl of acetonitrile was added and the solution was injected into a semi-preparative HPLC-system with a Waters X Terra Prep MSC18 10 µm 7.8 × 300 mm column. 0.1% formic

acid in water and 0.1 % formic acid in acetonitrile were utilized in the eluent gradient. Initially the gradient was an equal mixture of both eluents and gradually after 20 min changed to 70% of the acetonitrile-based eluent and at 15 min the desired ^{18}F-labelled intermediate eluted into R3 which was filled with 25 ml of water.

The intermediate product was loaded onto a preconditioned (3 ml dry ethanol followed by 5 ml of water) Waters Oasis® HLB Plus Light Cartridge and eluted with 1 ml of dry ethanol into R1. The vessel was heated to 90 °C under 100ml/min nitrogen flow until it was completely dry and cooled to 40 °C. The final step of the synthesis was removing protecting groups by adding 595 µl of trifluoroacetic acid and 5 µl of anisole and heating the mixture to 50 °C for 3 minutes after which the liquid was evaporated for further 2 minutes at 50 °C under 60 ml/min nitrogen gas flow. The product was then cooled to 40 °C and 2 ml of phosphate-buffered saline (PBS pH 6.5) was added to achieve the final product.

4.3.3 ^{18}F-AlF-NOTA-folate

Approximately 3.3 GBq of ^{18}F-F^- in physiological saline (50 µl) was added to a reaction vessel containing sodium acetate buffer (pH 4.0, 1 M, 25 µL) and $AlCl_3$ (2 mM). The mixture was kept at room temperature for 3 minutes after which NOTA-folate (250 µg) in water (50 µl) and acetonitrile (125 µl) was added, and the mixture was heated at 100 °C for 15 min, followed by dilution of the mixture with water containing 0.2% formic acid (1 ml). Next an HPLC purification with a semi-preparative C18 column (Jupiter 250 × 10 mm, Phenomenex Inc., Torrance, CA, USA) with both UV (254 nm) and radioactivity detection was performed producing solvent A which was water that contained 0.1% formic acid and solvent B which was acetonitrile that contained 0.1% formic acid. The elution was programmed as a gradient from 8% to 21% of solvent B over the time of 20 min, with a flow rate of 4 ml/min. The pH of the collected HPLC fraction was adjusted to 5.5 by adding potassium bicarbonate ($KHCO_3$) in water (1 M) after which the solvents were evaporated off. The residue was formulated in PBS (1–3 ml) containing 8% ethanol and 4–7% polypropylene glycol and at the end of the synthesis the product was sterile filtrated (0.22 µm, Millipore) into the end product vial.

4.4 PET/CT imaging

In studies II, III and IV, *in vivo* PET/CT imaging was performed before *ex vivo* measurements, whereas in study I, only *ex vivo* measurements were performed. Imaging of the mice was performed with a dedicated small animal PET/CT scanner (Inveon Multimodality, Siemens Medical Solutions, Knoxville, TN, USA). The mice were fasted for 2–4 h and then anesthetized with isoflurane (induction 4–5%,

maintenance 1.5–2.5%, oxygen as carrier). They were kept on a heating mat to maintain their body temperature and an intravenous catheter was inserted into the tail vein for the injection of the tracer. The tracer doses were as follows: 20 ± 2.0 MBq of ^{68}Ga-NODAGA-exendin-4 in study II, 13.9 ± 0.9 MBq of ^{18}F-FDG or 14.5± 0.8 MBq of (2*S*, 4*R*)-4-[^{18}F]fluoroglutamine (^{18}F-FGln) in study III and 10 ± 0.3 MBq of ^{18}F-FDG and 11 ± 0.7 MBq of ^{18}F-AlF-NOTA-folate (^{18}F-FOL) in study IV. Attenuation correction CT was performed before dynamic PET acquisition for 60 min (study II and III), or 90 min (study IV). PET imaging was followed by contrast-enhanced CT using an i.v. administered iodinated contrast agent (100–150 µL of eXIATM160XL, Binitio Biomedical Inc., Ottawa, ON, Canada) to get a better visualization of the aorta. In study III the mice were first imaged with ^{18}F-FDG and on the following day with ^{18}F-FGln and in study IV, the mice were first imaged with ^{18}F-FDG and on the following day with ^{18}F-FOL In addition to *in vivo* imaging, *ex vivo* imaging of excised mouse aortas (n= 1 LDLR$^{-/-}$ApoB$^{100/100}$ mouse, n = 1 LDLR$^{-/-}$ApoB$^{100/100}$ mouse with a 100-fold excess of folate glucosamine (blocking) and n = 1 C57BL/6N control mouse) was performed with ^{18}F-FOL. After the aortas were dissected, they were placed on an ultrasound gel covered Petri dish and PET data was acquired for 30 min. The PET data was reconstructed with either an ordered-subsets expectation maximization 2-dimentional algorithm (with two iterations) (study IV) or 3-dimensional algorithm (studies II and III). A Feldkamp based algorithm was used to reconstruct the contrast-enhanced CT images.

PET and CT images were automatically co-registered, and visually confirmed on the basis of anatomical landmarks. Carimas 2.9 software (Turku PET Center, Turku, Finland, www.turkupetcentre.fi/carimas/) was used to analyze PET/CT images. Regions of interest (ROIs) were determined for the aortic arch, vena cava (representing blood), and myocardium, using the contrast-enhanced CT as an anatomical reference. Additional ROIs were drawn in lungs, liver, kidneys, muscle, and urinary bladder as well as aortic root in study II. Results were expressed as standardized uptake values (SUVs), normalized for the injected radioactivity dose and animal body weight, and for the aorta as maximum TBR calculated as SUV_{max}, aortic arch/SUV_{mean}, blood.

In study IV, a clinical PET/CT scanner (Discovery VCT, General Electric Medical Systems, GEMS, Milwaukee, WI, USA) was utilized for imaging the rabbits. For the imaging studies, the rabbits were fasted for 4 h, sedated and anesthetized with a subcutaneous injection of medetomidine hydrochloride (Domitor, Orion Pharma; dose, 0.1 mg/kg) and ketamine (Ketalar, Pfizer; dose, 30 mg/kg), and to minimize accumulation of radioactivity in the bladder, a urinary catheter was inserted in the urethra. The rabbits were kept on a heating mat during anesthesia to maintain their body temperature and an i.v. catheter was inserted into the marginal ear vein for the injection of the tracer (dose 140 ± 29 MBq of ^{18}F-FDG

and 130 ± 37 MBq of ^{18}F-FOL) and another for collecting blood samples during imaging. Before PET imaging, a low-dose attenuation correction CT (voltage 80 or 120 kV, current 10−80 mA) was performed. The rabbits were first imaged with ^{18}F-FDG as a static 20 min PET acquisition (two bed positions, each for 10 min) 160 min post injection, and on the following day with ^{18}F-FOL with a dynamic 90 min PET acquisition where the bed positions were imaged in an interleaved manner. After PET imaging a CT with higher voltage and current (voltage 100 kV, current 450 mA) was performed to get a better visualization of the aorta and the field-of-view covered the area from the aortic arch to the bifurcation. The PET data was reconstructed with a 3-dimensional iterative algorithm (VUE point) with 28 subsets, 2 iterations, a standard z axis filter, and 2.00 mm full width at half maximum post-filtering. The aorta was divided into 2 cm segments and the maximum SUV was determined in each of them. The mean SUV in the blood was measured from the inferior vena cava to calculate maximum TBRs (SUV_{max}, aorta/SUV_{mean}, blood). Anatomical landmarks (e.g., renal arteries) were identified from CT images to match up the defined 2 cm aorta segments with the excised samples used for *ex vivo* measurements.

4.5 *Ex vivo* biodistribution

In study I, the mice were anesthetized with isoflurane (induction 4-5 %, maintenance 1.5-2.5 %, air as carrier). An i.v. catheter was placed into the tail vein for the tracer injection (dose 10 ± 0.23 MBq of ^{18}F-FDG). Blood glucose levels of the mice were measured before tracer injection and at the time of sacrifice using a glucometer (Contour Next, Bayer AG, Leverkusen, Germany). Sixty min after the tracer injection the mice were euthanized in deep anesthesia by cardiac puncture followed by cervical dislocation. Mice in studies II and III were euthanized in similar manner after PET-CT imaging and mice in study IV 120 mins after ^{18}F-AlF-NOTA-folate injection. Tissue samples were dissected, weighed and radioactivity measured using a gamma counter (Triathler 425-010, Hidex, Turku, Finland). The measurements were corrected for injected radioactivity dose and decay-corrected according to the physical half-life of the radionuclide. The results were expressed as percentage of injected radioactivity per gram of tissue (%ID/g, study IV) or as standardized uptake values (SUV, studies I, II and III) which were calculated as (radioactivity in tissue/tissue weight) / (injected radioactivity/mouse weight). TBR was calculated for the aorta by dividing the aortic SUV by blood SUV.

The rabbits in study IV were euthanized under deep medetomidine hydrochloride/ketamine anesthesia by cardiac puncture followed by an overdose of pentobarbital (Mebunat vet 60 mg/mL, Orion Pharma, Espoo, Finland) 120 mins after ^{18}F-FOL injection. Tissue samples were dissected, weighed and the radioactivity measured using a gamma counter (1480 Wizard 3″; Perkin

Elmer/Wallac, Turku, Finland). The aorta from the aortic arch to the iliac artery bifurcation was dissected and cut into 2 cm segments which were weighed, and the radioactivity of each aorta segment was measured. The radioactivity values were corrected for the injected radioactivity dose and decay of the tracer. The results were expressed as %ID/g.

4.6 Autoradiography studies

Ex vivo autoradiography (I–IV)

The tracer uptake in the aorta was determined in more detail using digital ARG (Figure 2.). The mouse aortas were carefully cleaned and rinsed and after the *ex vivo* measurements described in the previous chapter, the aortas were then frozen in dry-ice cooled isopentane and cut into 20 and 8 µm serial longitudinal sections (n = 6–8 sections/slide) and the rabbit aortas were divided into 3–6 transverse 2 cm segments, frozen, and cut into 20 µm sequential transverse sections with a cryomicrotome. In study I, a piece of the liver and in study II, the pancreas was similarly frozen and cut into 20- and 8 µm serial sections). The sections were airdried and opposed to a radiation-sensitive imaging plate (Fuji Imaging Plate BAS-TR2025, Fuji Photo Film Co., Ltd., Tokyo, Japan). The ARG was exposed for a specific time depending on the radionuclide used but for a minimum of two physical half-lives of the tracer and then scanned with a phosphoimager with an internal resolution of 25 µm (Fuji Analyzer BAS-5000, Fuji, Tokyo, Japan). The 20 µm sections were stained with hematoxylin and eosin (H&E) and the 8 µm sections were stored in -70 °C to be used later for immunohistochemical staining's.

The H&E slides were scanned using a slide scanner (Pannoramic 250 Flash, 3DHistech Ltd., Budapest, Hungary) and the outlines of the sections were then co-registered with the ARG images. From the aorta, 6–10 sections per animal and from the liver and pancreas, 6 sections per animal were analyzed with Tina 2.1 software (Raytest Isotopemessgeräte, GmbH, Straubenhardt, Germany) and the tracer accumulation was measured as count densities (photo-stimulated luminescence per square millimeter, PSL/mm^2). The background count densities were subtracted from the results and the PSL/mm^2 values decay-corrected for injection and exposure time and normalized for injected radioactivity dose for each animal.

For the mice the ROIs were determined in atherosclerotic plaques (excluding calcification and media), vessel wall with no lesion formation, and the brown adipose tissue around the aorta (adventitia). In study I, the whole liver section was encompassed by the ROI. In study II, the ROIs were placed on the islets of Langerhans and exocrine pancreas and the islet-to-exocrine ratio was determined. In the rabbit study the atherosclerotic plaques were divided into two categories based

of their histopathological characteristics seen in H&E: atherosclerotic plaques with large fibroatheroma lesions (mainly observed in denudated abdominal aorta) and mild atherosclerotic plaques with small lesions or intimal thickening (observed in non-denudated thoracic aorta). It was not possible to place a ROI in totally healthy vessel wall, as some plaque formation was also seen in non-denudated thoracic aorta due to the genetic background and advanced age of the rabbits.

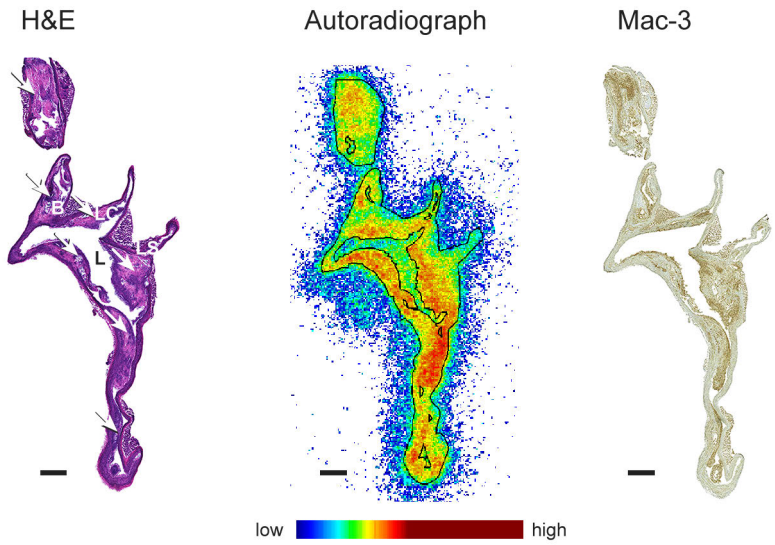

Figure 2. A representative image of an autoradiograph (middle) with corresponding H&E (left) and adjacent Mac-3 staining (right) of a mouse aorta. The white arrows depict atherosclerotic plaques. Plaques commonly build up in the aortic arch region and the aortic branches; brachiocephalic artery (B), left common carotid artery (LC) and left subclavian artery (LS). The lumen (L) is narrowed due to plaque buildup. Tracer uptake is highest in the macrophage rich plaques (red areas) and relatively low in the normal vessel wall and adventitia (green). (Adopted and modified from the original publication I with a permission (Fig. 2A, page 68). DOI: https://doi.org/10.1016/j.atherosclerosis.2020.05.009)

In vitro autoradiography (IV)

In vitro autoradiography was performed in study IV by using human (24 × 7 µm carotid cryosections from five patients), mouse (30 × 8 µm aorta cryosections from four atherosclerotic mice), and rabbit (46 × 20 µm aorta plaque cryosections from four Watanabe rabbits). The human samples were acquired from patients who underwent carotid endarterectomy, and the study was conducted according to the declaration of Helsinki, and the study protocol was approved by the ethics committee of the Hospital District of Southwest Finland. All of the patients gave their written

informed consent. The slides were pre-incubated in PBS (pH 7.4) at room temperature for 15 min and then in 0.2 nM ^{18}F-FOL in PBS with or without a 100-fold molar excess of folate glucosamine to also determine specificity of tracer binding. After incubation, the slides were washed twice with ice-cold PBS for 1 min, dipped in ice-cold distilled water, briefly dried with a hair dryer, and ARG was performed similarly as in the *ex vivo* studies.

4.7 Specificity of tracer binding (II, IV)

Specificity of tracer binding was assessed *ex vivo* in study II. 14 mg/kg of unlabeled exendin-4 peptide (ChinaPeptides Co. Ltd., Shanghai, China) was injected into 4 mice (results pooled n = 2 nondiabetic and n = 2 diabetic mice), 10 minutes prior to ^{68}Ga-NODAGA-exendin-4 injection, to block the specific binding sites of the tracer. The blocking peptide dose was ~100-fold amount (445 µg/mouse) compared with injected ^{68}Ga-NODAGA-exendin-4. The blocking was followed by autoradiography study as described in Chapter 4.6. In study IV, the specificity of the tracer was assessed *in vitro* (described in Chapter 4.6) and *ex vivo* by injecting a 100-fold molar excess of folate glucosamine ($C_{25}H_{30}N_8O_{10}$, molecular weight 602.56) (25–30 µl) i.v. into 3 LDLR$^{-/-}$ApoB$^{100/100}$ mice one minute before ^{18}F-FOL injection. The blocking was followed by ARG as described in the previous chapter.

4.7.1 *In vitro* binding (IV)

The binding of ^{18}F-FOL to macrophages was studied using peripheral blood mononuclear cells from buffy coats that were collected using Ficoll centrifugation method. Monocytes were enriched using magnetic-activated cell sorting (MACS) positive selection kit (Monocyte isolation kit with CD14 MicroBeads; Miltenyi Biotec, Bergisch Gladbach, Germany). MACS-purified monocytes were cultured in 12 well plates (1×10^6 cells/well) in the Iscove's Modified Dulbecco's medium (containing 2% AB serum and 2 mmol l-glutamine; Gibco, Thermo Fisher Scientific, Waltham, MA, USA) with M-CSF (20 ng/ml; Peprotech, London, UK) for 6 days (at 37 °C in a CO_2 incubator) to obtain macrophages (at day 3 half of the medium was replaced with fresh medium with M-CSF (20 ng/ml). At day 6, IFN-γ (50 ng/mL; Peprotech) and LPS (100 ng/ml; Sigma-Aldrich, St. Louis, MO, USA) were added to fresh medium to differentiate macrophages to M1, and M-CSF (20 ng/ml), IL-4 (10 ng/ml; Peprotech) and IL-10 (10 ng/ml; Peprotech) were added to the fresh medium to differentiate macrophages to M2. The cultures were incubated for another 2 days (at 37 °C in a CO_2 incubator). At day 8 the medium was removed from the wells, and ^{18}F-FOL (1 MBq/ml in fresh medium) was added to each well and incubated for 1 hour (at 37 °C in a CO_2 incubator). After the incubation the cells

were rinsed twice with PBS (1 mL) to remove any unbound radioactive materials and 1% sodium dodecyl sulfate in PBS (1 ml) was added to each well. Solubilized cells were collected into individual test tubes and the amount of bound tracer was measured with a gamma counter (1480 Wizard 3″; Perkin Elmer/Wallac, Turku, Finland). After this the cells were harvested to confirm the polarization to M1 and M2 macrophages, and after pre-blocking with human immunoglobulin (Ig 100 µg/ml; KIOVIG, Baxter, Vienna, Austria) they were incubated with Alexa Fluor 488-conjugated anti-human-CD206 antibody (mouse IgG1; BioLegend, San Diego, CA, USA) for cell surface staining or with isotype control (mouse IgG1; BD Biosciences, New Jersey, NJ, USA). For CD68 staining, the cells were permeabilized (15 s in ice-cold acetone), blocked and incubated with Alexa Fluor 488-conjugated anti-human-CD68 antibody (mouse IgG2a; BioLegend) or with isotype control (mouse IgG2a; BD Biosciences). As the last step, the cells were fixed using paraformaldehyde and analyzed using fluorescence-activated cell sorting (FACS) with Fortessa flow cytometer (BD Biosiences, CA, USA) and Flowing software (Turku Center of Biotechnology, Turku, Finland).

4.8 *In vivo* tracer stability (III, IV)

The *in vivo* stability and plasma protein binding of the tracer was assessed in studies III and IV. In study III, blood samples were taken from the mice at the end of PET/CT imaging (n = 4 atherosclerotic mice, n = 7 healthy controls). Whole blood was weighed, and radioactivity measured (Triathler 3″; Hidex, Turku, Finland) after which it was centrifuged (700 ×g at 4 °C for 5 minutes) to separate the plasma. The plasma sample was then weighed, and radioactivity measured before an aliquot was precipitated with 2.4 volumes of methanol, followed by vortexing and centrifugation (11,000 × g at room temperature for 10 min). The radioactivity of the supernatant and precipitated protein pellet was measured (1480 Wizard 3″; Perkin Elmer/Wallac, Turku, Finland). The precipitated plasma supernatants were further analyzed with HPLC to measure the fraction of intact ^{18}F-FGln. In study IV, blood samples were taken from all the rabbits and from a separate set of 6 atherosclerotic mice at timepoints of 5-60 minutes post injection of ^{18}F-FOL. Plasma was separated by centrifugation (2,100 × g for 4 min at 4 °C) after which it was weighed, and radioactivity measured. An aliquot of the plasma was precipitated by adding an equal volume of acetonitrile followed by vortexing and centrifugation (2,100 × g for 4 min at 4 °C). The radioactivity of the supernatant and precipitated protein pellet was measured. (1480 Wizard 3″; Perkin Elmer/Wallac, Turku, Finland). The supernatant was then filtered through a 0.45 µm Minispike filter (Waters Corporation, USA) to be further analyzed with HPLC. The column utilized in the HPLC was a semi-

preparative C18 column (Jupiter 250 × 10 mm, Phenomenex Inc., Torrance, CA, USA) and both UV (254 nm) and radioactivity detection were used.

4.9 Histology and immunohistochemistry

As the 20 μm cryosections of the aorta were used for H&E staining, adjacent 8 μm sections were used for different immunohistochemical staining's. In addition to the aorta cryosections, the aortic root of the mice was preserved in 10 % formalin and after fixation, dehydrated in 70 % ethanol, embedded in paraffin, and cut transversely into serial 6 μm sections at the level of the coronary ostia.

For immunohistochemical stainings in general, the sections were first thawed and fixed with 4 % formaldehyde and then boiled in citrate or tris-EDTA buffer. The sections were then incubated with the primary antibody followed by secondary and tertiary antibodies, depending on the staining. Detection of the stained regions was performed using 3.3′-diaminobenzidine tetrahydrochloride hydrate (DAB) and substrate (DakoCytomation K3468 or Bright-DAB, BS04-110, ImmunoLogic, Duiven, the Netherlands) and counterstained with Mayer's hematoxylin. Eight μm aorta cryosections were stained for macrophages with anti-mouse Mac-3 (clone M3/84, 1:1000 or 1:500, BD Biosciences, Franklin Lakes, NJ, USA) in all of the studies to investigate their co-localization with tracer uptake.

In study I, aortic root sections were stained with Mac-3, iNOS to detect M1 polarized macrophages, anti-mannose receptor C-type 1 antibody (MRC-1) to detect M2 polarized macrophages (anti-MRC-1 ab64693, 1:500 and anti-iNOS ab15323, 1:200; Abcam, Cambridge, UK) or modified Movat's pentachrome staining, which was used for histological evaluation of the plaques. Formalin-fixed, paraffin embedded piece of liver from each mouse was cut into 4 μm sections and stained with H&E or van Gieson's stain to study features of NAFLD (steatosis, inflammation, ballooning, and fibrosis). The evaluation was performed by two independent observers using the NAFLD activity scoring (NAS) scale, where the sum of three equal weighted features of steatosis (0–3), lobular inflammation (0–3) and hepatocellular ballooning (0–2) were used to calculate the score (Hjelkrem et al. 2011).

In study II, aortic root sections were co-stained with immunofluorescent GLP-1R antibody (7F38, 1:100; DSHB, IA, USA) and either Mac-3, iNOS or MRC-1. Immunofluorescent co-staining's were then performed with GLP-1R antibody in combination with EC antibody CD31 (NB100-2284, 1:100; Novus Biologicals, Abingdon, UK) SMC antibody or α-smooth muscle actin (α-SMA) (A5228, 1:2000 or 1:20 000; Merck, Darmstadt, GE). Pancreatic paraffin sections were additionally co-stained with GLP-1R and insulin antibodies (ab63820, 1:5000 or 1:1000; Abcam, Cambridge, UK).

In study III, co-localization of tracer uptake with glutamine transporters was studied in aorta cryosections by staining them with anti-SLC7A7 antibody (1:1,000; catalog number: PA5-113527; Thermo Fisher Scientific, Waltham, MA, USA). Aortic root sections were stained with Mac-3 and modified Movat's pentachrome and also with anti-SLC1A5 (1:500; NBP1-59732; Novus Biologicals, Centennial, CO, USA), anti-SCL3A2 (1:500; sc-390154; Santa Cruz Biotechnology, Dallas, TX, USA), and anti-SLC7A7 (1:500; PA5-113527; Thermo Fisher Scientific, Waltham, MA, USA)) antibodies to investigate the expression patterns of different glutamine transporters in atherosclerotic lesions.

In study IV, the mouse aortic root sections were stained with iNOS, MRC-1 and modified Movat's pentachrome staining. Mouse aorta cryosections were additionally stained with FR-β using a rabbit polyclonal anti-FR-β antibody (1:100, Biorbyt Ltd, Cambridge, UK), and anti-rabbit secondary antibody (Bright vision Poly-HRP-anti Rb, VWRKDPVR110HRP) to study the co-localization of the tracer with FR-β. The *ex vivo* imaged aortas were stained with Oil-Red-O. The rabbit aorta segments that were not used for ARG were fixed in 10% formalin, embedded in paraffin, and cut into 6 μm serial sections. For each aorta segment, adjacent sections were stained with either modified Movat's pentachrome or H&E for histological evaluation or mouse anti-rabbit RAM-11 antibody (M 0633, 1:1000, Envision, Dako, Carpinteria, CA, USA), followed by secondary anti-mouse antibody (K4001, Envision, Dako, Carpinteria, CA, USA) to detect macrophages. 8 μm human carotid artery cryosections were stained with mouse monoclonal anti-human CD68 antibody (mo876; 1:200, PG-M1, Dako, Glostrup, Denmark), to detect macrophages or biotinylated anti-human FR-β antibody (m909, 1:100), followed by secondary antibody (P0397, 1:200, Dako) to detect FR- β positive areas.

After staining the slides were scanned using a slide scanner (Pannoramic 250 Flash, for histology or MIDI for immunofluorescence, 3DHistech Ltd., Budapest, Hungary). For each aortic root and liver staining, 3 sections per mouse were analyzed using the ImageJ software (Fiji, National Institutes of Health, Bethesda, MD, USA). The aortic roots were outlined based on the histology, using the image processing software GIMP2 so that the intima and media were separated, and the absolute area of intima (mm^2) and intima-to-media ratio could be calculated. The percentage of intimal area positive for different macrophages was measured with a color deconvolution method that detects the DAB-stained areas.

4.10 Measurement of plasma biomarkers (I, II)

Plasma concentration of different biomarkers were measured in studies I and II. In study I, fasting plasma concentration of glucose and insulin were measured during the oGTT's as previously mentioned and TG's (Triglyceride Determination Kit,

Sigma-Aldrich, St. Louis, MO, USA) and total cholesterol (Cholesterol ChOD-PAP kit, MTI-diagnostics GmbH, Idstein, Germany) concentrations were measured before and at the end of treatment. As previously described by Darsalia et al. (2016), plasma DPP-4 and GLP-1 activity was measured from a separate set of linagliptin treated and high-fat diet mice at the end of the 3-month intervention.

In study II, plasma concentrations of total cholesterol (CHOD-PAP kit, Roche Diagnostics, Basel, Switzerland), LDL, HDL (as described by Yan et al. 2007) and TG's (GPO-PAP kit, Roche Diagnostics, Basel, Switzerland) were measured. Additionally, plasma levels of C-peptide, glucagon, insulin, and leptin were measured from blood samples taken before tracer injection, using a Luminex assay (MILLIPLEX MAP Mouse Metabolic Hormone Magnetic Bead Panel, Merck Millipore, Billerica, MA, USA).

4.11 Statistical analyses

The results were expressed as mean ± standard deviation (SD) and statistical significance was accepted when $p < 0.05$ in all of the studies. Analyses were performed using Microsoft Excel or IBM SPSS Statistics 25 (IBM Corp., Armonk, NY, USA). In study I, normally distributed datasets were analyzed using Student's t-test for unpaired data to compare the differences between linagliptin and HFD group or HFD and chow group. Evaluation of NAFLD scores was performed using Fisher's exact test, and correlations were evaluated using Spearman's rho. In study II, a Shapiro–Wilk test was used to examine normality, and equality of variances was tested with Levene's test. Multiple comparisons were made by one-way analysis of variance (ANOVA) followed by Dunnett's post hoc test for the control group or the competition group. Student's t test for unpaired or paired data was used to compare differences between nondiabetic and diabetic groups. In study III, normality was examined by a Shapiro–Wilk test, and equality of variances was tested with an F test. A two-tailed unpaired Student's t test was used for normally distributed datasets, to compare differences between the groups. In study IV, independent samples t tests was used to compare differences between groups and one-way ANOVA with Tukey's correction to compare multiple groups. Paired t tests were applied for comparisons of tracer uptake between different tissues in the same animals. In the rabbit studies, general linear mixed models were used to test associations between continuous variables, where the animal was used as a random effect to account for within-subject correlation, and classified aorta segments were used as a repeated effect to account for the difference between segments when appropriate. Pearson's correlation coefficient (r) was used to assess correlations between continuous variables.

5 Results

5.1 Study animal characteristics

5.1.1 Histology and immunohistochemistry

All atherosclerotic mice (both ApoB$^{100/100}$LDLR$^{-/-}$ and IGF-II/ApoB$^{100/100}$LDLR$^{-/-}$,) developed extensive macrophage-rich atherosclerotic lesions on HFD, whereas the IGF-II/ApoB$^{100/100}$LDLR$^{-/-}$ mice that were kept on chow diet only developed small lesions, which were similarly infiltrated with macrophages. No lesion development was observed in the C57BL/6N or C57BL/6Rj control mice.

In study I, the intima-to-media ratio in the aortic root was similar in the linagliptin and HFD group (4.0 ± 1.2 vs. 4.8 ± 2.4, $p = 0.24$) but in the chow group it was significantly lower than in high-fat diet group (0.9 ± 0.64, $p = 0.002$). All mice showed similar distributions of M1 and M2 polarized macrophages in the lesions. Mice in linagliptin and HFD group showed prominent hepatic micro- and macrovesicular steatosis, but linagliptin-treated mice had significantly less inflammation compared to HFD mice (steatosis 2.0 ± 1.1 vs. 2.3 ± 1.0, $p = 0.85$; inflammation 0.93 ± 0.59 vs. 1.4 ± 1.3, $p = 0.04$, respectively). In addition, the number of ballooned cells was similar and there was minimal to no fibrosis in all of the groups. There were no differences between linagliptin and HFD groups with respect to NAS or fibrosis. Compared to HFD group, mice on chow diet showed significantly less steatosis (0.80 ± 0.45, $p = 0.02$), but there were no differences in inflammation, NAS, or fibrosis.

In study II, the intima-to-media ratio was similar in nondiabetic and diabetic mice (1.7 ± 0.47 vs. 1.7 ± 0.37, $p = 0.98$). No GLP-1R expression was seen in the control mice but in the atherosclerotic mice, GLP-1R-positive protein immunostaining was found in the lesions mainly in the macrophage-rich areas stained with Mac-3, iNOS, and MRC-1. GLP-1R expression co-localized most prominently with M2 polarized macrophages. Scattered GLP-1R-positive staining was also observed in the CD31-positive endothelium and additional GLP-1R positive staining was observed in deeper areas of the lesions, which did not however colocalize with α-SMA-positive VSMCs. In the pancreatic sections, GLP-1R

immunostaining colocalized with insulin staining in pancreatic β-cells of islets of Langerhans.

In study III, glutamine transporters SLC1A5, SLC3A2, and SLC7A7 were expressed in atherosclerotic lesions in the aortic root, but with unique expression profiles. SLC1A5 was expressed predominantly in aortic valve leaflets, whereas SLC3A2 was expressed in the intima. Expression of SLC7A7 was prominent in both the aortic valve and intima and it colocalized with Mac-3-positive macrophages which was also observed in aortic arch cryosections.

In study IV, the intima-to-media ratio was 3.7 ± 2.1 and lesions showed infiltration of both M1 and M2 polarized macrophages that were also FR-β-positive. The endarterectomized carotid artery samples showed co-localization of CD68 and FR-β positive macrophages in the lesions. In rabbits, staining with HE and anti-RAM-11 antibody showed that the aortic segments within the denudated part of the aorta contained large fibroatheroma-type lesions infiltrated with macrophages. The non-denudated aorta showed only small fibroatheroma-type lesions or mild intimal thickening.

5.1.2 Plasma biomarkers

In study I, fasting blood glucose and insulin levels were similar in linagliptin and HFD group (fasting glucose 9.8 ± 1.5 vs. 9.6 ± 3.0 mmol/l, $p = 0.77$, fasting insulin 0.56 ± 0.18 vs. 0.60 ± 0.27 ng/ml, $p = 0.69$, respectively) as well as total cholesterol and TG levels (total cholesterol 35 ± 8.3 vs. 35 ± 14 mmol/l, p = 0.99, TG 2.5 ± 0.83 vs. 2.3 ± 0.54 mmol/l, $p = 0.30$, respectively). However, total cholesterol was significantly lower in the chow group compared to HFD group (8.0 ± 3.2 mmol/l, $p < 0.001$). The mean intake of linagliptin during the intervention was 7.7 ± 0.98 mg/kg/day, measured from the food intake of the mice. Linagliptin treatment lowered plasma DPP-4 activity by 83 % and increased GLP-1 activity by 81% compared with HFD mice (DPP-4 activity 749 ± 127 vs. 4,488 ± 783 relative fluorescence units, $p < 0.001$, GLP-1 activity 16 ± 5.2 vs. 2.9 ± 2.3 pg/ml, respectively; $p < 0.001$).

In study II, total cholesterol was similar in the nondiabetic and diabetic hypercholesterolemic mice (46 ± 7.8 vs. 50 ± 6.6 mmol/l, $p = 0.24$), but significantly lower in the healthy controls (2.0 ± 0.41 mmol/l, $p < 0.01$). HDL and TG levels were similar between the groups. Plasma leptin levels were significantly higher in both non-diabetic (6,300 ± 1,800 pg/ml) and diabetic mice (6,500 ± 2,800 pg/ml) compared to healthy controls (2,700 ± 2,600 pg/ml, $p < 0.05$). Additionally, the diabetic mice showed a tendency towards higher fasting plasma levels of insulin and C-peptide (insulin 2,700 ± 1,600 vs. 1,300 ± 1,200 pg/ml, $p = 0.11$; C-peptide 1,700 ± 1,100 vs. 1,000 ± 670 pg/ml, $p = 0.17$) compared to non-diabetic mice.

5.1.3 Glucose tolerance tests

In study I, baseline oGTT showed similar glucose tolerance between the groups, but at the end of the intervention, linagliptin treated mice exhibited significantly improved glucose tolerance compared to baseline (Area under the curve 0–120 min, ($AUC_{0–120\ min}$) 1,365 ± 313 mmol·min/l vs. 2,033 ± 435; $p < 0.001$) and HFD mice ($AUC_{0–120\ min}$ 1,365 ± 313 vs. 1,720 ± 397 mmol·min/l; $p = 0.01$). At the end of the intervention, linagliptin treated mice also showed a significant increase in insulin secretion compared to baseline ($AUC_{0–120\ min}$ 75 ± 14 vs. 143 ± 59 ng·min/ml; $p = 0.001$)(Figure 3.).

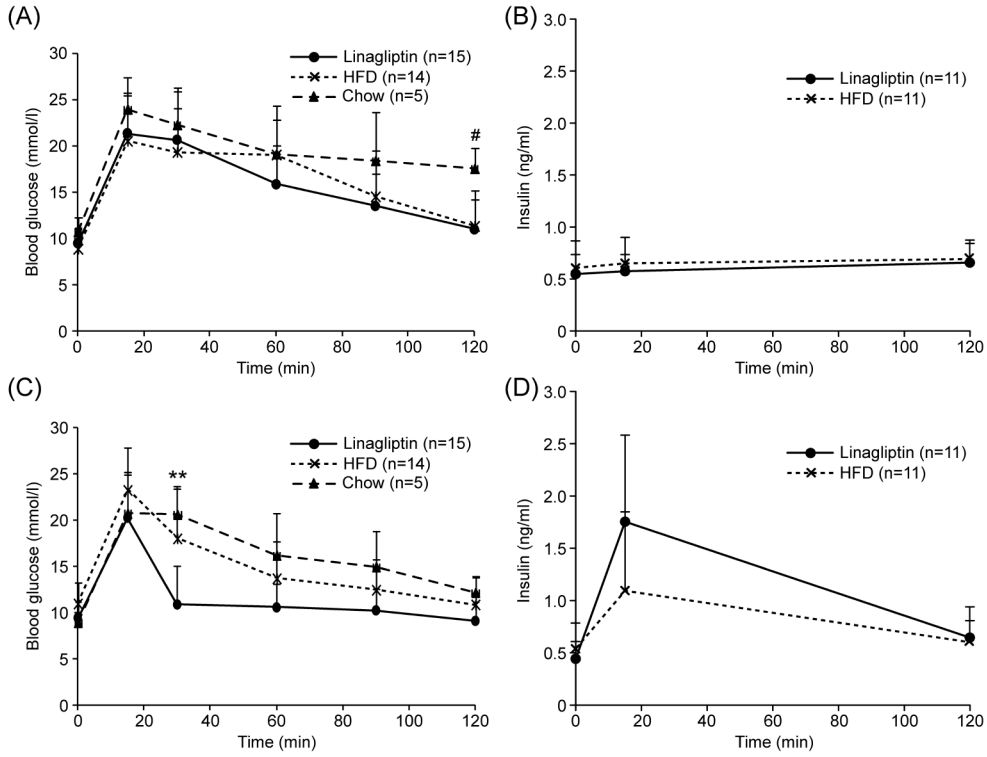

Figure 3. Oral glucose tolerance test in study I. Baseline oGTT was performed before the start of the intervention (A) and the insulin levels were measured during the test (B). At the end of the intervention the oGTT (C) and insulin measurements (D) were repeated. Linagliptin treatment significantly improved glucose tolerance of the mice compared to baseline ($p < 0.001$) and increased insulin secretion during oGTT ($p = 0.001$). # HFD vs. chow $p < 0.01$; ** Linagliptin vs. HFD $p < 0.001$. (Adopted from the original publication I with a permission (Fig. 1, page 67). DOI: https://doi.org/10.1016/j.atherosclerosis.2020.05.009)

In study II, the diabetic mice exhibited significantly impaired glucose tolerance (peak ipGTT value at 20 min 29 ± 4.6 mmol/l) compared to non-diabetic mice (14 ± 2.6 mmol/l, $p < 0.001$) and healthy controls (13 ± 1.6 mmol/l, $p < 0.001$).

5.2 Specificity of tracer binding (II, IV)

In study II, i.v. injection of unlabeled exendin-4 prior to ^{68}Ga-NODAGA-exendin-4, showed reduced lesion-to-wall ratio (block 1.4 ± 0.10, $p = 0.0018$ vs. nondiabetic and $p = 0.0025$ vs. diabetic mice) and completely blocked tracer uptake in islets of Langerhans, indicating that the tracer uptake is specifically mediated by GLP-1R. In study IV, mice were i.v. injected with 100-fold excess of folate glucosamine 1 min prior to ^{18}F-FOL which reduced uptake of the tracer by ~ 92% in the atherosclerotic plaques *ex vivo*.

5.2.1 *In vitro* binding (IV)

In vitro incubation of mouse aorta and human carotid artery cryosections in folate glucosamine prior to ^{18}F-FOL reduced the total binding of the tracer by 89 ± 3.5% and 88 ± 8.9%, respectively)(Original article IV, Fig. 2, page 3). *In vitro* incubation of macrophages showed that the tracer binds to both M1 and M2 polarized macrophages, but there's significantly more binding to M2 polarized macrophages ($p = 0.011$) (Original article IV, supplement, Fig. S1, page 2, DOI: https://doi.org/10.1038/s41598-018-27618-4).

5.3 *In vivo* tracer stability (III, IV)

In vivo tracer stability was examined in studies III and IV. In study III, on average the red blood cell uptake of the radioactivity was 46.8 ± 1.5% and plasma protein binding was 24.6 ± 4.4% ~ 70 min post injection of ^{18}F-FGln in both atherosclerotic mice and healthy controls. HPLC analysis showed that 78.2 ± 4.0% of the tracer was intact at this timepoint. In study IV, the plasma protein binding of i.v. injected ^{18}F-FOL was 16 ± 6.4% in mice and 15 ± 9.5% in rabbits. In mice, 85 ± 6.0% of the tracer was still intact up to 60 min post-injection. The results indicated good *in vivo* stability of the tracer in both of the studies.

5.4 PET/CT imaging

PET/CT imaging was performed in studies II, III and IV. In study II, at 50–60 min post injection of ^{68}Ga-NODAGA-exendin-4, uptake of the tracer was significantly higher in the atherosclerotic aorta than in the control aorta as determined by

increased SUV_{max} (0.26 ± 0.039 vs. 0.17 ± 0.048, $p = 0.029$) and TBR (SUV_{max}, aorta/SUV_{mean}, blood 1.3 ± 0.15 vs. 1.1 ± 0.13, $p = 0.040$). Myocardial uptake was relatively low, although the hypercholesterolemic mice had significantly higher uptake compared to controls (SUV_{mean} 0.16 ± 0.011 vs. 0.11 ± 0.026, $p < 0.01$). *In vivo* uptake of the tracer in other tissues studied was similar between atherosclerotic and control mice.

In study III, uptake of ^{18}F-FGln in the atherosclerotic aortic arch could be visualized from the PET/CT images whereas uptake of ^{18}F-FDG was not detectable. There was a tendency towards higher TBR of ^{18}F-FGln in the atherosclerotic aortic arch compared to healthy controls (SUV_{max}, aorta/SUV_{mean}, blood 1.95 ± 0.42 vs. 1.44 ± 0.10, $p = 0.09$), but there was no difference in TBR of ^{18}F-FDG (SUV_{max}, aorta/SUV_{mean}, blood 2.77 ± 0.71 vs. 2.74 ± 0.77, $p = 0.96$, respectively). Myocardial uptake of ^{18}F-FGln was significantly lower than that of ^{18}F-FDG (SUV_{mean} 0.43 ± 0.06 vs. 10.84 ± 1.10, $p < 0.0001$).

In study IV, 60-90 min post injection of ^{18}F-FOL, the atherosclerotic mice showed significantly higher TBR in the aortic arch compared to healthy controls (SUV_{max}, aortic arch/SUV_{mean}, blood, 1.5 ± 0.34 vs. 0.71 ± 0.18, $p = 0.00019$). Myocardial uptake of ^{18}F-FOL was significantly lower than that of ^{18}F-FDG (SUV_{max} 0.36 ± 0.069 vs. 12 ± 4.3, $p < 0.0001$, respectively). Blood radioactivity was also significantly lower for ^{18}F-FOL compared to ^{18}F-FDG (SUV_{mean} 0.39 ± 0.15 vs. 0.68 ± 0.22, $p = 0.0057$), indicating a faster clearance from the circulation. *Ex vivo* PET imaging of excised mouse aortas 120 minutes after ^{18}F-FOL injection showed highest tracer uptake in atherosclerotic lesions in the aortic arch. In the rabbits, TBR in the atherosclerotic aorta was similar with both ^{18}F-FOL and ^{18}F-FDG and there was an association in the same segments of the aorta between the TBR obtained from the two tracers (linear mixed model $p = 0.0088$). The average uptake of ^{18}F-FOL in the whole aorta was similar to that of ^{18}F-FDG (SUV_{max}, aorta/SUV_{mean}, blood, 2.6 ± 0.63 vs. 1.9 ± 0.45, $p = 0.074$). TBR of ^{18}F-FOL had a high association with the areal percentage of RAM-11-positive macrophages (linear mixed model $p = 0.0031$) in the corresponding segment of the aorta. Representative images of rabbit PET/CT are presented in Figure 4.

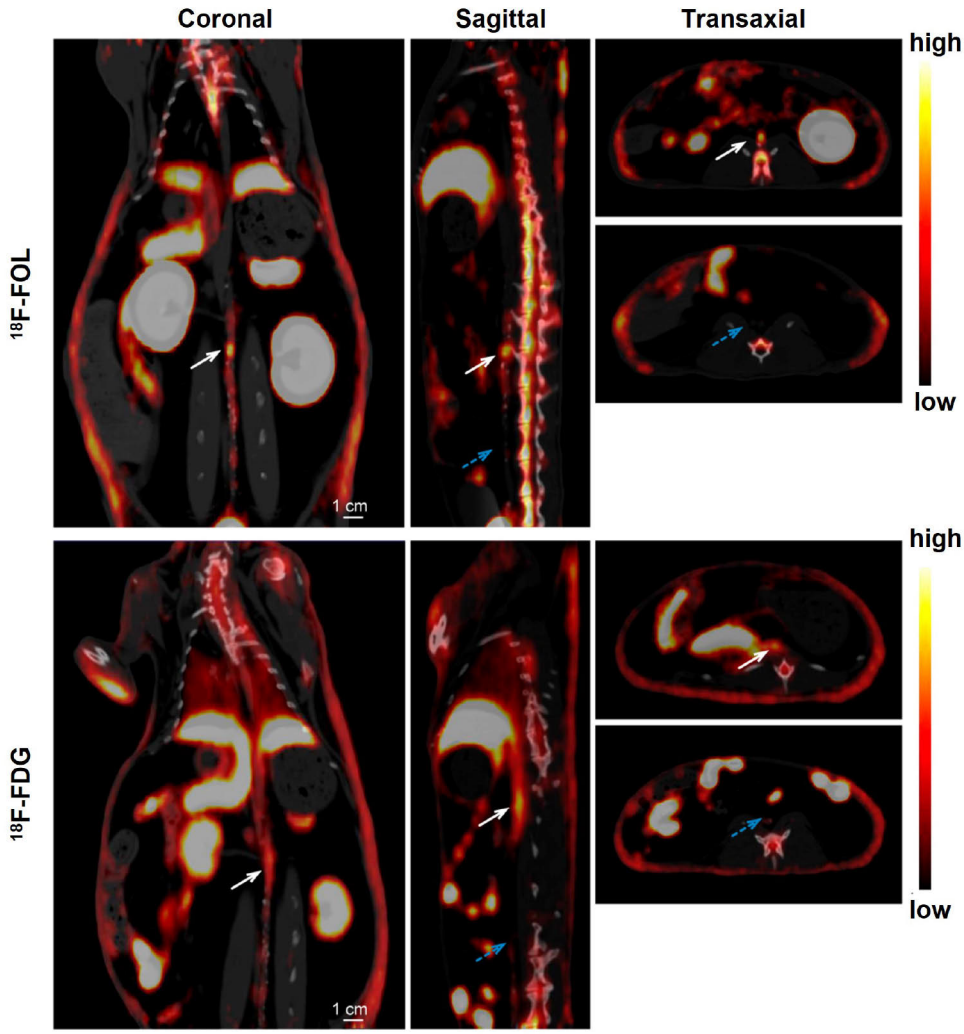

Figure 4. Representative images of rabbit PET/CT with ^{18}F-FOL and ^{18}F-FDG from coronal (left), sagittal (middle) and transaxial (right) view. The white arrows indicates a segment with advanced atherosclerosis with high tracer uptake in the abdominal aorta and the blue arrows indicate segments of aorta with mild atherosclerosis and lower tracer uptake. The color scale is the same in all of the PET images portrayed. (Adopted from the original publication IV with a permission (Fig. 5A, page 8). DOI: https://doi.org/10.1038/s41598-018-27618-4).

5.5 *Ex vivo* biodistribution

Ex vivo biodistribution studies were performed in all of the studies. In study I, there was no difference in ^{18}F-FDG uptake in the aorta between linagliptin treated and HFD mice (SUV 1.0 ± 0.23 vs. 1.1 ± 0.27, $p = 0.74$; aorta-to-blood ratio 3.2 ± 0.78 vs. 3.0 ± 0.58, $p = 0.60$) or between HFD and chow groups (SUV 1.1 ± 0.27 vs. 1.2

± 0.60; $p = 0.54$; aorta-to-blood ratio 3.0 ± 0.58 vs. 2.5 ± 0.70; $p = 0.12$). Uptake of ^{18}F-FDG was similar between the groups in other tissues as well, however linagliptin treated mice had significantly lower uptake in white adipose tissue compared to HFD group (SUV 0.07 ± 0.02 vs. 0.10 ± 0.04, $p = 0.04$).

In study II, at 60 min post injection of ^{68}Ga-NODAGA-exendin-4, both non-diabetic and diabetic hypercholesterolemic mice had significantly higher uptake in the aorta compared to healthy controls (SUV 0.23 ± 0.06 vs. 0.22 ± 0.05 vs. 0.15 ± 0.05, $p = 0.009$; $p = 0.016$, respectively). Highest radioactivity was observed in the kidneys and urine of all the mice.

In study III, atherosclerotic mice had significantly higher uptake of ^{18}F-FGln in the aorta compared to healthy controls (SUV 0.35 ± 0.06 vs. 0.20 ± 0.08, $p = 0.03$). Highest uptake of ^{18}F-FGln was observed in the pancreas. Interestingly, the uptake in the pancreas and liver was significantly lower in atherosclerotic mice compared to controls (SUV pancreas 2.64 ± 0.62 vs. 4.77 ± 0.90, $p = 0.004$, SUV liver 1.20 ± 0.24 vs. 1.90 ± 0.14, $p = 0.0001$).

In study IV, aortic uptake of ^{18}F-FOL 120 min post-injection was significantly higher in atherosclerotic mice compared to controls (%ID/g 2.4 ± 0.56 vs. 1.3 ± 0.46, $p < 0.001$) and atherosclerotic mice from the blocking study (%ID/g 0.28 ± 0.15, $p = 0.0040$). Additionally, when the aortic uptake was compared to blood radioactivity, there was a 5-fold difference in the radioactivity concentration (%ID/g aorta 2.4 ± 0.56 vs. %ID/g blood 0.48 ± 0.20, $p < 0.0001$). The highest radioactivity was found in the kidneys which are known to express FR and the radioactivity was excreted in the urine. The aorta with advanced atherosclerosis in the rabbits had higher uptake of ^{18}F-FOL than aorta with mild atherosclerosis (%ID/g 0.075 ± 0.026 vs. 0.048 ± 0.018, $p = 0.04$). As with the mice, aortic uptake was significantly higher compared to blood radioactivity as intra-animal comparison showed that aorta-to-blood ratio was 16 ± 10, $p = 0.013$. Highest uptake of the tracer was observed in the kidneys, spleen, and liver of the rabbits.

5.6 Autoradiography

In study I, no differences were observed in the uptake of ^{18}F-FDG in atherosclerotic lesions and non-atherosclerotic vessel wall between linagliptin and HFD group (plaque-to-wall ratio, 1.7 ± 0.25 vs. 1.6 ± 0.21, $p = 0.24$). Uptake in the surrounding adventitia was also similar between linagliptin and HFD mice (95 ± 27 vs. 88 ± 18 PSL/mm^2, $p = 0.45$) as was the uptake in the liver (116 ± 29 vs. 134 ± 36 PSL/mm^2, $p = 0.17$). However, hepatic ^{18}F-FDG uptake was significantly lower in the chow group compared to HFD group (93 ± 16 vs. 134 ± 36 PSL/mm^2, $p = 0.03$).

In study II, uptake of ^{68}Ga-NODAGA-exendin-4 was significantly higher in atherosclerotic lesions than in normal vessel walls in both nondiabetic (plaque-to-wall ratio 1.6 ± 0.10, P < 0.0001) and diabetic mice (plaque-to-wall ratio 1.6 ± 0.078, P < 0.0001). Uptake in adventitia was significantly higher in both hypercholesterolemic non-diabetic and diabetic mice compared to healthy controls (21 ± 2.5 vs. 20 ± 3.8 vs. 10 ± 1.3 PSL/mm^2, $p < 0.0001$). All groups showed focally increased uptake of the tracer in the islets of Langerhans. The ratio between islets and exocrine pancreas was similar in nondiabetic and diabetic mice (9.0 ± 3.3 vs. 7.8 ± 2.5, $p = 0.56$) and control mice (11 ± 1.7, $p = 0.42$ vs. non-diabetic and $p = 0.14$ vs. diabetic mice). Tracer uptake in the islets of Langerhans weas completely blocked by the unlabeled exendin-4 peptide.

In study III, uptake of ^{18}F-FGln in atherosclerotic plaques was significantly higher than in normal vessel wall (89.05 ± 18.09 vs. 34.60 ± 5.23 PSL/mm^2, $p = 0.002$) or adventitia (35.48 ± 10.34 PSL/mm^2, $p = 0.001$). The average plaque-to-wall ratio was significantly higher with ^{18}F-FGln than with ^{18}F-FDG (2.90 ± 0.42 vs. 1.93 ± 0.22, $p = 0.004$). The uptake of both tracers in atherosclerotic lesions co-localized with Mac-3- and SLC7A7- positive macrophages. No uptake was observed in the healthy control aortas.

In study IV, uptake of ^{18}F-FOL in mouse atherosclerotic plaques was significantly higher than in healthy vessel wall (plaque-to- wall ratio 2.6 ± 0.58, $p < 0.0001$) or adventitia (plaque-to-adventitia ratio 2.4 ± 0.55, $p < 0.0001$). The tracer uptake co-localized with Mac-3- and FR-β- positive macrophages in the atherosclerotic lesions. In rabbits the sections of aorta with advanced atherosclerosis had significantly higher uptake of ^{18}F-FOL than the sections with only mild atherosclerosis or intimal thickening (41 ± 7.0 vs. 17 ± 2.7 PSL/mm^2, $p = 0.0028$).

6 Discussion

6.1 Imaging in different animal models of atherosclerosis

The hypercholesterolemic mouse model ApoB$^{100/100}$LDLR$^{-/-}$ and its diabetic counterpart IGF-II/ApoB$^{100/100}$LDLR$^{-/-}$ are useful models to study atherosclerosis, but they have some disadvantages in their use. While the mice resemble FH in humans both in the lipid profile and lesion formation, they still lack CETP expression, which in humans transfers esterified cholesterol from HDL to LDL and VLDL (Zhao et al. 2020). The plaque profile is also different from human atherosclerosis where the whole range of atherosclerotic plaques from early fatty streaks to large fibroatheromas and plaque ruptures occur throughout the arteries, whereas the mice mainly develop fibroatheromas in the aorta. The diabetic mice also do not have a fully comparable phenotype as T2DM human patients. The mechanisms why these mice develop insulin resistance is not fully understood, which is why the model requires further characterization. A common side effect of feeding the mice a HFD is, that they develop xanthomas which also happened with some of the mice used in these studies. One mouse had to be euthanized in study I during the intervention period due to the severity of the xanthomas. Overall, mice are the most commonly used experimental animals in atherosclerosis research.

In vivo imaging of mouse aortas is challenging due to the small size of the animals and their vessels. Utilizing PET tracers that have a lot of spillover, such as ^{18}F-FDG due to its high uptake in the myocardium, can hamper the analysis process and thus requires meticulous analysis of the images. Co-registration with contrast-enhanced CT is required for the analysis and the placement of the ROIs needs to be considered carefully. The ROIs in this study were drawn in the aortic arch and aortic root regions whereas it was not possible to completely analyze other parts of the aorta due to the spillover from the myocardium and liver or high activity in the kidneys. However, our studies as well as several other studies suggest that studies in mice can provide an initial proof-of-concept for suitability of a tracer for atherosclerosis imaging using combined *in vivo* and *ex vivo* approaches (Silvola et al. 2011; Hellberg et al. 2016; 2017a; Moisio et al. 2020).

As there are limitations in using mice in *in vivo* imaging due to their small size, the Watanabe rabbit serves as an alternative for imaging atherosclerosis. The rabbits highly resemble human FH in that they develop hypercholesterolemia with high levels of LDL and extremely low levels of HDL and a wide range of atherosclerotic lesions in the aorta and coronary arteries and even exhibit plaque ruptures. The advanced plaques also resemble the plaques seen in humans, having calcification and a lipid or necrotic core that is covered by a fibrotic cap. (Fan et al. 2015.)

The larger size of the rabbits is more compatible with the spatial resolution of *in vivo* PET imaging, although a high-resolution CT is still required to get a proper anatomical view. The downside of using Watanabe rabbits is that they need to be maintained for a much longer period of time than mice for them to develop large atherosclerotic lesions; in study IV for a total of 45 months. Additional procedures such as balloon denudation may be needed to promote lesion development that requires appropriate equipment and a trained professional to conduct the procedures. Also, the development of the lesions does not necessarily happen similarly to human disease. In addition to the costs and time it takes for rabbits to develop the disease, rabbits do not fit the traditional small animal scanner. Rabbits are also timid animals that are easily stressed, which may lead to anorexia and digestive issues, requiring intense care from the researchers and animal technicians. In this study all of the rabbits had to be force fed for a short period of time after they arrived at the Central Animal Laboratory of the University of Turku to ensure their wellbeing. So even though Watanabe rabbits are useful in atherosclerosis research, due to the above-mentioned technical reasons, the other research included in the thesis was mainly done utilizing mice.

6.1.1 Plaque characterization

Plaque burden and immunohistochemical staining and detection of different macrophages were analyzed from aortic root sections of the different mouse strains. Mac-3 is a glycoprotein, which is expressed by macrophages, but not by lymphocytes or granulocytes, and it was used as a general macrophage marker in the studies since it had been used in several previous studies and had a working protocol (Ho & Springer 1983). Mac-3 is also expressed by vascular ECs, DCs and fibroblasts, but it can still be used to successfully distinguish macrophages (Flotte et al. 1983; Inoue et al. 2005). In future studies, F4/80 could be considered as a more specific macrophage marker for mice (Austyn & Gordon 1981). CD68 is expressed on the surface of activated macrophages in humans and is commonly used as a macrophage marker (Ramprasad et al 1996). However, like Mac-3, it is not specific to only macrophages since CD68 also stains fibroblasts and VSMCs (Kunisch et al. 2004; Andreeva et al. 1996). For the rabbits in study IV, RAM-11 was chosen as a

macrophage marker, as it has been widely used in vascular research and staining was technically feasible (Tsukada et al. 1986; Bi et al. 2012; Kim et al. 2017).

The markers for M1 (iNOS) and M2 (MRC-1) polarized macrophages were chosen based on literature and previous studies. iNOS is an intracellular enzyme that mediates production of NO, and it is exclusively expressed in M1 macrophages. Transcription of iNOS is induced by proinflammatory cytokine IFN-γ and upon microbial infection also TNF and INF-α/β are involved. (MacMicking et al. 1997.) MRC-1 is an endocytic surface receptor that mediates binding and ingestion of mannosylated proteins and macromolecules. It is expressed in M2 macrophages and is induced by the anti-inflammatory cytokine IL-4. (Stein et al. 1992.) However, MRC-1 is not exclusively expressed in M2 macrophages as studies have shown that also M1 macrophages express MRC-1 and it cannot also be ruled out that other types of macrophages express MRC-1 (Martinez et al. 2006; Ambarus et al. 2012). MRC-1 is still commonly used as an M2 macrophage marker as its expression has been widely reported in M2 macrophages (Madsen et al. 2013; Lv et al. 2017; Wei et al. 2021).

In our study, aortic root sections were chosen for the evaluation of plaque burden as the sections were cut from the level of coronary ostia, and therefor provide more comparable sections between animals, unlike other vascular parts for example the aortic arch. There were slight differences on the level of the sections, which could be seen from the presence or absence of aortic valve leaflets, but the results obtained from the analysis still provided a reliable result of plaque burden in each animal. The sections were stained with modified Movat's pentachrome, rather than HE, as Movat stains different tissues with different colors (lipids are green, muscle is red, collagen yellow, and cell nuclei black), enabling reliable separation of intima and media.

6.2 GLP-1 therapy

GLP-1 targeting therapies are used to treat hyperglycemia and help maintain glycemic control in T2DM patients. Different types of pharmaceuticals have been developed to inhibit the enzymatic functions of DPP-4, which increases the amount of active circulating GLP-1. On the other hand, GLP-1RAs have been developed, which can avoid the proteolytic effects of DPP-4 and have a longer half-life than the native GLP-1. In addition to glycemic control, many of the GLP-1RAs and DPP-4 inhibitors have shown cardioprotective effects, as well as other beneficial cardiovascular effects. (Nauck et al. 2020.) The expression pattern of GLP-1R in the vasculature is poorly known, but studies have reported GLP-1R expression in mouse and rat aortas (Green et al. 2008; Richards et al. 2014; Zhang et al. 2020). Several GLP-1RAs have shown atheroprotective effects by stabilizing and decreasing the size of the lesions, suppressing the formation of foam cells and inhibiting monocyte

and macrophage infiltration as well as inducing a shift towards M2 polarized macrophages (Rakipovski et al. 2018; Bruen et al. 2019; Nagashima et al. 2011; Arakawa et al. 2010; Helmstädter et al. 2020).

6.2.1 Effects of linagliptin therapy

DPP-4 inhibitors in general have shown atheroprotective effects in different animal models of atherosclerosis and treatment with linagliptin has been reported to decrease atherosclerotic lesion formation and size (Salim et al. 2016; Nishida et al. 2020) and reduce oxLDL induced foam cell formation (Wang et al. 2020). In our study, area of the intima and IMR were similar in the linagliptin, and HFD group. Chow fed mice had significantly smaller area of the intima and IMR than HFD mice, which was expected as HFD is known to promote lesion growth (Silvola et al. 2011; Hellberg et al. 2017a). Plaque inflammation was similar in all groups, although linagliptin treated mice had a tendency towards an increase in M1 polarized macrophages in the plaques. This finding was not consistent with a previous study, where treatment with linagliptin increased M2 macrophage polarization in atherosclerotic mouse aortas (Nishida et al. 2020). Contrasting results on the effects of another DPP-4 inhibitor sitagliptin have also been reported as it was found to increase M2 macrophage polarization in ApoE$^{-/-}$ mice (Brenner et al. 2015), however in a more recent study no effect on macrophage polarization was observed in cultured cells (De Nigris et al. 2021). In our study, the amount of M2 polarized macrophages still surpassed the amount of M1 polarized macrophages, which is consistent with a previous study utilizing the same mouse model (Hellberg et al. 2016). Clinical studies have shown little to no beneficial effects of linagliptin treatment on cardiovascular health outcomes, including major atherosclerotic complications (de Boer et al. 2017; Tripolt et al. 2018; McGuire et al. 2019), suggesting there is only limited benefit of linagliptin treatment on atherosclerosis.

DPP-4 levels rise in different liver conditions such as hepatitis C and NAFLD/ non-alcoholic steatohepatitis (NASH) and it is likely the cause of decreased glucose tolerance and insulin resistance (Sharma et al. 2022). In NAFLD, DPP-4 expression can be increased by 15-fold compared to healthy livers and is negatively correlated with homeostasis model assessment-insulin resistance and body mass index (Miyazaki et al. 2012). In clinical trials, treatment with DPP-4 inhibitor sitagliptin reduced hepatic steatosis in NASH (Alam et al. 2018) but not in NAFLD (Cui et al. 2016). Linagliptin treatment has previously reported to alleviate hepatic steatosis and inflammation in preclinical mouse models of NASH (Klein et al. 2014) and NAFLD (Santos et al. 2020) however, in our study linagliptin treatment only improved glucose tolerance and reduced hepatic inflammation but had no effect on steatosis. The different outcome concerning hepatic steatosis in NAFLD could be explained

by the higher dose of linagliptin, 30 mg/kg/day, whereas in our study the dose was only 10 mg/kg/day. However, the same dose has been shown to alleviate hepatic steatosis in *db/db* mice (Michurina et al. 2016). In these mouse models NAFLD is more pronounced than in IGF-II/LDLR$^{-/-}$ApoB$^{100/100}$ mice, which in part may explain the different outcomes of the interventions.

DPP-4 inhibition in general has shown anti-inflammatory effects which was also observed in our study in WAT where uptake of ^{18}F-FDG was significantly decreased suggesting decreased inflammation. The results are in line with other studies reporting reduced macrophage infiltration and shift to M2 macrophage polarization in WAT (Dobrian et al. 2011; Zhuge et al. 2016).

6.2.2 SGLT2 therapy

Sodium-glucose co-transporter-2 (SGLT2) inhibitors are antidiabetic drugs that lower blood glucose levels by promoting urinary excretion of glucose. Initial randomized control trials showed unprecedented cardiovascular benefits of SGLT2 inhibitors including lower rates of deaths from cardiovascular causes and hospitalization due to heart failure (Zinman et al. 2015; Wiviott et al. 2019) as well as lower risk of cardiovascular events (Neal et al. 2017). This has piqued the interest for further research and there are several different theories of how SGLT2 inhibitors exert their cardioprotective effects. The so called “thrifty substrate” hypothesis explained the cardioprotective effects of SGLT2 inhibitor empagliflozin by a shift in myocardial metabolism to utilize energy-efficient ketone bodies instead of glucose or FFAs, improving myocardial efficiency and function (Ferrannini et al. 2016; Mudaliar et al. 2016). An untargeted metabolomic study revealed that 162 metabolites were altered by empagliflozin, suggesting increased utilization of ketone bodies and branched chain amino acids catabolism (Kappel et al. 2017). A recent randomized control study utilizing PET/CT imaging, reported that SGLT2 inhibition by empagliflozin reduced myocardial glucose uptake but had no effect on FFA uptake or myocardial oxygen consumption, suggesting that myocardial substrate utilization does indeed shift towards other sources (Lauritsen et al. 2021). However, empagliflozin has also been reported to reduce myocardial oxygen consumption at rest which could contribute to its cardioprotective effects (Søndergaard et al. 2022). Reduction in heart failure hospitalization is suggested to be due to the diuretic effects of empagliflozin, which results in fluid clearance from the interstitial fluid space, thus easing congestion (Hallow et al. 2018). In a preclinical study, dapagliflozin regulated M2 macrophage polarization via reactive oxygen and nitrogen species signal transducer and activator of transcription 3 pathway, resulting in reduced myofibroblast infiltration and cardiac fibrosis (Lee et al. 2017). There are still many unanswered questions about the effects of SGLT2 inhibitors in patients with T2DM

and CVD and further research is needed to elucidate the full spectrum of cardiovascular effects of these treatments.

6.3 Evaluation of the PET tracers for imaging atherosclerotic disease activity

PET imaging of atherosclerosis gives valuable information about plaque biology such as inflammation and neovascularization. ^{18}F-FDG is the most widely used PET tracer for atherosclerosis imaging, but due to its unspecific nature as well as high myocardial uptake and competing with blood glucose for GLUT receptors, its use has its limitations. Tracers targeting macrophages provide more specific information about the inflammatory activity in atherosclerosis since they are the most abundant cell type in advanced lesions and express several different surface molecules that can be targeted by PET tracers. (Hyafil & Vigne, 2019.)

6.3.1 ^{68}Ga-NODAGA-exendin-4

GLP-1 is known for controlling blood glucose homeostasis, but its protective effects on the cardiovascular system have been widely reported (Hernandez et al. 2018; Rakipovski et al. 2018; Gerstein et al. 2019; Verma et al. 2022; Ying et al. 2023). Therefore, we designed a study to investigate a GLP-1R targeting tracer in imaging atherosclerosis. Uptake of ^{68}Ga-NODAGA-exendin-4 in atherosclerotic aorta could be visualized from the *in vivo* PET/CT images, which was further verified in *ex vivo* ARG analysis of the aortas, where the tracer uptake was evident in the macrophage rich atherosclerotic plaques in both non-diabetic (LDLR$^{-/-}$ApoB$^{100/100}$) and diabetic (IGF-II/LDLR$^{-/-}$ApoB$^{100/100}$) mice. Uptake in the healthy vessel wall was significantly lower than in the plaques, and the aortas of healthy control mice (C57BL/6N) showed very little uptake of the tracer. Blocking with pre-injected unlabeled exendin-4 significantly reduced uptake of the tracer in atherosclerotic lesions, however some uptake still remained. This could be explained by unspecific radioactivity in the necrotic cores of the lesions, which has been previously reported (Ståhle et al. 2020). Even though uptake of ^{68}Ga-NODAGA-exendin-4 could be visualized from the *in vivo* PET/CT images, the TBR was only 1.3 which is relatively low if we compare it to ^{18}F-FDG where a TBR of 2.1 has been reported (Hellberg et al. 2017b). However, the myocardial and lung uptake of ^{68}Ga-NODAGA-exendin-4 was low, providing only low amount of background activity and thus enabling *in vivo* imaging of GLP-1R expression in atherosclerotic lesions in the nearby vessels.

The immunohistochemical stainings showed that GLP-1R expression co-localized with macrophage-rich areas with both M1 (iNOS) and M2 (MRC-1) polarized macrophages, though the co-localization was most prominent with M2

macrophages. The results are in line with previous studies reporting that GLP-1R activation induces a shift from M1 polarization to M2 (Vinué et al. 2017; Bruen et al. 2019). Expression of GLP-1R has also been shown to increase during MI (Pan et al. 2017; Ståhle et al. 2020) and in M2 polarized macrophages in coronary heart disease patients (Yang et al. 2021), providing more protective effects during MI healing and progression of atherosclerosis.

Even though the ARG and immunofluorescence staining both confirmed that GLP-1R is expressed in atherosclerotic lesions, the expression pattern was very diffuse. M2 polarized macrophages are usually related to the resolution of inflammation, so a study using different time-points concerning the development of atherosclerosis could shed new light into the expression pattern of GLP-1Rs during atherogenesis. In our study, no expression of GLP-1R was seen in the aortic ECs or VSMCs of the mice. These results are in line with a previous study where GLP-1R expression was not seen in human coronary artery ECs or VSMCs (Baggio et al. 2018). However, contrasting results have also been reported from several preclinical studies. Mice with endovascular injury showed GLP-1R expression that co-localized with α-SMA positive VSMCs in the media and neointima of the lesions (Hirata et al. 2013). GLP-1RA liraglutide attenuated cultured VSMC migration, proliferation, and apoptosis via direct activation of GLP-1R (Shi et al. 2015).

Even though ^{68}Ga-NODAGA-exendin-4 detected GLP-1R expression in inflamed atherosclerotic lesions *in vivo*, additional research is needed to elucidate the expression pattern of GLP-1R in healthy and atherosclerotic vessels in mice and humans. This would provide further information about the translational relevance of the tracer.

6.3.2 ^{18}F-FGln

Glutamine is an amino acid that has many roles from metabolism to nucleotide synthesis. It is an essential nutrient for lymphocytes, macrophages, and neutrophils and during infection, the consumption rate of glutamine is greater than glucose in all immune cells. (Cruzat et al. 2018.) Macrophages utilize glucose, FAs, and glutamine in their metabolic pathways, but the role of glutamine is especially important in phagocytic and secretory activity of the cells (Newsholme et al. 1996). The product of glutaminolysis, α-ketoglutarate, promotes M2 macrophage polarization and activation and suppresses production of proinflammatory cytokines by restricting M1 macrophage activation (Liu et al. 2017).

Although glutamine-based PET-imaging has successfully been used to image different cancers and infections, its efficacy in atherosclerosis imaging has not yet been established. Our study was the first to report that ^{18}F-FGln uptake can be visualized in mouse atherosclerotic aortic arch in PET/CT images, although the TBR

did not statistically differ from that of healthy controls. However, *in vivo* uptake of ^{18}F-FDG was high in the myocardium and uptake in the atherosclerotic aortic arch could therefore not be detected. Myocardial uptake of ^{18}F-FGln on the other hand was significantly lower than that of ^{18}F-FDG allowing detection of atherosclerotic lesions in the aortic arch. So eventhough the use of ^{18}F-FGln has its limitations, it is still a noteworthy tracer for *in vivo* atherosclerosis imaging.

In LDLR$^{-/-}$ mice, atherosclerotic lesions rich with M2 macrophages expressing SLC1A5 could be distinguished by the increased uptake of ^{11}C-glutamine *ex vivo* (Tavakoli et al. 2017). In our study, analysis of the ARG and immunohistochemistry showed, that ^{18}F-FGln was also taken up in atherosclerotic plaques rich with macrophages, and co-localized with expression of SLC7A7. The uptake was significantly higher in the plaques than healthy vessel wall or adventitia and no uptake was observed in the healthy control aortas. ^{18}F-FGln also had significantly higher plaque-to-healthy vessel wall ratio than ^{18}F-FDG. As we only studied macrophages and the expression of SLC7A7 in the aortic arch, it cannot be excluded that also other cell types and glutamine transporters may be involved in the uptake of ^{18}F-FGln. As mentioned previously, lymphocytes and neutrophils also utilize glutamine in their metabolism and both cell types are present in atherosclerotic lesions. In our study, immunohistochemical staining of aortic root sections also revealed the presence of other glutamine transporters, which did not co-localize with macrophages but are in line with previous reports of glutamine transporters and their expression patterns (Tavakoli et al. 2017). An *in vitro* blocking study could provide more insight whether other glutamine transporters are also involved in the cellular uptake of ^{18}F-FGln.

Interestingly, the uptake of ^{18}F-FGln was significantly lower in the pancreas and liver of atherosclerotic mice compared to healthy controls. The reason for this can only be speculated, as we have no histological data from these organs, nor do we have any information about plasma biomarkers from these mice. In the pancreas, glutamine and its metabolite glutamate are important factors in the regulation of β-cell function and insulin secretion, but the exact interplay with other factors such as glucose, involved in these processes remains unclear. In the liver, glutamine and glutamate are utilized in gluconeogenesis. (Newsholme et al. 2003.) As both organs have an integral role in glucose homeostasis, one could speculate, that the atherosclerotic mice might have had reduced glucose tolerance. Feeding mice a HFD has been reported to induce glucose intolerance and hepatic steatosis, which could explain the difference between the atherosclerotic mice and controls in our study (Saxena et al. 2022). It would also be of high interest to evaluate the tracer using the hypercholesterolemic and diabetic IGF-II/ApoB$^{100/100}$LDLR$^{-/-}$ mice to see, if the diabetic state affects tracer uptake.

6.3.3 ^{18}F-AlF-NOTA-folate

FR-β is a promising target for atherosclerotic inflammation imaging as it is highly expressed in macrophages (Nakashima-Matsushita et al. 1999; Steintz et al. 2022). In previous studies, FR-β based tracers have been successfully used to detect atherosclerotic lesions both *in vitro* and *in vivo* in SPECT-imaging (Ayala-López et al. 2010; Jager et al. 2014; Müller et al. 2014; Winkel et al. 2014). Therefore, we designed a study to evaluate FR-β targeting PET-tracer in imaging atherosclerotic inflammation. ^{18}F-FOL was rapidly removed from the circulation and the myocardial uptake was low, enabling *in vivo* visualization of atherosclerotic lesions in mouse and rabbit aortas with a comparable TBR to ^{18}F-FDG. Uptake of the tracer showed specificity to FR-β as blocking with folate glucosamine significantly reduced tracer binding. It was recently discovered that in addition to FR-β, ^{18}F-FOL also binds FR-α in a rat glioma model and the uptake was similarly blocked with folate glucosamine (Miner et al. 2023). As FR-α is only expressed in epithelial and cancer cells (Elnakat & Ratnam 2004), it should not account for any of the binding observed in our study. Tracer uptake was significantly higher in advanced lesions than mild lesions, suggesting that it could be useful in discerning high and low risk plaques as well as monitoring disease progression.

After the study included in this thesis, imaging of atherosclerotic inflammation with NOTA-folate has now also been evaluated using a ^{68}Ga label. ^{68}Ga-NOTA-folate uptake in atherosclerotic lesions could be detected *in vivo* in atherosclerotic mice and *ex vivo* studies confirmed uptake in atherosclerotic plaques rich with macrophages. The tracer had low myocardial uptake and the plaque-to-healthy vessel wall ratio was higher than with ^{18}F-FDG. (Moisio et al. 2020.)

Cell binding studies showed that ^{18}F-FOL binds more to M2 polarized rather than M1 polarized macrophages, which is in line with a previous study where (99m) Tc-folate accumulated in M2 macrophage rich lesions and FR-β mRNA expression was significantly increased in M2 macrophages compared to M1 macrophages (Jager et al. 2014). Another study further verified, that ^{18}F-FOL preferentially binds M2 polarized macrophages in a rat model of experimental autoimmune encephalomyelitis (Elo et al. 2019). However, it was also reported that ^{18}F-FOL readily binds M1 rather than M2 polarized macrophages in a rat model of autoimmune myocarditis (Jahandideh et al. 2020). Indeed, both macrophage types express FR-β, but studies indicate that the expression tends to be higher in M2 polarized macrophages (Puig-Kröger et al. 2009; Jager et al. 2014; Warmink et al. 2022). In addition, FR-β expression has been observed in human proinflammatory monocytes (Shen et al. 2012).

While FR-β based tracers in general have high specificity to target activated macrophages, there are reports of unspecific uptake. ^{18}F-fluorophenylfolate has shown high unspecific uptake in the intestine and bile due to hepatobiliary excretion

(Bettio et al. 2006; Ross et al. 2008). In our study, uptake in the small intestine was higher than most other tissues, but the highest uptake was observed in the kidneys in both mice and rabbits. This is most likely due to the tracer being secreted through urine rather than the hepatobiliary system and specific uptake in the kidneys which are known to express FRs (Selhub & Franklin, 1984; Sandoval et al. 2014).

As ^{18}F-FOL showed promising results in detecting inflamed atherosclerotic lesions *in vivo*, *ex vivo* and *in vitro*, clinical studies seem warranted to determine whether the tracer could be utilized to image atherosclerotic inflammation in patients.

6.4 Future aspects of PET imaging of atherosclerosis

PET/CT and also PET/MR imaging of atherosclerosis provides valuable information about disease mechanisms and enables monitoring of disease progression. As such it will continue to serve as a valuable tool for researchers. Novel tracers targeting different aspects of the disease are being developed and methods like single cell RNA-sequencing and transcriptomics expand our knowledge about atherosclerosis and can reveal new target molecules for both imaging and therapeutic purposes (Pasterkamp et al. 2022; Örd et al. 2023; Maier et al. 2024).

Total body PET enables simultaneous imaging of the whole body as the detector rings cover the entire body and allow highly accurate detection of the emitted radiation from the body, providing up to 40-fold increase in sensitivity (Cherry et al. 2018). As atherosclerosis can affect arteries in different regions of the body, total body PET allows simultaneous quantitative imaging of different organs and can provide valuable information about regional differences for example in blood flow and enable early detection of atherosclerotic plaque development (Knuuti et al. 2023; Maier et al. 2024). Indeed, imaging technology is constantly improving giving the new devises better resolution, higher sensitivity, and shorter imaging time as well as improvements on image quality, reconstruction and even implementation of AI (Meester et al. 2019; Prenosil et al. 2022; Aide et al. 2022).

7 Summary and Conclusions

The thesis investigated the effects of linagliptin on atherosclerotic plaque formation and inflammation as well as hepatic inflammation and steatosis. In addition, three novel PET tracers for imaging atherosclerotic disease activity were evaluated in mouse and rabbit models of atherosclerosis.

1. Three month treatment with linagliptin significantly improved glucose tolerance and increased insulin secretion of hypercholesterolemic and diabetic mice. Linagliptin treatment showed no effect on plaque formation or inflammation, determined by histology and aortic ^{18}F-FDG uptake. There was no effect on hepatic steatosis, but linagliptin treatment significantly decreased hepatic inflammation.

2. ^{68}Ga-NODAGA-exendin-4 detected GLP-1R expression in atherosclerotic lesions in both diabetic and non-diabetic hypercholesterolemic mice. Uptake of the tracer co-localized with M1 and M2 polarized macrophages, though it was most prominent with M2 macrophages.

3. ^{18}F-FGln uptake could be visualized in atherosclerotic aortic arch of hypercholesterolemic mice *in vivo*, but the TBR did not differ from the control mice. The uptake of ^{18}F-FGln co-localized with Mac-3 and SLC7A7 positive macrophages.

4. ^{18}F-FOL showed rapid clearance from the circulation and the uptake in atherosclerotic lesions could be visualized *in vivo* in hypercholesterolemic mice and atherosclerotic rabbits. TBR was comparable to ^{18}F-FDG but uptake in the myocardium was lower with ^{18}F-FOL. Lesional uptake of the tracer co-localized with macrophages and the uptake was higher in advanced lesions.

All of the three tracers studied showed potential in imaging atherosclerotic disease activity *in vivo*, although there were some limitations to their use.

Acknowledgements

This study was conducted in Turku PET Centre, Institute of Clinical Medicine, Department of Clinical Physiology and Nuclear Medicine, Turku University Hospital and University of Turku, Turku, Finland during the years 2015–2022. It was conducted within the Finnish Centre of Excellence in Cardiovascular and Metabolic Diseases supported by the Academy of Finland, University of Turku, Turku University Hospital and Åbo Akademi University. I want to express my gratitude to former and present Heads of the Department of Clinical Physiology and Nuclear Medicine, Professor Emeritus Jaakko Hartiala and Professor Jukka Kemppainen and Director of Turku PET Centre Professor Juhani Knuuti, for providing excellent facilities for the research.

This study was financially supported by the Drug Reasearh Doctoral Programme, University of Turku Graduate school, Innovative Medicines Initiative Joint Undertaking, resources of which are composed of financial contribution from the European Union's Seventh Framework Programme and EFPIA companies' kind contribution, grants from the Sigrid Jusélius Foundation, the Finnish Foundation for Cardiovascular Research, Jane and Aatos Erkko Foundation, State Research Funding of Turku University Hospital, Jalmari and Rauha Ahokas Foundation, Ida Montin Foundation, the Instrumentarium Science Foundation, Academy of Finland, InFLAMES Flagship Programme of the Academy of Finland and Orion Research Foundation.

I want to warmly thank my supervisors, Professor Anne Roivainen and Professor Antti Saraste. You provided me help and guidance throughout these years and made this thesis possible. Anne, your expertise in preclinical imaging has helped me immensely to conduct research and find myself as a researcher and I have always felt welcomed if I've had any questions or worries. Antti, your profound knowledge of cardiovascular research and encouragement have been invaluable throughout this journey.

I wish to thank the official reviewers of my thesis: Docent Katariina Öörni and Associate Professor Kirsten Bouchelouche. I appreciate the time and effort you took to review my thesis and the valuable comments and suggestions you had to improve the quality of it. I am also very grateful to Professor Sohvi Hörkkö for accepting the

invitation to act as my opponent. I want to thank my Follow-up Committee members, Professor Eriika Savontaus, Professor Pirjo Nuutila and Professor Juhani Knuuti for the help and guidance during this journey. The Director of Drug Research Doctoral Programme Professor Ullamari Pesonen as well as Coordinator Eeva Valve are also thanked.

The projects included in this thesis would not have been possible without teamwork and collaboration. Professor Seppo Ylä-Herttuala from the University of Eastern Finland and Professor Maria Gomez from the University of Lund are warmly thanked for the collaboration within the CoE. Adjunct Professor Matti Jauhiainen from Minerva Institute for Medical Research is aknowledged for the help and expertise in lipid analyses and metabolism. I wish to thank Adjunct Professor Mirva Södersröm and Professor Emeritus Pekka Saukko for providing expertise in pathological analyses and Docent Harri Hakovirta for providing crucial artery samples for the research. The radiochemists are warmly thanked for providing the tracers for the studies. Thank you Adjunct Professor Xiang-Guo Li, Olli Eskola, Olli Metsälä, Olli Moisio, Maxwell Miner and and all the other personel involved in the radiochemistry processes. Professor Philip Low, Professor Minna Kaikkonen, Qingshou Chen, Tiit Öörd, Aarthi Ravindran, Miikka Tarkia, Jenni Huusko, Virva Saunavaara, Saija Hurme, Senthil Palani, and Jarkko Hytönen are acknowledged for their expertise, scientific contribution and collaboration. I also want to show my appreciation to Timo Kattelus for the skilled processing of images and figures for the manuscripts.

I want to show my appreciation to Johanna Silvola, Mia Ståhle and Sanna Hellberg for introducing me to the wonderful world of atherosclerosis research and teaching me all that I need to know about preclinical PET studies. A very special thank you to Heidi Liljenbäck who has been a vital part of all the animal studies and a teacher to many of the different techniques I've learned during these past years. Your expertise in animal studies is truly inspiring. Thank you also to Aake Honkaniemi for taking care of animal imaging and helping with the studies, I truly appreciate it. I want to thank Marja-Riitta Kajaala and Erica Nyman for your skilled contribution to histology and immunohistochemical stainings. The staff of Central Animal Laboratory of University of Turku took wonderful care of the study animals. Thank you former and present Director Ulla-Marjut Jaakkola and Emrah Yatkin, office staff Nina Kulmala and Aila Saari and all the animal technicians for your hard work.

I wish to thank my present and former colleagues in Roivainen-Saraste group: Andriana, Erika, Arina, Mia, Heidi, Sanna, Helena, Riikka, Anu, Meeri, Maria, Petri, Olli, Max, Maxwell, Johanna, Senthil, Aida, Sauli, Imran, Arman and Miikka and undergraduates Reija and Aino. Thank you for the supportive work space and being there when I needed help. We've all had our ups and downs but as a team and as

friends, we've survived and prospered. I want to thank the expert personnel at the Turku PET Centre for all your help. Special thanks to Sanna, Eija, Emilia, Minna, Kalle, Tuula, Rami, Marko, Heidi, Jarmo and Leena.

I want to thank my dear friends in my life. My fellow biologists Julia, Ella, Tarja, Hanna and Tuuli, thank you for all the fun times in and out of university. Our little cooking and board game nights have always brightened up my days. Thank you Jordan for all the fun times we've shared (and tea spilled) and all your support, I treasure our friendship dearly. A very special thank you to Taru and Alisa, for being the best friends a girl could ever have and keeping me sane. Taru, we've been friends for what feels like an eternity. You have always been there for me when I needed someone to talk to, we've had fun (though sometimes a bit rough) trips to cat shows and even funnier times at the stables. Alisa, even though you live across the pond you are one of the most important people in my life and I'm truly greatful to have met you. Our gamenights and late night talks have become a necessity for me. I shall never stop sending you endless amounts of memes and funny videos.

Finally, I would like to thank my parents Riitta and Markku, my sister Jonna and my partner Mika for all your support. Thank you for always being there for me and believing in me. Without you, I wouldn't be here.

Turku, June 2024
Jenni Virta

References

Abarbanell A M., Herrmann J L., Weil B R., Wang Y., Tan J., Moberly S P., Fiege J W. & Meldrum D R., 2010. Animal models of myocardial and vascular injury. *J Surg Res*. 162(2), p. 239-249. Available at: https://doi.org/10.1016/j.jss.2009.06.021.

Aide N., Lasnon C., Desmonts C., Armstrong I S., Walker M D. & McGowan D R., 2022. Advances in PET/CT Technology: An Update. *Semin Nucl Med.* 52(3), p. 286-301. Available at: https://doi.org/10.1053/j.semnuclmed.2021.10.005.

Aini K., Fukuda D., Tanaka K., Higashikuni Y., Hirata Y., Yagi S., Kusunose K., Yamada H., Soeki T. & Sata M., 2019. Vildagliptin, a DPP-4 Inhibitor, Attenuates Endothelial Dysfunction and Atherogenesis in Nondiabetic Apolipoprotein E-Deficient Mice. *Int Heart J*. 60(6), p. 1421-1429. Available at: https://doi.org/10.1536/ihj.19-117.

Alam S., Ghosh J., Mustafa G., Kamal M. & Ahmad N., 2018. Effect of sitagliptin on hepatic histological activity and fibrosis of nonalcoholic steatohepatitis patients: a 1-year randomized control trial. *Hepat Med*.10, p. 23-31. Available at: https://doi.org/10.2147/HMER.S158053.

Ambarus C A., Krausz S., van Eijk M., Hamann J., Radstake T R D J., Reedquist K A., Tak P P. & Baeten D L P., 2012. Systematic validation of specific phenotypic markers for in vitro polarized human macrophages. *J Immunol Methods.* 375(1-2), p. 196-206. Available at: https://doi.org/10.1016/j.jim.2011.10.013.

Ancuta P., Rao R., Moses A., Mehle A., Shaw S K., Luscinskas F W. & Gabuzda D., 2003. Fractalkine preferentially mediates arrest and migration of CD16+ monocytes. *J Exp Med*. 197(12), p. 1701-1707. Available at: https://doi.org/10.1084/jem.20022156.

Andreeva E R., Pugach I M. & Orekhov A N., 1997. Subendothelial smooth muscle cells of human aorta express macrophage antigen in situ and in vitro. *Atherosclerosis*. 135(1), p. 19-27. Available at: https://doi.org/10.1016/s0021-9150(97)00136-6.

Antoniades C. & West H W., 2021. Coronary CT angiography as an 'one-stop shop' to detect the high-risk plaque and the vulnerable patient. *Eur Heart J.* 42(37), p. 3853-3855. Available at: https://doi.org/10.1093/eurheartj/ehab538.

Arakawa M., Mita T., Azuma K., Ebato C., Goto H., Nomiyama T., Fujitani Y., Hirose T., Kawamori R. & Watada H., 2010. Inhibition of monocyte adhesion to endothelial cells and attenuation of atherosclerotic lesion by a glucagon-like peptide-1 receptor agonist, exendin-4. *Diabetes.* 59(4), p. 1030-1037. Available at: https://doi.org/10.2337/db09-1694.

Armani C., Catalani E., Balbarini A, Bagnoli P. & Cervia D., 2007. Expression, pharmacology, and functional role of somatostatin receptor subtypes 1 and 2 in human macrophages. *J Leukoc Biol.* 81(3), p. 845-855. Available at: https://doi.org/10.1189/jlb.0606417.

Austyn J M. & Gordon S., 1981. F4/80, a monoclonal antibody directed specifically against the mouse macrophage. *Eur J Immunol.* 11(10), p. 805-815. Available at: https://doi.org/10.1002/eji.1830111013.

Ayala-López W., Xia W., Varghese B. & Low P S., 2010. Imaging of atherosclerosis in apoliprotein e knockout mice: targeting of a folate-conjugated radiopharmaceutical to activated macrophages. *J Nucl Med*. 51(5), p. 768-774. Available at: https://doi.org/10.2967/jnumed.109.071324

Badimon L. & Vilahur G., 2014. Thrombosis formation on atherosclerotic lesions and plaque rupture. *J Intern Med*. 276(6), p. 618-632. Available at: https://doi.org/10.1111/joim.12296.

Bae E J., 2016. DPP-4 inhibitors in diabetic complications: role of DPP-4 beyond glucose control. *Arch Pharm Res.* 39(8), p. 1114-1128. Available at: https://doi.org/10.1007/s12272-016-0813-x.

Bandara N., Zheleznyak A., Cherukuri K., Griffith D A., Limberakis C., Tess D A., Jianqing C., Waterhouse R. & Lapi S E., 2016. Evaluation of Cu-64 and Ga-68 Radiolabeled Glucagon-Like Peptide-1 Receptor Agonists as PET Tracers for Pancreatic β cell Imaging. *Mol Imaging Biol.* 18(1), p. 90-98. Available at: https://doi.org/10.1007/s11307-015-0861-5.

Bartoli-Leonard F., Wilkinson F L., Schiro A., Serracino Inglott F., Alexander M Y. & Weston R., 2021. Loss of SIRT1 in diabetes accelerates DNA damage-induced vascular calcification. *Cardiovasc Res*. 117(3), p. 836-849. Available at: https://doi.org/10.1093/cvr/cvaa134.

Beckman J A., Creager M A & Libby P., 2002. Diabetes and atherosclerosis: epidemiology, pathophysiology, and management. *JAMA*. 287(19), p. 2570-2581. Available at: https://doi.org/10.1001/jama.287.19.2570.

Bentzon J F. & Falk E., 2010. Atherosclerotic lesions in mouse and man: is it the same disease? *Curr Opin Lipidol*. 21(5), p. 434-440. Available at: https://doi.org/10.1097/MOL.0b013e32833ded6a.

Bentzon J F., Otsuka F., Virmani R. & Falk E., 2014. Mechanisms of Plaque Formation and Rupture. *Circ Res.,* 114(12):1852-66. Available at: https://do.org/10.1161/CIRCRESAHA.114.302721.

Bettio A., Honer M., Müller C., Brühlmeier M., Müller U., Schibli R., Groehn V., Schubiger A P. & Ametamey S M., 2006. Synthesis and preclinical evaluation of a folic acid derivative labeled with 18F for PET imaging of folate receptor-positive tumors. *J Nucl Med.* 47(7), p. 1153-1160.

Bhori M., Rastogi V., Tungare K. & Marar T., 2022. A review on interplay between obesity, lipoprotein profile and nutrigenetics with selected candidate marker genes of type 2 diabetes mellitus. *Mol Biol Rep*.49(1), p. 687-703. Available at: https://doi.org/10.1007/s11033-021-06837-5.

Bi Y., Xu K., Zhong H., Qi X., Zhang Z. & Ni Y., 2012. A novel in vivo rabbit model of abdominal aortic aneurysm induced by periarterial incubation of papain. *J Vasc Interv Radiol*. 23(11), p. 1529-1536. Available at: https://doi.org/10.1016/j.jvir.2012.08.007.

Bird J L E., Izquierdo-Garcia D., Davies J R., Rudd J H F., Probst K C., Figg N., Clark J C., Weissberg P L., Davenport A P. & Warburton E A., 2010. Evaluation of translocator protein quantification as a tool for characterising macrophage burden in human carotid atherosclerosis. *Atherosclerosis.* 210(2), p. 388-391. Available at: https://doi.org/10.1016/j.atherosclerosis.2009.11.047.

Bjørklund M M., Hollensen A K., Hagensen M K., Dagnaes-Hansen F., Christoffersen C., Mikkelsen J G. & Bentzon J F., 2014. Induction of atherosclerosis in mice and hamsters without germline genetic engineering. *Circ Res.* 114(11), p. 1684-1689. Available at: https://doi.org/10.1161/CIRCRESAHA.114.302937.

Blin M G., Bachelier R., Fallague K., Moussouni K., Aurrand-Lions M., Fernandez S., Guillet B., Robert S., Foucault-Bertaud A., Bardin N., Blot-Chabaud M., Dignat-George F. & Leroyer A S., 2019. CD146 deficiency promotes plaque formation in a mouse model of atherosclerosis by enhancing RANTES secretion and leukocyte recruitment. *J Mol Cell Cardiol.* 130, p. 76-87. Available at: https://doi.org/10.1016/j.yjmcc.2019.03.017.

Blomberg B A. & Høilund-Carlsen P F., 2015. [^{18}F]-fluorodeoxyglucose PET imaging of atherosclerosis. *PET Clin.* 10(1), p. 1-7. Available at: https://doi.org/10.1016/j.cpet.2014.09.001.

Blykers A., Schoonooghe S., Xavier C., D'hoe K., Laoui D., D'Huyvetter M., Vaneycken I., Cleeren F., Bormans G., Heemskerk J., Raes G., De Baetselier P., Lahoutte T., Devoogdt N., Van Ginderachter J A. & Caveliers V., 2015. PET Imaging of Macrophage Mannose Receptor-Expressing Macrophages in Tumor Stroma Using ^{18}F-Radiolabeled Camelid Single-Domain Antibody Fragments. *J Nucl Med*. 56(8), p. 1265-1271. Available at: https://doi.org/10.2967/jnumed.115.156828.

Bonthu S., Heistad D D., Chappell D A., Lamping K G. & Faraci F M., 1997. Atherosclerosis, vascular remodeling, and impairment of endothelium-dependent relaxation in genetically altered

hyperlipidemic mice. *Arterioscler Thromb Vasc Biol*. 17(11), p. 2333-2340. Available at: https://doi.org/10.1161/01.atv.17.11.2333.

Borén J. & Williams K J., 2016. The central role of arterial retention of cholesterol-rich apolipoprotein-B-containing lipoproteins in the pathogenesis of atherosclerosis: a triumph of simplicity. *Curr Opin Lipidol*. 27(5), p. 473-483. Available at: https://doi.org/10.1097/MOL.0000000000000330.

Borén J., Chapman M J., Krauss R M., Packard C J., Bentzon J F., Binder C J., Daemen M J., Demer L L., Hegele R A., Nicholls S J., Nordestgaard B G., Watts G F., Bruckert E., Fazio S., Ference B A., Graham I., Horton J D., Landmesser U., Laufs U., Masana L., Pasterkamp G., Raal F J., Ray K K., Schunkert H., Taskinen M R., van de Sluis B., Wiklund O., Tokgozoglu L., Catapano A L. & Ginsberg H N., 2020. Low-density lipoproteins cause atherosclerotic cardiovascular disease: pathophysiological, genetic, and therapeutic insights: a consensus statement from the European Atherosclerosis Society Consensus Panel. *Eur Heart J.* 41(24), p. 2313-2330. Available at: https://doi.org/10.1093/eurheartj/ehz962.

Borén J., Taskinen M R., Björnson E. & Packard C J., 2022. Metabolism of triglyceride-rich lipoproteins in health and dyslipidaemia. *Nat Rev Cardiol.* 19(9), p. 577-592. Available at: https://doi.org/10.1038/s41569-022-00676-y.

Boyle J J., Johns M., Kampfer T., Nguyen A T., Game L., Schaer D J., Mason J C. & Haskard D O., 2012. Activating Transcription Factor 1 Directs Mhem Atheroprotective Macrophages Through Coordinated Iron Handling and Foam Cell Protection. *Circ Res*.110(1), p. 20-33. Available at: https://doi.org/10.1161/CIRCRESAHA.111.247577.

Brenner C., Franz W M., Kühlenthal S., Kuschnerus K., Remm F., Gross L., Theiss H D., Landmesser U. & Kränkel N., 2015. DPP-4 inhibition ameliorates atherosclerosis by priming monocytes into M2 macrophages. *Int J Cardiol*. 199, p. 163-169. Available at: https://doi.org/10.1016/j.ijcard.2015.07.044.

Bruen R., Curley S., Kajani S., Crean D., O'Reilly M E., Lucitt M B., Godson C G., McGillicuddy F C. & Belton O., 2017. Liraglutide dictates macrophage phenotype in apolipoprotein E null mice during early atherosclerosis. *Cardiovasc Diabetol.* 16(1): 143. Available at: https://doi.org/10.1186/s12933-017-0626-3.

Bruen R., Curley S., Kajani S., Lynch G., O'Reilly M E., Dillon E T., Brennan E P., Barry M., Sheehan S. McGillicuddy F C. & Belton O., 2019. Liraglutide Attenuates Preestablished Atherosclerosis in Apolipoprotein E-Deficient Mice via Regulation of Immune Cell Phenotypes and Proinflammatory Mediators. *J Pharmacol Exp Ther*. 370(3), p. 447-458. Available at: https://doi.org/10.1124/jpet.119.258343.

Cagnin A., Gerhard A. & Banati R B., 2002. In vivo imaging of neuroinflammation. *Eur Neuropsychopharmacol.* 12(6), p. 581-586. Available at: https://doi.org/10.1016/s0924-977x(02)00107-4.

Carr M E., 2001. Diabetes mellitus: a hypercoagulable state. *J Diabetes Complications.* 15(1), p. 44-54. Available at: https://doi.org/10.1016/s1056-8727(00)00132-x.

Cherry S R., Jones T., Karp J S., Qi J., Moses W W. & Badawi R D. 2018. Total-Body PET: Maximizing Sensitivity to Create New Opportunities for Clinical Research and Patient Care. *J Nucl Med.* 59(1), p. 3-12. Available at: https://doi.org/10.2967/jnumed.116.184028.

Chinetti-Gbaguidi G., Colin S. & Staels B., 2015. Macrophage subsets in atherosclerosis. *Nat Rev Cardiol.*12(1), p. 10-17. Available at: https://doi.org/10.1038/nrcardio.2014.173.

Christ E., Wild D., Forrer F., Brändle M., Sahli R., Clerici T., Gloor B., Martius F., Maecke H. & Reubi J C., 2009. Glucagon-like peptide-1 receptor imaging for localization of insulinomas. *J Clin Endocrinol Metab.* 94(11), p. 4398-4405. Available at: https://doi.org/10.1210/jc.2009-1082.

Co C M., Mulgaonkar A., Zhou N., Harris S., Öz O K., Tang L. & Sun X., 2022. PET Imaging of Active Invasive Fungal Infections with d-[5-^{11}C]-Glutamine. *ACS Infect Dis.* 8(8), p. 1663-1673. Available at: https://doi.org/10.1021/acsinfecdis.2c00249.

Cohen A S., Grudzinski J., Smith G T., Peterson T E., Whisenant J G., Hickman T L., Ciombor K K., Cardin D., Eng C., Goff L W., Das S., Coffey R J., Berlin J D. & Manning H C., 2022. First-in-

Human PET Imaging and Estimated Radiation Dosimetry of l-[5-^{11}C]-Glutamine in Patients with Metastatic Colorectal Cancer. *J Nucl Med.* 63(1), p. 36-43. Available at: https://doi.org/10.2967/jnumed.120.261594.

Corti R. & Fuster V., 2011. Imaging of atherosclerosis: magnetic resonance imaging. *Eur Heart J.* 32(14), p. 1709-1719b. Available at: https://doi.org/10.1093/eurheartj/ehr068.

Cruzat V., Rogero M M., Keane K N., Curi R. & Newsholme P., 2018. Glutamine: Metabolism and Immune Function, Supplementation and Clinical Translation. *Nutrients.* 10(11):1564. Available at: https://doi.org/10.3390/nu10111564.

Cui J., Philo L., Nguyen P., Hofflich H., Hernandez C., Bettencourt R., Richards L., Salotti J., Bhatt A., Hooker J., Haufe W., Hooker C., Brenner D A., Sirlin C B. & Loomba R., 2016. Sitagliptin vs. placebo for non-alcoholic fatty liver disease: A randomized controlled trial. *J Hepatol.* 65(2), p. 369-376. Available at: https://doi.org/10.1016/j.jhep.2016.04.021.

Cybulsky M I., Iiyama K., Li H., Zhu S., Chen M., Iiyama M., Davis V., Gutierrez-Ramos J C., Connelly P W. & Milstone D S., 2001. A major role for VCAM-1, but not ICAM-1, in early atherosclerosis. *J Clin Invest*. 107(10), p. 1255-1262. Available at: https://doi.org/10.1172/JCI11871.

Darsalia V., Larsson M., Lietzau G., Nathanson D., Nyström T., Klein T. & Patrone C., 2016. Gliptin-mediated neuroprotection against stroke requires chronic pretreatment and is independent of glucagon-like peptide-1 receptor. *Diabetes Obes Metab*. 18(5), p. 537-541. Available at: https://doi.org/10.1111/dom.12641.

de Boer S A., Heerspink H J L., Juárez Orozco L E., van Roon A M., Kamphuisen P W., Smit A J., Slart R H J A., Lefrandt J D. & Mulder D J., 2017. Effect of linagliptin on pulse wave velocity in early type 2 diabetes: A randomized, double-blind, controlled 26-week trial (RELEASE). *Diabetes Obes Metab.* 19(8), p. 1147-1154. Available at: https://doi.org/10.1111/dom.12925.

De Man F H., Cabezas M C., Van Barlingen H H., Erkelens D W. & de Bruin T W., 1996. Triglyceride-rich lipoproteins in non-insulin-dependent diabetes mellitus: post-prandial metabolism and relation to premature atherosclerosis. *Eur J Clin Invest.* 26(2), p. 89-108. Available at: https://doi.org/10.1046/j.1365-2362.1996.114256.x.

De Nigris V., Prattichizzo F., Iijima H. & Ceriello A., 2021. DPP-4 Inhibitors Have Different Effects on Endothelial Low-Grade Inflammation and on the M1-M2 Macrophage Polarization Under Hyperglycemic Conditions. *Diabetes Metab Syndr Obes*. 14, p. 1519-1531. Available at: https://doi.org/10.2147/DMSO.S302621.

Demer L L. & Tintut Y., 2014. Inflammatory, metabolic, and genetic mechanisms of vascular calcification. *Arterioscler Thromb Vasc Biol.* 34(4), p. 715-723. Available at: https://doi.org/10.1161/ATVBAHA.113.302070.

Dinarello C A., 2009. Immunological and inflammatory functions of the interleukin-1 family. *Annu Rev Immunol*. 27, p. 519-550. Available at: https://doi.org/10.1146/annurev.immunol.021908.132612.

Dobrian A D., Ma Q., Lindsay J W., Leone K A., Ma K., Coben J., Galkina E V. & Nadler J L., 2011. Dipeptidyl peptidase IV inhibitor sitagliptin reduces local inflammation in adipose tissue and in pancreatic islets of obese mice. *Am J Physiol Endocrinol Metab*. 300(2), p. E410-421. Available at: https://doi.org/10.1152/ajpendo.00463.2010.

Domschke G. & Gleissner C A., 2019. CXCL4-induced macrophages in human atherosclerosis. *Cytokine*. 122: 154141. Available at: https://doi.org/10.1016/j.cyto.2017.08.021.

Dragoljevic D., Veiga C B., Michell D L., Shihata W A., Al-Sharea A., Head G A., Murphy A J., Kraakman M J. & Lee M K S., 2021. A spontaneously hypertensive diet-induced atherosclerosis-prone mouse model of metabolic syndrome. *Biomed Pharmacother*. 139:111668. Available at: https://doi.org/10.1016/j.biopha.2021.111668.

Duncan R E., Ahmadian M., Jaworski K., Sarkadi-Nagy E. & Sul H S., 2007. Regulation of lipolysis in adipocytes. *Annu Rev Nutr.* 27, p. 79-101. Available at: https://doi.org/10.1146/annurev.nutr.27.061406.093734.

Duran E K., Aday A W., Cook N R., Buring J E., Ridker P M. & Pradhan A D., 2020. Triglyceride-Rich Lipoprotein Cholesterol, Small Dense LDL Cholesterol, and Incident Cardiovascular Disease. *J Am Coll Cardiol.* 75(17), p. 2122-2135. Available at: https://doi.org/10.1016/j.jacc.2020.02.059.

Elnakat H. & Ratnam M., 2019. Distribution, functionality and gene regulation of folate receptor isoforms: implications in targeted therapy. *Adv Drug Deliv Rev*.56(8), p. 1067-1084. Available at: https://doi.org/10.1016/j.addr.2004.01.001.

Emerging Risk Factors Collaboration, 2023. Life expectancy associated with different ages at diagnosis of type 2 diabetes in high-income countries: 23 million person-years of observation. *Lancet Diabetes Endocrinol.* 11(10), p. 731-742. Available at: https://doi.org/10.1016/S2213-8587(23)00223-1.

Emini Veseli B., Perrotta P., De Meyer G R A., Roth L., Van der Donckt C., Martinet W. & De Meyer G R Y., 2017. Animal models of atherosclerosis. *Eur J Pharmacol.* 816, p. 3-13. Available at: https://doi.org/10.1016/j.ejphar.2017.05.010.

Elo P., Li X G., Liljenbäck H., Helin S., Teuho J., Koskensalo K., Saunavaara V., Marjamäki P., Oikonen V., Virta J., Chen Q., Low P S., Knuuti J., Jalkanen S., Airas L. & Roivainen A., 2019. Folate receptor-targeted positron emission tomography of experimental autoimmune encephalomyelitis in rats. *J Neuroinflammation.* 16(1):252. Available at: https://doi.org/10.1186/s12974-019-1612-3.

Erbel C., Tyka M., Helmes C.M., Akhavanpoor M., Rupp G., Domschke G., Linden F., Wolf A., Doesch A., Lasitschka F., Katus H A. & Gleissner C A., 2015. CXCL4-induced plaque macrophages can be specifically identified by co-expression of MMP7+S100A8+ in vitro and in vivo. *Innate Immun*. 21(3), p. 255-265. Available at: https://doi.org/10.1177/1753425914526461.

Falk E., Shah P K. & Fuster V., 1995. Coronary plaque disruption. *Circulation*. 1;92(3), p. 657-671. Available at: https://doi.org/10.1161/01.cir.92.3.657.

Falk E., 2006. Pathogenesis of Atherosclerosis. *J Am Coll Cardiol,* 47(8 Suppl), p. C7-12. Available at: https://doi.org/10.1016/j.jacc.2005.09.068.

Fan A P., An H., Moradi F., Rosenberg J., Ishii Y., Nariai T., Okazawa H. & Zaharchuk G., 2020. Quantification of brain oxygen extraction and metabolism with [^{15}O]-gas PET: A technical review in the era of PET/MRI. *Neuroimage.* 220:117136. Available at: https://doi.org/10.1016/j.neuroimage.2020.117136.

Fan J., Kitajima S., Watanabe T., Xu J., Zhang J., Liu E. & Chen Y E., 2015. Rabbit models for the study of human atherosclerosis: from pathophysiological mechanisms to translational medicine. *Pharmacol Ther.* 146, p. 104-119. Available at: https://doi.org/10.1016/j.pharmthera.2014.09.009.

Farkas R., Siwowska K., Ametamey S M., Schibli R., van der Meulen N P. & Müller C., 2016. (64)Cu- and (68)Ga-Based PET Imaging of Folate Receptor-Positive Tumors: Development and Evaluation of an Albumin-Binding NODAGA-Folate. *Mol Pharm*. 13(6), p. 1979-1987. Available at: https://doi.org/10.1021/acs.molpharmaceut.6b00143.

Ferrannini E., Mark M. & Mayoux E., 2016. CV Protection in the EMPA-REG OUTCOME Trial: A "Thrifty Substrate" Hypothesis. *Diabetes Care.* 39(7), p. 1108-1114. Available at: https://doi.org/10.2337/dc16-0330.

Ferreira J P., Sharma A., Vasques-Nóvoa F., Angélico-Gonçalves A., Leite A R., Borges-Canha M., Carvalho D., Packer M., Zannad F., Leite-Moreira A. & Neves J S., 2020. Albiglutide in patients with type 2 diabetes and heart failure: a post-hoc analysis from Harmony Outcomes. *Eur J Heart Fail.* 24(10), p. 1792-1801. Available at: https://doi.org/10.1002/ejhf.2660.

Figueroa A L., Abdelbaky A., Truong Q A., Corsini E., MacNabb M H., Lavender Z R., Lawler M A., Grinspoon S K., Brady T J., Nasir K., Hoffmann U. & Tawakol A., 2013. Measurement of arterial activity on routine FDG PET/CT images improves prediction of risk of future CV events. *JACC Cardiovasc Imaging*. 6(12), p. 1250-1259. Available at: https://doi.org/10.1016/j.jcmg.2013.08.006.

Finn A V., Nakano M., Polavarapu R., Karmali V., Saeed O., Zhao X O., Yazdani S., Otsuka F., Davis T., Habib A., Narula J., Kolodgie F D. & Virmani R., 2012. Hemoglobin directs macrophage differentiation and prevents foam cell formation in human atherosclerotic plaques. *J Am Coll Cardiol.* 59(2), p. 166-177. Available at: https://doi.org/10.1016/j.jacc.2011.10.852.

Flotte T J., Springer T A. & Thorbecke G J., 1983. Dendritic cell and macrophage staining by monoclonal antibodies in tissue sections and epidermal sheets. *Am J Pathol*. 111(1), p. 112-24.

Folco E J., Sheikine Y., Rocha V Z., Christen T., Shvartz E., Sukhova G K., Di Carli M F. & Libby P., 2011. Hypoxia but not inflammation augments glucose uptake in human macrophages: Implications for imaging atherosclerosis with 18fluorine-labeled 2-deoxy-D-glucose positron emission tomography. *J Am Coll Cardiol.*58(6), p. 603-614. Available at: https://doi.org/10.1016/j.jacc.2011.03.044.

Gaemperli O., Shalhoub J., Owen D.R., Lamare F., Johansson S., Fouladi N., Davies A H., Rimoldi O E. & Camici P G., 2012. Imaging intraplaque inflammation in carotid atherosclerosis with 11C-PK11195 positron emission tomography/computed tomography. *Eur Heart J.* 33(15), p. 1902-1910. Available at: https://doi.org/10.1093/eurheartj/ehr367.

Gallego-Colon E., Wojakowski W. & Francuz T., 2018. Incretin drugs as modulators of atherosclerosis. *Atherosclerosis*. 278, p. 29-38. Available at: https://doi.org/10.1016/j.atherosclerosis.2018.09.011.

Gallino A., Stuber M., Crea F., Falk E., Corti R., Lekakis J., Schwitter J., Camici P., Gaemperli O., Di Valentino M., Prior J., Garcia-Garcia H M., Vlachopoulos C., Cosentino F., Windecker S., Pedrazzini G., Conti R., Mach F., De Caterina R. & Libby P., 2012 "In vivo" imaging of atherosclerosis. *Atherosclerosis.* 224(1), p. 25-36. Available at: https://doi.org/10.1016/j.atherosclerosis.2012.04.007.

Gao X., Mao D., Zuo X., Hu F., Cao J., Zhang P., Sun J Z., Liu J., Liu B. & Tang B Z., 2019. Specific Targeting, Imaging, and Ablation of Tumor-Associated Macrophages by Theranostic Mannose-AIEgen Conjugates. *Anal Chem.* 91(10), p. 6836-6843. Available at: https://doi.org/10.1021/acs.analchem.9b01053.

Georgakis M K., Bernhagen J., Heitman L H., Weber C. & Dichgans M., 2022. Targeting the CCL2-CCR2 axis for atheroprotection. *Eur Heart J.* 43(19), p. 1799-1808. Available at: https://doi.org/10.1093/eurheartj/ehac094.

Gent Y Y J., Weijers K., Molthoff C F M., Windhorst A D., Huisman M C., Smith D E C., Kularatne S A., Jansen G., Low P S., Lammertsma A A. & van der Laken C J., 2013. Evaluation of the novel folate receptor ligand [18F]fluoro-PEG-folate for macrophage targeting in a rat model of arthritis. *Arthritis Res Ther.* 15(2):R37. Available at: https://doi.org/10.1186/ar4191.

Gerstein H C., Colhoun H M., Dagenais G R., Diaz R., Lakshmanan M., Pais P., Probstfield J., Riesmeyer J S., Riddle M C., Rydén L., Xavier D., Atisso C M., Dyal L., Hall S., Rao-Melacini P., Wong G., Avezum A., Basile J., Chung N., Conget I., Cushman W C., Franek E., Hancu N., Hanefeld M., Holt S., Jansky P., Keltai M., Lanas F., Leiter L A., Lopez-Jaramillo P., Cardona Munoz E G., Pirags V., Pogosova N., Raubenheimer P.J., Shaw J E., Sheu W H., Temelkova-Kurktschiev T. & REWIND Investigators, 2019. Dulaglutide and cardiovascular outcomes in type 2 diabetes (REWIND): a double-blind, randomised placebo-controlled trial. *Lancet.* 394(10193), p. 121-130. Available at: https://doi.org/10.1016/S0140-6736(19)31149-3.

Gimbrone Jr M A. & García-Cardeña G., 2016 Endothelial Cell Dysfunction and the Pathobiology of Atherosclerosis. *Circ Res.* 118(4), p. 620-636. Available at: https://doi.org/10.1161/CIRCRESAHA.115.306301.

Ginsberg H N., Packard C J., Chapman M J., Borén J., Aguilar-Salinas C A., Averna M., Ference B A., Gaudet D., Hegele R A., Kersten S., Lewis G F., Lichtenstein A H., Moulin P., Nordestgaard B G., Remaley A T., Staels B., Stroes E S G., Taskinen M R., Tokgözoğlu L S., Tybjaerg-Hansen A., Stock J K. & Catapano A L., 2021. Triglyceride-rich lipoproteins and their remnants: metabolic insights, role in atherosclerotic cardiovascular disease, and emerging therapeutic strategies-a consensus statement from the European Atherosclerosis Society. *Eur Heart J.* 42(47), p. 4791-4806. Available at: https://doi.org/10.1093/eurheartj/ehab551.

Green B D., Hand K V., Dougan J E., McDonnell B M., Cassidy R S. & Grieve D J., 2008. GLP-1 and related peptides cause concentration-dependent relaxation of rat aorta through a pathway involving KATP and cAMP. *Arch Biochem Biophys*. 478(2), p. 136-142. Available at: https://doi.org/10.1016/j.abb.2008.08.001.

Guérin M., Le Goff W., Lassel T S., Van Tol A., Steiner G. & Chapman M J., 2001. Proatherogenic Role of Elevated CE Transfer From HDL to VLDL1 and Dense LDL in Type 2 Diabetes. *Arterioscler Thromb Vasc Biol.* 21(2), p. 282-288. Available at: https://doi.org/10.1161/01.atv.21.2.282.

Habib A. & Finn A V., 2014. The role of iron metabolism as a mediator of macrophage inflammation and lipid handling in atherosclerosis. *Front Pharmacol*. 5:195. Available at: https://doi.org/10.3389/fphar.2014.00195.

Hajhosseiny R., Bustin A., Munoz C., Rashid I., Cruz G., Manning W J., Prieto C. & Botnar R M. 2020. Coronary Magnetic Resonance Angiography: Technical Innovations Leading Us to the Promised Land? *JACC Cardiovasc Imaging.* 13(12), p. 2653-2672. Available at: https://doi.org/10.1016/j.jcmg.2020.01.006.

Hallow K M., Helmlinger G., Greasley P J., McMurray J J V. & Boulton D W., 2018. Why do SGLT2 inhibitors reduce heart failure hospitalization? A differential volume regulation hypothesis. *Diabetes Obes Metab.* 20(3), p. 479-487. Available at: https://doi.org/10.1111/dom.13126.

Hansson G K. & Libby P., 2006. The immune response in atherosclerosis: a double-edged sword. *Nat Rev Immunol*. 6(7), p. 508-519. Available at: https://doi.org/10.1038/nri1882.

Haribabu B., Zhelev D V., Pridgen B C., Richardson R M., Ali H. & Snyderman R., 1999. Chemoattractant receptors activate distinct pathways for chemotaxis and secretion. Role of G-protein usage. *J Biol Chem.* 274(52), p. 37087-37092. Available at: https://doi.org/10.1074/jbc.274.52.37087.

Harper E., Forde H., Davenport C., Rochfort K D., Smith D. & Cummins P M., 2016. Vascular calcification in type-2 diabetes and cardiovascular disease: Integrative roles for OPG, RANKL and TRAIL. *Vascul Pharmacol.* 82, p. 30-40. Available at: https://doi.org/10.1016/j.vph.2016.02.003.

Heinonen S E., Leppänen P., Kholová I., Lumivuori H., Häkkinen S-K., Bosch F., Laakso M. & Ylä-Herttuala S., 2007. Increased atherosclerotic lesion calcification in a novel mouse model combining insulin resistance, hyperglycemia, and hypercholesterolemia. *Circ Res.* 101(10), p. 1058-1067. Available at: https://doi.org/10.1161/CIRCRESAHA.107.154401.

Hellberg S., Silvola J M U., Kiugel M., Liljenbäck H., Metsälä O., Viljanen T., Metso J., Jauhiainen M., Saukko P., Nuutila P., Ylä-Herttuala S., Knuuti J., Roivainen A. & Saraste A., 2016. Type 2 diabetes enhances arterial uptake of choline in atherosclerotic mice: an imaging study with positron emission tomography tracer ^{18}F-fluoromethylcholine. *Cardiovasc Diabetol*. 15:26. Available at: https://doi.org/10.1186/s12933-016-0340-6.

Hellberg S., Silvola J M U., Kiugel M., Liljenbäck H., Savisto N., Li X G., Thiele A., Lehmann L., Heinrich T., Vollmer S., Hakovirta H., Laine J O., Ylä-Herttuala S., Knuuti J., Roivainen A. & Saraste A., 2017a. 18-kDa translocator protein ligand 18F-FEMPA: Biodistribution and uptake into atherosclerotic plaques in mice. *J Nucl Cardiol*. 24(3), p. 862-871. Available at: https://doi.org/10.1007/s12350-016-0527-y.

Hellberg S., Sippola S., Liljenbäck H., Virta J., Silvola J M U., Ståhle M., Savisto N., Metso J., Jauhiainen M., Saukko P., Ylä-Herttuala S., Nuutila P., Knuuti J., Roivainen A. & Saraste A., 2017b. Effects of atorvastatin and diet interventions on atherosclerotic plaque inflammation and [^{18}F]FDG uptake in Ldlr$^{-/-}$Apob$^{100/100}$ mice. *Atherosclerosis.* 263, p. 369-376. Available at: https://doi.org/10.1016/j.atherosclerosis.2017.04.004.

Hellberg S., Liljenbäck H., Eskola O., Morisson-Iveson V., Morrison M., Trigg W., Saukko P., Ylä-Herttuala S., Knuuti J., Saraste A. & Roivainen A., 2018. Positron Emission Tomography Imaging of Macrophages in Atherosclerosis with ^{18}F-GE-180, a Radiotracer for Translocator Protein (TSPO). *Contrast Media Mol Imaging*. 9186902. Available at: https://doi.org/10.1155/2018/9186902.

Helmstädter J., Frenis K., Filippou K., Grill A., Dib M., Kalinovic S., Pawelke F., Kus K., Kröller-Schön S., Oelze M., Chlopicki S., Schuppan D., Wenzel P., Ruf W., Drucker D J., Münzel T., Daiber A. & Steven S., 2020. Endothelial GLP-1 (Glucagon-Like Peptide-1) Receptor Mediates Cardiovascular Protection by Liraglutide In Mice With Experimental Arterial Hypertension. *Arterioscler Thromb Vasc Biol*. 40(1), p. 145-158. Available at: https://doi.org/10.1161/atv.0000615456.97862.30.

Henein M Y., Vancheri S., Longo G. & Vancheri F., 2022. The Role of Inflammation in Cardiovascular Disease. *Int J Mol Sci. 23*(21):12906. Available at: https://doi.org/10.3390/ijms232112906.

Heo K-S., Fujiwara K. & Abe J-i., 2014. Shear stress and atherosclerosis. *Mol Cells*. 37(6), p. 435-440. Available at: https://doi.org/10.14348/molcells.2014.0078.

Hermans M., Lennep J R V., van Daele P. & Bot I., 2019. Mast Cells in Cardiovascular Disease: From Bench to Bedside. *Int J Mol Sci.* 20(14):3395. Available at: https://doi.org/10.3390/ijms20143395.

Hernandez A F., Green J B., Janmohamed S., D'Agostino Sr R B., Granger C B., Jones N P., Leiter L A., Rosenberg A E., Sigmon K N., Somerville M C., Thorpe K M., McMurray J J V., Del Prato S. & Harmony Outcomes committees and investigators, 2018. Albiglutide and cardiovascular outcomes in patients with type 2 diabetes and cardiovascular disease (Harmony Outcomes): a double-blind, randomised placebo-controlled trial. *Lancet*. 392(10157), p. 1519-1529. Available at: https://doi.org/10.1016/S0140-6736(18)32261-X.

Herrington W., Lacey B., Sherliker P., Armitage J. & Lewington S., 2016. Epidemiology of Atherosclerosis and the Potential to Reduce the Global Burden of Atherothrombotic Disease. *Circ Res.* 118(4), p. 535-546. Available at: https://doi.org/10.1161/CIRCRESAHA.115.307611.

Hirano K., Young S G., Farese Jr R V., Ng J., Sande E., Warburton C., Powell-Braxton L M. & Davidson N O., 1996. Targeted disruption of the mouse apobec-1 gene abolishes apolipoprotein B mRNA editing and eliminates apolipoprotein B48. *J Biol Chem.* 271(17), p. 9887-9890. Available at: https://doi.org/10.1074/jbc.271.17.9887.

Hirata Y., Kurobe H., Nishio C., Tanaka K., Fukuda D., Uematsu E., Nishimoto S., Soeki T., Harada N., Sakaue H., Kitagawa T., Shimabukuro M., Nakaya Y. & Sata M., 2013. Exendin-4, a glucagon-like peptide-1 receptor agonist, attenuates neointimal hyperplasia after vascular injury. *Eur J Pharmacol*. 699(1-3), p. 106-111. Available at: https://doi.org/10.1016/j.ejphar.2012.11.057.

Hjelkrem M., Stauch C., Shaw J. & Harrison S A., 2011. Validation of the non-alcoholic fatty liver disease activity score. *Aliment Pharmacol. Ther*. 34, p. 214-218. Available at: https://doi.org/10.1111/j.1365-2036.2011.04695.x.

Ho M K. & Springer T A., 1983. Tissue distribution, structural characterization, and biosynthesis of Mac-3, a macrophage surface glycoprotein exhibiting molecular weight heterogeneity. *J Biol Chem.* 258(1), p. 636-642.

Holman R R., Bethel M A., Mentz R J., Thompson V P., Lokhnygina Y., Buse J B., Chan J C., Choi J., Gustavson S M., Iqbal N., Maggioni A P., Marso S P., Öhman P., Pagidipati N J., Poulter N., Ramachandran A., Zinman B., Hernandez A F.; EXSCEL Study Group, 2017. Effects of Once-Weekly Exenatide on Cardiovascular Outcomes in Type 2 Diabetes. *N Engl J Med.* 377(13), p. 1228-1239. Available at: https://doi.org/10.1056/NEJMoa1612917.

Holst J J., Vilsbøll T. & Deacon C F., 2009. The incretin system and its role in type 2 diabetes mellitus. *Mol Cell Endocrinol.* 297(1-2), p. 127-136. Available at: https://doi.org/10.1016/j.mce.2008.08.012.

Hopfner R L. & Gopalakrishnan V., 1999. Endothelin: emerging role in diabetic vascular complications. *Diabetologia.* 42(12), p. 1383-1394. Available at: https://doi.org/10.1007/s001250051308.

Huang J., Gu J-X., Bao H-Z., Li S-S., Yao X-Q., Yang M., Li Y., Zhang A-M., Yin Y., Zhang N., Jia M. & Su M., 2021. Elevated Serum Small Dense Low-Density Lipoprotein Cholesterol May Increase the Risk and Severity of Coronary Heart Disease and Predict Cardiovascular Events in Patients with Type 2 Diabetes Mellitus. *Dis Markers*. 2021: 5597028. Available at: https://doi.org/10.1155/2021/5597028.

Hyafil F., Cornily J-C., Rudd J H F., Machac J., Feldman L J. & Fayad Z A., 2009. Quantification of inflammation within rabbit atherosclerotic plaques using the macrophage-specific CT contrast agent N1177: a comparison with 18F-FDG PET/CT and histology. *J Nucl Med.* 50(6), p. 959-965. Available at: https://doiorg/10.2967/jnumed.108.060749.

Hyafil F. & Vigne J., 2019. Nuclear Imaging: Focus on Vascular Probes. *Arterioscler Thromb Vasc Biol.* 39(7), p. 1369-1378. Available at: https://doi.org/10.1161/ATVBAHA.119.312586

Ikezaki H., Furusyo N., Yokota Y., Ai M., Asztalos B F., Murata M., Hayashi J. & Schaefer E J., 2000. Small Dense Low-Density Lipoprotein Cholesterol and Carotid Intimal Medial Thickness Progression. *J Atheroscler Thromb.* 27(10), p. 1108-1122. Available at: https://doi.org/10.5551/jat.54130.

Inoguchi T., Li P., Umeda F., Yu H Y., Kakimoto M., Imamura M., Aoki T., Etoh T., Hashimoto T., Naruse M., Sano H., Utsumi H. & Nawata H., 2000. High glucose level and free fatty acid stimulate reactive oxygen species production through protein kinase C--dependent activation of NAD(P)H oxidase in cultured vascular cells. *Diabetes.* 49(11), p. 1939-1945. Available at: https://doi.org/10.2337/diabetes.49.11.1939.

Inoue T., Plieth D., Venkov C D., Xu C. & Neilson E G., 2005. Antibodies against macrophages that overlap in specificity with fibroblasts. *Kidney Int.* 67(6), p. 2488-2493. Available at: https://doi.org/10.1111/j.1523-1755.2005.00358.x.

Ishibashi S., Brown M S., Goldstein J L., Gerard R D., Hammer R E. & Herz J., 1993. Hypercholesterolemia in low density lipoprotein receptor knockout mice and its reversal by adenovirus-mediated gene delivery. *J Clin Invest.* 92(2), p. 883-893. Available at: https://doi.org/10.1172/JCI116663.

Ishibashi S., Goldstein J L., Brown M S., Herz J. & Burns D K., 1994. Massive xanthomatosis and atherosclerosis in cholesterol-fed low density lipoprotein receptor-negative mice. *J Clin Invest.* 93(5), p. 1885-1893. Available at: https://doi.org/10.1172/JCI117179.

Jager N A., Westra J., Golestani R., van Dam G M., Low P S., Tio R A., Slart R H., Boersma H H., Bijl M. & Zeebregts C J., 2014. Folate receptor-β imaging using 99mTc-folate to explore distribution of polarized macrophage populations in human atherosclerotic plaque. *J Nucl Med*. 55(12), p. 1945-1951. Available at: https://doi.org/10.2967/jnumed.114.143180.

Jahandideh A., Uotila S., Ståhle M., Virta J., Li X G., Kytö V., Marjamäki P., Liljenbäck H., Taimen P., Oikonen V., Lehtonen J., Mäyränpää M I., Chen Q., Low P S., Knuuti J., Roivainen A. & Saraste A., 2020. Folate Receptor β-Targeted PET Imaging of Macrophages in Autoimmune Myocarditis. *J Nucl Med.* 61(11), p. 1643-1649. Available at: https://doi.org/10.2967/jnumed.119.241356.

Jarr K-U., Ye J., Kojima Y., Nanda V., Flores A M., Tsantilas P., Wang Y., Hosseini-Nassab N., Eberhard A V., Lotfi M., Käller M., Smith B R., Maegdefessel L. & Leeper N J., 2020. ^{18}F-Fluorodeoxyglucose-Positron Emission Tomography Imaging Detects Response to Therapeutic Intervention and Plaque Vulnerability in a Murine Model of Advanced Atherosclerotic Disease-Brief Report. *Arterioscler Thromb Vasc Biol.* 40(12), p. :2821-2828. Available at: https://doiorg/10.1161/ATVBAHA.120.315239.

Ji Y., Ge Y., Xu X., Ye S., Fan Y., Zhang J., Mei L., Zhang X., Ying L., Yang T. & Li C., 2019. Vildagliptin Reduces Stenosis of Injured Carotid Artery in Diabetic Mouse Through Inhibiting Vascular Smooth Muscle Cell Proliferation via ER Stress/NF-κB Pathway. *Front Pharmacol.* 10:142. Available at: https://doi.org/10.3389/fphar.2019.00142.

Jiang C., Cai H., Peng X., Zhang P., Wu X. & Tian R., 2017. Targeted Imaging of Tumor-Associated Macrophages by Cyanine 7-Labeled Mannose in Xenograft Tumors. *Mol Imaging.* 16:1536012116689499. Available at: https://doi.org/10.1177/1536012116689499.

Jinnouchi H., Sato Y., Sakamoto A., Cornelissen A., Mori M., Kawakami R., Gadhoke N V., Kolodgie F D., Virmani R. & Finn A V., 2020a. Calcium deposition within coronary atherosclerotic lesion: Implications for plaque stability. *Atherosclerosis*. 306, p. 85-95. Available at: https://doi.org/10.1016/j.atherosclerosis.2020.05.017.

Jinnouchi H., Guo L., Sakamoto A., Torii S., Sato Y., Cornelissen A., Kuntz S., Paek K H., Fernandez R., Fuller D., Gadhoke N., Surve D., Romero M., Kolodgie F D., Virmani R. & Finn A V., 2020b. Diversity of macrophage phenotypes and responses in atherosclerosis. *Cell Mol Life Sci.* 77(10), p. 1919-1932. Available at: https://doi.org/10.1007/s00018-019-03371-3.

Johnsrud K., Skagen K., Seierstad T., Skjelland M., Russell D. & Revheim M-E., 2019. ^{18}F-FDG PET/CT for the quantification of inflammation in large carotid artery plaques. *J Nucl Cardiol.* 26(3), p. 883-893. Available at: https://doi.org/10.1007/s12350-017-1121-7.

Kadl A., Meher A K., Sharma P R., Lee M Y., Doran A C., Johnstone S R., Elliott M R., Gruber F., Han J., Chen W., Kensler T., Ravichandran K S., Isakson B E., Wamhoff B R. & Leitinger N., 2010. Identification of a novel macrophage phenotype that develops in response to atherogenic phospholipids via Nrf2. *Circ Res*. 107(6), p. 737-746. Available at: https://doi.org/10.1161/CIRCRESAHA.109.215715.

Kaeppeli S A M., Jodal A., Gotthardt M., Schibli R. & Béhé M., 2019. Exendin-4 Derivatives with an Albumin-Binding Moiety Show Decreased Renal Retention and Improved GLP-1 Receptor Targeting. *Mol Pharm.* 16(9), p. 3760-3769. Available at: https://doi.org/10.1021/acs.molpharmaceut.9b00271.

Kalff V., Iravani A., Akhurst T., Pattison D A., Eu P., Hofman M S. & Hicks R J., 2021. Utility of ^{68}Ga-DOTA-Exendin-4 positron emission tomography-computed tomography imaging in distinguishing between insulinoma and nesidioblastosis in patients with confirmed endogenous hyperinsulinaemic hypoglycaemia. *Intern Med J.* 51(10), p. 1657-1664. Available at: https://doi.org/10.1111/imj.15141.

Kang H., Li X., Xiong K., Song Z., Tian J., Wen Y., Sun A. & Deng X., 2021. The Entry and Egress of Monocytes in Atherosclerosis: A Biochemical and Biomechanical Driven Process. *Cardiovasc Ther.* 2021: 6642927. Available at: https://doi.org/10.1155/2021/6642927.

Kappel B A., Lehrke M., Schütt K., Artati A., Adamski J., Lebherz C. & Marx N., 2017. Effect of Empagliflozin on the Metabolic Signature of Patients With Type 2 Diabetes Mellitus and Cardiovascular Disease. *Circulation.* 136(10), p. 969-972. Available at: https://doi.org/10.1161/CIRCULATIONAHA.117.029166.

Kaur R., Kaur M. & Singh J., 2018. Endothelial dysfunction and platelet hyperactivity in type 2 diabetes mellitus: molecular insights and therapeutic strategies. *Cardiovasc Diabetol.* 17(1):121. Available at: https://doi.org/10.1186/s12933-018-0763-3.

Kiesewetter D O., Gao H., Ma Y., Niu G., Quan Q., Guo N. & Chen X., 2012. 18F-radiolabeled analogs of exendin-4 for PET imaging of GLP-1 in insulinoma. *Eur J Nucl Med Mol Imaging.* 39(3), p. 463-473. Available at: https://doi.org/10.1007/s00259-011-1980-0.

Kim C J., Han E J., Chu E-H., Hwang B-H., Kim J-J., Seung K-B., Kim S H., O J H. & Chang K., 2020. Effect of moderate-intensity statin therapy on plaque inflammation in patients with acute coronary syndrome: A prospective interventional study evaluated by 18F-FDG PET/CT of the carotid artery. *Cardiol J*. 27(6), p. 762-771. Available at: https://doi.org/10.5603/CJ.a2018.0069.

Kim E J., Kim S., Seo H S., Lee Y J., Eo J S., Jeong J M., Lee B., Kim J Y., Park Y M. & Jeong M., 2016. Novel PET Imaging of Atherosclerosis with 68Ga-Labeled NOTA-Neomannosylated Human Serum Albumin. *J Nucl Med.* 57(11), p. 1792-1797. Available at: https://doi.org/10.2967/jnumed.116.172650.

Kim J S., Lee S G., Oh J., Park S., Park S I., Hong S Y., Kim S., Lee S H., Ko Y G., Choi D., Hong M K. & Jang Y., 2017. Development of Advanced Atherosclerotic Plaque by Injection of Inflammatory Proteins in a Rabbit Iliac Artery Model. *Yonsei Med J.* 57(5), p. 1095-1105. Available at: https://doi.org/10.3349/ymj.2016.57.5.1095.

Klein T., Fujii M., Sandel J., Shibazaki Y., Wakamatsu K., Mark M. & Yoneyama H., 2014. Linagliptin alleviates hepatic steatosis and inflammation in a mouse model of non-alcoholic steatohepatitis. *Med Mol Morphol*. 47(3), p.137-149. Available at: https://doi.org/10.1007/s00795-013-0053-9.

Knuuti J., Tuisku J., Kärpijoki H., Iida H., Maaniitty T., Latva-Rasku A., Oikonen V., Nesterov S V., Teuho J., Jaakkola M K., Klén R., Louhi H., Saunavaara V., Nuutila P., Saraste A., Rinne J. &

Nummenmaa L., 2023. Quantitative Perfusion Imaging with Total-Body PET. *J Nucl Med*. 64(Suppl 2), p. 11S-19S. Available at: https://doi.org/10.2967/jnumed.122.264870.

Kolodgie F D., Gold H K., Burke A P., Fowler D R., Kruth H S., Weber D K., Farb A., Guerrero L J., Hayase M., Kutys R., Narula J., Finn A V. & Virmani R., 2003 Intraplaque Hemorrhage and Progression of Coronary Atheroma. *N Engl J Med.* 349(24), p. 2316-2325. Available at: https://doi.org/10.1056/NEJMoa035655.

Kolossváry M., Szilveszter B., Merkely B. & Maurovich-Horvat P., 2017. Plaque imaging with CT-a comprehensive review on coronary CT angiography based risk assessment. *Cardiovasc Diagn Ther.* 7(5), p. 489-506. Available at: https://doi.org/10.21037/cdt.2016.11.06.

Kopecky C., Pandzic E., Parmar A., Szajer J., Lee V., Dupuy A., Arthur A., Fok S., Whan R., Ryder W J., Rye K A. & Cochran B J., 2019. Translocator protein localises to CD11b+ macrophages in atherosclerosis. *Atherosclerosis*.284, p. 153-159. Available at: https://doi.org/10.1016/j.atherosclerosis.2019.03.011.

Kunisch E., Fuhrmann R., Roth A., Winter R., Lungershausen W. & Kinne R W., 2004. Macrophage specificity of three anti-CD68 monoclonal antibodies (KP1, EBM11, and PGM1) widely used for immunohistochemistry and flow cytometry. *Ann Rheum Dis.* 63(7), p. 774-784. Available at: https://doi.org/10.1136/ard.2003.013029.

Kurosawa T., Li Y., Sudo M., Haruta H., Hagikura K., Takayama T., Hiro T., Shiomi M., Hao H., Matsumoto T., Hirayama A. & Okumura Y., 2021. Effect of the dipeptidyl peptidase-4 inhibitor linagliptin on atherosclerotic lesions in Watanabe heritable hyperlipidemic rabbits: iMap-IVUS and pathological analysis. *Heart Vessels.* 36(1), p. 127-135. Available at: https://doi.org/10.1007/s00380-020-01689-8.

Laitinen I., Marjamäki P., Haaparanta M., Savisto N., Laine V.J., Soini S L., Wilson I., Leppänen P., Ylä-Herttuala S., Roivainen A. & Knuuti J., 2006. Non-specific binding of [18F]FDG to calcifications in atherosclerotic plaques: experimental study of mouse and human arteries. *Eur J Nucl Med Mol Imaging.* 33(12), p. 1461-1467. Available at: https://doi.org/10.1007/s00259-006-0159-6.

Laitinen I., Marjamäki P., Någren K., Laine V J., Wilson I., Leppänen P., Ylä-Herttuala S., Roivainen A. & Knuuti J., 2009. Uptake of inflammatory cell marker [11C]PK11195 into mouse atherosclerotic plaques. *Eur J Nucl Med Mol Imaging.* 36(1), p. 73-80. Available at: https://doi.org/10.1007/s00259-008-0919-6.

Lauritsen K M., Nielsen B R R., Tolbod L P., Johannsen M., Hansen J., Hansen T K., Wiggers H., Møller N., Gormsen L C. & Søndergaard E., (2021) SGLT2 Inhibition Does Not Affect Myocardial Fatty Acid Oxidation or Uptake, but Reduces Myocardial Glucose Uptake and Blood Flow in Individuals With Type 2 Diabetes: A Randomized Double-Blind, Placebo-Controlled Crossover Trial. *Diabetes.* 70(3), p. 800-808. Available at: https://doi.org/10.2337/db20-0921.

Laws A., Hoen H M., Selby J V., Saad M F., Haffner S M. & Howard B V., 1997. Differences in insulin suppression of free fatty acid levels by gender and glucose tolerance status. Relation to plasma triglyceride and apolipoprotein B concentrations. Insulin Resistance Atherosclerosis Study (IRAS) Investigators. *Arterioscler Thromb Vasc Biol.* 17(1), p. 64-71. Available at: https://doi.org/10.1161/01.atv.17.1.64.

Lee S J., Thien Quach C H., Jung K H., Paik J Y., Lee J H., Park J W. & Lee K H., 2014. Oxidized low-density lipoprotein stimulates macrophage 18F-FDG uptake via hypoxia-inducible factor-1α activation through Nox2-dependent reactive oxygen species generation. *J Nucl Med.* 55(10), p. 1699-1705. Available at: https://doi.org/10.2967/jnumed.114.139428.

Lee T-M., Chang N-C. & Lin S-Z., 2017. Dapagliflozin, a selective SGLT2 Inhibitor, attenuated cardiac fibrosis by regulating the macrophage polarization via STAT3 signaling in infarcted rat hearts. *Free Radic Biol Med.* 104, p. 298-310. Available at: https://doi.org/10.1016/j.freeradbiomed.2017.01.035.

Lee Y T., Lin H Y., Chan Y W., Li K H., To O T., Yan B P., Liu T., Li G., Wong W T., Keung W. & Tse G., 2017. Mouse models of atherosclerosis: a historical perspective and recent advances. *Lipids Health Dis.* 16(1):12. Available at: https://doi.org/10.1186/s12944-016-0402-5.

Lewis G F., Uffelman K D., Szeto L W. & Steiner G., 1993. Effects of acute hyperinsulinemia on VLDL triglyceride and VLDL apoB production in normal weight and obese individuals. *Diabetes*. 42(6), p. 833-842. Available at: https://doi.org/10.2337/diab.42.6.833.

Li B., Luo Y R., Tian F., Chen Y D., Tian J W., Ding Y., Zhu M., Li J W., Zhang Y Q. & Shi W M., 2020. Sitagliptin attenuates the progression of coronary atherosclerosis in patients with coronary disease and type 2 diabetes. *Atherosclerosis.* 300, p. 10-18. Available at: https://doi.org/10.1016/j.atherosclerosis.2020.03.015.

Li B., Luo Y R., Zhang Q., Fu S H., Chen Y D., Tian J W. & Guo Y., 2021. Sitagliptin, a dipeptidyl peptidase-4 inhibitor, attenuates apoptosis of vascular smooth muscle cells and reduces atherosclerosis in diabetic apolipoprotein E-deficient mice. *Vascul Pharmacol*. 140:106854. Available at: https://doi.org/10.1016/j.vph.2021.106854.

Li C., Huang S., Guo J., Wang C., Huang Z., Huang R., Liu L., Liang S. & Wang H., 2019. Metabolic Evaluation of MYCN-Amplified Neuroblastoma by 4-[^{18}F]FGln PET Imaging. *Mol Imaging Biol*. 21(6), p. 1117-1126. Available at: https://doi.org/10.1007/s11307-019-01330-9.

Li X., Samnick S., Lapa C., Israel I., Buck A K., Kreissl M C. & Bauer W., 2012. 68Ga-DOTATATE PET/CT for the detection of inflammation of large arteries: correlation with18F-FDG, calcium burden and risk factors. *EJNMMI Res*. 2(1):52. Available at: https://doi.org/10.1186/2191-219X-2-52.

Li X., Bauer W., Kreissl M C., Weirather J., Bauer E., Israel I., Richter D., Riehl G., Buck A. & Samnick S., 2013. Specific somatostatin receptor II expression in arterial plaque: (68)Ga-DOTATATE autoradiographic, immunohistochemical and flow cytometric studies in apoE-deficient mice. *Atherosclerosis.* 230(1), p. 33-39. Available at: https://doi.org/10.1016/j.atherosclerosis.2013.06.018.

Libby P., Ridker P M. & Maseri A., 2002. Inflammation and Atherosclerosis. *Circulation*. 105, p. 1135-1143. Available at: https://doi.org/10.1161/hc0902.104353.

Libby P., 2017. Interleukin-1 Beta as a Target for Atherosclerosis Therapy: The Biological Basis of CANTOS and Beyond. *J Am Coll Cardiol.* 70(18), p. 2278–2289. Available at: https://doi.org/10.1016/j.jacc.2017.09.028.

Libby P., Buring J E., Badimon L., Hansson G K., Deanfield J., Bittencourt M S., Tokgözoğlu L. & Lewis E F., 2019. Atherosclerosis. *Nat Rev Dis Primers*. 5(1):56. Available at: https://doi.org/10.1038/s41572-019-0106-z.

Liu K., Chen B., Zeng F., Wang G., Wu X., Liu Y., Li G., Yan J. & Zhang S., 2022. ApoE/ NOS3 Knockout Mice as a Novel Cardiovascular Disease Model of Hypertension and Atherosclerosis. *Genes (Basel)*. 13(11):1998. Available at: https://doi.org/10.3390/genes13111998.

Liu P S., Wang H., Li X., Chao T., Teav T., Christen S., Di Conza G., Cheng W C., Chou C H., Vavakova M., Muret C., Debackere K., Mazzone M., Huang H D., Fendt S M., Ivanisevic J. & Ho P C., 2017. α-ketoglutarate orchestrates macrophage activation through metabolic and epigenetic reprogramming. *Nat Immunol.* 18(9), p. 985-994. Available at: https://doi.org/10.1038/ni.3796.

Lutgens E., Daemen M., Kockx M., Doevendans P., Hofker M., Havekes L., Wellens H. & de Muinck E D., 1999. Atherosclerosis in APOE*3-Leiden transgenic mice: from proliferative to atheromatous stage. *Circulation.* 99(2), p. 276-283. Available at: https://doi.org/10.1161/01.cir.99.2.276.

Lv R., Bao Q. & Li Y., 2017. Regulation of M1-type and M2-type macrophage polarization in RAW264.7 cells by Galectin-9. *Mol Med Rep*. 16(6), p. 9111-9119. Available at: https://doi.org/10.3892/mmr.2017.7719.

Ma X., Liu Z., Ilyas I., Little P J., Kamato D., Sahebka A., Chen Z., Luo S., Zheng X., Weng J. & Xu S., 2021. GLP-1 receptor agonists (GLP-1RAs): cardiovascular actions and therapeutic potential. *Int J Biol Sci*. 17(8), p. 2050-2068. Available at: https://doi.org/10.7150/ijbs.59965.

MacMicking J., Xie Q W. & Nathan C., 1997. Nitric oxide and macrophage function. *Annu Rev Immunol*. 15, p. 323-350. Available at: https://doi.org/10.1146/annurev.immunol.15.1.323.

Madsen D H., Leonard D., Masedunskas A., Moyer A., Jürgensen H J., Peters D E., Amornphimoltham P., Selvaraj A., Yamada S S., Brenner D A., Burgdorf S., Engelholm L H., Behrendt N., Holmbeck K., Weigert R. & Bugge T H., 2013. M2-like macrophages are responsible for collagen degradation through a mannose receptor-mediated pathway. *J Cell Biol.* 202(6), p. 951-966. Available at: https://doi.org/10.1083/jcb.201301081.

Maier A., Teunissen A J P., Nauta S A., Lutgens E., Fayad Z A. & van Leent M M T., 2024. Uncovering atherosclerotic cardiovascular disease by PET imaging. *Nat Rev Cardiol*. Online ahead of print. Available at: https://doi.org/10.1038/s41569-024-01009-x.

Mallat Z., Gojova A., Marchiol-Fournigault C., Esposito B., Kamaté C., Merval R., Fradelizi D. & Tedgui A., 2001. Inhibition of transforming growth factor-beta signaling accelerates atherosclerosis and induces an unstable plaque phenotype in mice. *Circ Res.* 89(10), p. 930-934. Available at: https://doi.org/10.1161/hh2201.099415.

Mani P., Puri R., Schwartz G G., Nissen S E., Shao M., Kastelein J J P., Menon V., Lincoff A M. & Nicholls S J., 2019. Association of Initial and Serial C-Reactive Protein Levels With Adverse Cardiovascular Events and Death After Acute Coronary Syndrome: A Secondary Analysis of the VISTA-16 Trial. *JAMA Cardiol*. 4(4), p. 314-320. Available at: https://doi.org/10.1001/jamacardio.2019.0179.

Martinez F O., Gordon S., Locati M. & Mantovani A., 2006. Transcriptional profiling of the human monocyte-to-macrophage differentiation and polarization: new molecules and patterns of gene expression. *J Immunol*. 177(10), p. 7303-7311. Available at: https://doi.org/10.4049/jimmunol.177.10.7303.

Masteling M G., Zeebregts C J., Tio R A., Breek J-C., Tietge U J F., de Boer J F., Glaudemans A W J M., Dierckx R A J O., Boersma H H. & Slart R H J A., 2011. High-resolution imaging of human atherosclerotic carotid plaques with micro18F-FDG PET scanning exploring plaque vulnerability. *J Nucl Cardiol.* 18(6), p. 1066–1075. Available at: https://doi.org/10.1007/s12350-011-9460-2.

McGuire D K., Alexander J H., Johansen O E., Perkovic V., Rosenstock J., Cooper M E., Wanner C., Kahn S E., Toto R D., Zinman B., Baanstra D., Pfarr E., Schnaidt S., Meinicke T., George J T., von Eynatten M., Marx N. & CARMELINA Investigators, 2019. Linagliptin Effects on Heart Failure and Related Outcomes in Individuals With Type 2 Diabetes Mellitus at High Cardiovascular and Renal Risk in CARMELINA. *Circulation.* 139(3), p. 351-361. Available at: https://doi.org/10.1161/CIRCULATIONAHA.118.038352.

Meester E J., Krenning B J., de Swart J., Segbers M., Barrett H E., Bernsen M R., Van der Heiden K. & de Jong M., 2019. Perspectives on Small Animal Radionuclide Imaging; Considerations and Advances in Atherosclerosis. *Front Med (Lausanne).* 6:39. Available at: https://doi.org/10.3389/fmed.2019.00039.

Meier J J., 2012. GLP-1 receptor agonists for individualized treatment of type 2 diabetes mellitus. *Nat Rev Endocrinol*. 8(12), p. 728-742. Available at: https://doiorg/10.1038/nrendo.2012.140.

Michurina S V., Ishenko I J., Klimontov V V., Archipov S A., Myakina N E., Cherepanova M A., Zavjalov E L., Koncevaya G V. & Konenkov V I., 2016. Linagliptin alleviates fatty liver disease in diabetic db/ db mice. *World J Diabetes.*7(19), p. 534-546. Available at: https://doi.org/10.4239/wjd.v7.i19.534.

Midha A D., Zhou Y., Queliconi B B., Barrios A M., Haribowo A G., Chew B T L., Fong C O Y., Blecha J E., VanBrocklin H., Seo Y. & Jain I H., 2023. Organ-specific fuel rewiring in acute and chronic hypoxia redistributes glucose and fatty acid metabolism. *Cell Metab.* 35(3), p. 504-516.e5. Available at: https://doi.org/10.1016/j.cmet.2023.02.007.

Mikkola K., Yim C B., Fagerholm V., Ishizu T., Elomaa V V., Rajander J., Jurttila J., Saanijoki T., Tolvanen T., Tirri M., Gourni E., Béhé M., Gotthardt M., Reubi J C., Mäcke H., Roivainen A., Solin O. & Nuutila P., 2014. 64Cu- and 68Ga-labelled [Nle(14),Lys(40)(Ahx-NODAGA)NH2]-

exendin-4 for pancreatic beta cell imaging in rats. *Mol Imaging Biol*. 16(2), p. 255-263. Available at: https://doi.org/10.1007/s11307-013-0691-2.

Milzi A., Burgmaier M., Burgmaier K., Hellmich M., Marx N. & Reith S., 2017. Type 2 diabetes mellitus is associated with a lower fibrous cap thickness but has no impact on calcification morphology: an intracoronary optical coherence tomography study. *Cardiovasc Diabetol.* 16(1):152. Available at: https://doi.org/10.1186/s12933-017-0635-2.

Miner M W G., Liljenbäck H., Virta J., Kärnä S., Viitanen R., Elo P., Gardberg M., Teuho J., Saipa P., Rajander J., Mansour H M A., Cleveland N A., Low P S., Li X G. & Roivainen A., 2023. High folate receptor expression in gliomas can be detected in vivo using folate-based positron emission tomography with high tumor-to-brain uptake ratio divulging potential future targeting possibilities. *Front Immunol*. 14:1145473. Available at: https://doi.org/10.3389/fimmu.2023.1145473.

Mita T., Katakami N., Yoshii H., Onuma T., Kaneto H., Osonoi T., Shiraiwa T., Kosugi K., Umayahara Y., Yamamoto T., Yokoyama H., Kuribayashi N., Jinnouchi H., Gosho M., Shimomura I., Watada H. & Collaborators on the Study of Preventive Effects of Alogliptin on Diabetic Atherosclerosis (SPEAD-A) Trial, 2016. Alogliptin, a Dipeptidyl Peptidase 4 Inhibitor, Prevents the Progression of Carotid Atherosclerosis in Patients With Type 2 Diabetes: The Study of Preventive Effects of Alogliptin on Diabetic Atherosclerosis (SPEAD-A). *Diabetes Care.* 39(1), p. 139-148. Available at: https://doi.org/10.2337/dc15-0781.

Mita T., Katakami N., Shiraiwa T., Yoshii H., Gosho M., Shimomura I. & Watada H., 2017. Dose-Dependent Effect of Sitagliptin on Carotid Atherosclerosis in Patients with Type 2 Diabetes Mellitus Receiving Insulin Treatment: A Post Hoc Analysis. *Diabetes Ther.* 8(5), p. 1135-1146. Available at: https://doi.org/10.1007/s13300-017-0309-9.

Miyashita Y., Shirai K., Itoh Y., Sasaki H., Totsuka M., Murano T. & Watanabe H., 2002. Low lipoprotein lipase mass in preheparin serum of type 2 diabetes mellitus patients and its recovery with insulin therapy. *Diabetes Res Clin Pract.* 56(3), p. 181-187. Available at: https://doi.org/10.1016/s0168-8227(01)00369-2.

Miyazaki M., Kato M., Tanaka K., Tanaka M., Kohjima M., Nakamura K., Enjoji M., Nakamuta M., Kotoh K. & Takayanagi R., 2012. Increased hepatic expression of dipeptidyl peptidase-4 in non-alcoholic fatty liver disease and its association with insulin resistance and glucose metabolism. *Mol Med Rep.* 5(3), p. 729-733. Available at: https://doi.org/10.3892/mmr.2011.707.

Moisio O., Palani S., Virta J., Elo P., Liljenbäck H., Tolvanen T., Käkelä M., Miner M G., Atencio Herre E., Marjamäki P., Örd T., Heinäniemi M., Kaikkonen M U., Zhang F., Srinivasarao M., Knuuti J., Low P S., Saraste A., Li X G. & Roivainen A., 2020. Radiosynthesis and preclinical evaluation of [^{68}Ga]Ga-NOTA-folate for PET imaging of folate receptor β-positive macrophages. Sci Rep. 10(1):13593. Available at: https://doi.org/10.1038/s41598-020-70394-3.

Moore K J. & Tabas I., 2011. Macrophages in the Pathogenesis of Atherosclerosis. *Cell*. 145(3), p. 341–355. Available at: https://doi.org/10.1016/j.cell.2011.04.005.

Mudaliar S., Alloju S. & Henry R R., 2016. Can a Shift in Fuel Energetics Explain the Beneficial Cardiorenal Outcomes in the EMPA-REG OUTCOME Study? A Unifying Hypothesis. *Diabetes Care.* 39(7), p. 1115-1122. Available at: https://doi.org/10.2337/dc16-0542.

Müller T D., Finan B., Bloom S R., D'Alessio D., Drucker D J., Flatt P R., Fritsche A., Gribble F., Grill H J., Habener J F., Holst J J., Langhans W., Meier J J., Nauck M A., Perez-Tilve D., Pocai A., Reimann F., Sandoval D A., Schwartz T W., Seeley R J., Stemmer K., Tang-Christensen M., Woods S C., DiMarchi R D. & Tschöp M H., 2019. Glucagon-like peptide 1 (GLP-1). *Mol Metab.* 30, p. 72-130. Available at: https://doi.org/10.1016/j.molmet.2019.09.010.

Müller A., Beck K., Rancic Z., Müller C., Fischer C R., Betzel T., Kaufmann P A., Schibli R., Krämer S D. & Ametamey S M., 2014. Imaging atherosclerotic plaque inflammation via folate receptor targeting using a novel 18F-folate radiotracer. *Mol Imaging.* 13, p. 1-11.

Nagashima M., Watanabe T., Terasaki M., Tomoyasu M., Nohtomi K., Kim-Kaneyama J., Miyazaki A. & Hirano T., 2011. Native incretins prevent the development of atherosclerotic lesions in

apolipoprotein E knockout mice. *Diabetologia.* 54(10), p. 2649-2659. Available at: https://doi.org/10.1007/s00125-011-2241-2.

Nagel T., Resnick N., Atkinson W J., Dewey Jr C F. & Gimbrone Jr M A., 1994. Shear stress selectively upregulates intercellular adhesion molecule-1 expression in cultured human vascular endothelial cells. *J Clin Invest.* 94, p. 885–891. Available at: https://doi.org/10.1172/JCI117410.

Nakashima Y., Plump A S., Raines E W., Breslow J L. & Ross R., 1994. ApoE-deficient mice develop lesions of all phases of atherosclerosis throughout the arterial tree. *Arterioscler Thromb.* 14(1), p. 133-140. Available at: https://doi.org/10.1161/01.atv.14.1.133.

Nakashima Y., Raines E W., Plump A S., Breslow J L. & Ross R., 1998. Upregulation of VCAM-1 and ICAM-1 at atherosclerosis-prone sites on the endothelium in the ApoE-deficient mouse. *Arterioscler Thromb Vasc Biol* 18(5), p. 842-851. Available at: https://doi.org/10.1161/01.atv.18.5.842.

Nakashima-Matsushita N., Homma T., Yu S., Matsuda T., Sunahara N., Nakamura T., Tsukano M., Ratnam M. & Matsuyama T., 1999. Selective expression of folate receptor beta and its possible role in methotrexate transport in synovial macrophages from patients with rheumatoid arthritis. *Arthritis Rheum.* 42(8), p. 1609-1616. Available at: https://doi.org/10.1002/1529-0131(199908)42:8<1609::AID-ANR7>3.0.CO;2-L.

Nauck M A., Quast D R., Wefers J. & Meier J J., 2021. GLP-1 receptor agonists in the treatment of type 2 diabetes - state-of-the-art. *Mol Metab.* 46:101102. Available at: https://doi.org/10.1016/j.molmet.2020.101102.

Neal B., Perkovic V., Mahaffey K W., de Zeeuw D., Fulcher G., Erondu N., Shaw W., Law G., Desai M., Matthews D R.; CANVAS Program Collaborative Group, 2017. Canagliflozin and Cardiovascular and Renal Events in Type 2 Diabetes. *N Engl J Med.* 377(7), p. 644-657. Available at: https://doi.org/10.1056/NEJMoa1611925.

Newsholme P., Costa Rosa L F., Newsholme E A. & Curi R., 1996. The importance of fuel metabolism to macrophage function. *Cell Biochem Funct.* 14(1), p. 1-10. Available at: https://doi.org/10.1002/cbf.644.

Newsholme P., Procopio J., Lima M M., Pithon-Curi T C. & Curi R., 2003. Glutamine and glutamate--their central role in cell metabolism and function. *Cell Biochem Funct.* 21(1), p. 1-9. Available at: https://doi.org/10.1002/cbf.1003.

Nishida S., Matsumura T., Senokuchi T., Murakami-Nishida S., Ishii N., Morita Y., Yagi Y., Motoshima H., Kondo T. & Araki E., 2020. Inhibition of inflammation-mediated DPP-4 expression by linagliptin increases M2 macrophages in atherosclerotic lesions. *Biochem Biophys Res Commun*. 524(1), p. 8-15. Available at: https://doi.org/10.1016/j.bbrc.2020.01.027.

Nomura-Kitabayashi A. & Kovacic J C., 2018. Mouse Model of Wire Injury-Induced Vascular Remodeling. *Methods Mol Biol*. 1816, p. 253-268. Available at: https://doi.org/10.1007/978-1-4939-8597-5_20.

Noyan-Ashraf M H., Momen M A., Ban K., Sadi A-M., Zhou Y-Q., Riazi A M., Baggio L L., Henkelman R M., Husain M. & Drucker D J., 2009. GLP-1R agonist liraglutide activates cytoprotective pathways and improves outcomes after experimental myocardial infarction in mice. *Diabetes.* 58(4), p. 975-983. Available at: https://doi.org/10.2337/db08-1193.

Otsuka F., Sakakura K., Yahagi K., Joner M. & Virmani R., 2014. Has our understanding of calcification in human coronary atherosclerosis progressed? Arterioscler Thromb Vasc Biol. 34(4), p. 724-736. Available at: https://doi.org/10.1161/ATVBAHA.113.302642.

Paigen B., Morrow A., Brandon C., Mitchell D. & Holmes P., 1985. Variation in susceptibility to atherosclerosis among inbred strains of mice. *Atherosclerosis.* 57(1), p. 65-73. Available at: https://doi.org/10.1016/0021-9150(85)90138-8.

Pan X., Xu Q., Chen J., Wang T., Zhang M., Wang H. & Gao H., 2019. Preliminary evaluation of 18F-AlF-NOTA-MAL-Cys40-Exendin-4 in rodent heart after myocardial ischemia and reperfusion. *Mol Med Rep*. 20(3), p. 2276-2284. Available at: https://doi.org/10.3892/mmr.2019.10432.

Pasterkamp G., den Ruijter H M. & Giannarelli C., 2022. False Utopia of One Unifying Description of the Vulnerable Atherosclerotic Plaque: A Call for Recalibration That Appreciates the Diversity of Mechanisms Leading to Atherosclerotic Disease. *Arterioscler Thromb Vasc Biol*. 42(4), p. e86-e95. Available at: https://doi.org/10.1161/ATVBAHA.121.316693.

Paulmier B., Duet M., Khayat R., Pierquet-Ghazzar N., Laissy J-P., Maunoury C., Hugonnet F., Sauvaget E., Trinquart L. & Faraggi M., 2008. Arterial wall uptake of fluorodeoxyglucose on PET imaging in stable cancer disease patients indicates higher risk for cardiovascular events. *J Nucl Cardiol.* 15(2), p. 209-217. Available at: https://doi.org/10.1016/j.nuclcard.2007.10.009.

Pedersen S F., Græbe M., Hag A M F., Højgaard L., Sillesen H. & Kjær A., 2013. (18)F-FDG imaging of human atherosclerotic carotid plaques reflects gene expression of the key hypoxia marker HIF-1α. *Am J Nucl Med Mol Imaging*.3(5), p. 384-392.

Pedersen S F., Sandholt B V., Keller S H., Hansen A E., Clemmensen A E., Sillesen H., Højgaard L., Ripa R S. & Kjær A., 2015. 64Cu-DOTATATE PET/MRI for Detection of Activated Macrophages in Carotid Atherosclerotic Plaques: Studies in Patients Undergoing Endarterectomy. *Arterioscler Thromb Vasc Biol*. 35(7), p. 1696-1703. Available at: https://doi.org/10.1161/ATVBAHA.114.305067.

Pfeffer M A., Claggett B., Diaz R., Dickstein K., Gerstein H C., Køber L V., Lawson F C., Ping L., Wei X., Lewis E F., Maggioni A P., McMurray J J V., Probstfield J L., Riddle M C., Solomon S D., Tardif J-C.; ELIXA Investigators, 2015. Lixisenatide in Patients with Type 2 Diabetes and Acute Coronary Syndrome. *N Engl J Med.* 373(23), p. 2247-2257. Available at: https://doi.org/10.1056/NEJMoa1509225.

Philippidis P., Mason J C., Evans B J., Nadra I., Taylor K M., Haskard D O. & Landis R C., 2004. Hemoglobin scavenger receptor CD163 mediates interleukin-10 release and heme oxygenase-1 synthesis: antiinflammatory monocyte-macrophage responses in vitro, in resolving skin blisters in vivo, and after cardiopulmonary bypass surgery. *Circ Res.* 94(1), p. 119-126. Available at: https://doiorg/10.1161/01.RES.0000109414.78907.F9.

Piccirillo F., Mastroberardino S., Nusca A., Frau L., Guarino L., Napoli N., Ussia G P. & Grigioni F., 2023. Novel Antidiabetic Agents and Their Effects on Lipid Profile: A Single Shot for Several Cardiovascular Targets. *Int J Mol Sci.* 24(12):10164. Available at: https://doi.org/10.3390/ijms241210164.

Piedrahita J A., Zhang S H., Hagaman J R., Oliver P M. & Maeda N., 1992. Generation of mice carrying a mutant apolipoprotein E gene inactivated by gene targeting in embryonic stem cells. *Proc Natl Acad Sci U S A.* 89(10), p. 4471-4475. Available at: https://doi.org/10.1073/pnas.89.10.4471.

Plump A S., Smith J D., Hayek T., Aalto-Setälä K., Walsh A., Verstuyft J G., Rubin E M. & Breslow J L., 1992. Severe hypercholesterolemia and atherosclerosis in apolipoprotein E-deficient mice created by homologous recombination in ES cells. *Cell*. 71(2), p. 343-353. Available at: https://doi.org/10.1016/0092-8674(92)90362-g.

Plump A S. & Breslow J L., 1995. Apolipoprotein E and the apolipoprotein E-deficient mouse. *Annu Rev Nutr*.15, p. 495-518. Available at: https://doi.org/10.1146/annurev.nu.15.070195.002431.

Potteaux S., Esposito B., van Oostrom O., Brun V., Ardouin P., Groux H., Tedgui A. & Mallat Z., 2004. Leukocyte-derived interleukin 10 is required for protection against atherosclerosis in low-density lipoprotein receptor knockout mice. *Arterioscler Thromb Vasc Biol.* 24(8), p. 1474-1478. Available at: https://doi.org/10.1161/01.ATV.0000134378.86443.cd.

Powell-Braxton L., Véniant M., Latvala R D., Hirano K I., Won W B., Ross J., Dybdal N., Zlot C H. & Young S G., 1998. A mouse model of human familial hypercholesterolemia: markedly elevated low density lipoprotein cholesterol levels and severe atherosclerosis on a low-fat chow diet. *Nat Med*. 4(8), p. 934-938. Available at: https://doi.org/10.1038/nm0898-934.

Poznyak A V., Grechko A V., Poggio P., Myasoedova V A., Alfieri V. & Orekhov A N., 2020. The Diabetes Mellitus-Atherosclerosis Connection: The Role of Lipid and Glucose Metabolism and Chronic Inflammation. *Int J Mol Sci*. 21(5): 1835. Available at: https://doi.org/10.3390/ijms21051835.

Poznyak A V., Sukhorukov V N., Surkova R., Orekhov N A. & Orekhov A N., 2023. Glycation of LDL: AGEs, impact on lipoprotein function, and involvement in atherosclerosis. *Front Cardiovasc Med.* 10:1094188. Available at: https://doi.org/10.3389/fcvm.2023.1094188.

Prenosil G A., Sari H., Fürstner M., Afshar-Oromieh A., Shi K., Rominger A. & Hentschel M., 2022. Performance Characteristics of the Biograph Vision Quadra PET/CT System with a Long Axial Field of View Using the NEMA NU 2-2018 Standard. *J Nucl Med*. 63(3), p. 476-484. Available at: https://doi.org/10.2967/jnumed.121.261972.

Pugliese F., Gaemperli O., Kinderlerer A R., Lamare F., Shalhoub J., Davies A H., Rimoldi O E., Mason J C. & Camici P G., 2010. Imaging of vascular inflammation with [11C]-PK11195 and positron emission tomography/computed tomography angiography. *J Am Coll Cardiol*. 56(8), p. 653-661. Available at: https://doi.org/10.1016/j.jacc.2010.02.063.

Puig-Kröger A., Sierra-Filardi E., Domínguez-Soto A., Samaniego R., Corcuera M T., Gómez-Aguado F., Ratnam M., Sánchez-Mateos P. & Corbí A L., 2009. Folate receptor beta is expressed by tumor-associated macrophages and constitutes a marker for M2 anti-inflammatory/regulatory macrophages. *Cancer Res.* 69(24), p. 9395-9403. Available at: https://doi.orh/10.1158/0008-5472.CAN-09-2050.

Pyke C., Heller R S., Kirk R K., Ørskov C., Reedtz-Runge S., Kaastrup P., Hvelplund A., Bardram L., Calatayud D. & Bjerre Knudsen L., 2014. GLP-1 receptor localization in monkey and human tissue: novel distribution revealed with extensively validated monoclonal antibody. *Endocrinology.* 155(4), p. 1280-1290. Available at: https://doi.org/10.1210/en.2013-1934.

Qiao Y N., Zou Y L. & Guo S D., 2022. Low-density lipoprotein particles in atherosclerosis. *Front Physiol*. 13: 931931. Available at: https://doi.org/10.3389/fphys.2022.931931.

Qiao L., Fisher E., McMurray L., Milicevic Sephton S., Hird M., Kuzhuppilly-Ramakrishnan N., Williamson D J., Zhou X., Werry E., Kassiou M., Luthra S., Trigg W. & Aigbirhio F I., 2019. Radiosynthesis of (R,S)-[^{18}F]GE387: A Potential PET Radiotracer for Imaging Translocator Protein 18 kDa (TSPO) with Low Binding Sensitivity to the Human Gene Polymorphism rs6971. *ChemMedChem.* 14(9), p. 982-993. Available at: https://doi.org/10.1002/cmdc.201900023.

Rakipovski G., Rolin B., Nøhr J., Klewe I., Frederiksen K S., Augustin R., Hecksher-Sørensen J., Ingvorsen C., Polex-Wolf J. & Knudsen L B., 2018. The GLP-1 Analogs Liraglutide and Semaglutide Reduce Atherosclerosis in ApoE-/- and LDLr-/- Mice by a Mechanism That Includes Inflammatory Pathways. *JACC Basic Transl Sci.* 3(6), p. 844-857. Available at: https://doi.org/10.1016/j.jacbts.2018.09.004.

Ramprasad M P., Terpstra V., Kondratenko N., Quehenberger O. & Steinberg D., 1996. Cell surface expression of mouse macrosialin and human CD68 and their role as macrophage receptors for oxidized low density lipoprotein. *Proc Natl Acad Sci U S A*. 93(25), p. 14833-14838. Available at: https://doi.org/10.1073/pnas.93.25.14833.

Reijrink M., de Boer S A., Te Velde-Keyzer C A., Sluiter J K E., Pol R A., Heerspink H J L., Greuter M J W., Hillebrands J L., Mulder D J. & Slart R H J A., 2022. [^{18}F]FDG and [^{18}F]NaF as PET markers of systemic atherosclerosis progression: A longitudinal descriptive imaging study in patients with type 2 diabetes mellitus. *J Nucl Cardiol*. 29(4), p. 1702-1709. Available at: https://doi.org/10.1007/s12350-021-02781-w.

Reijrink M., Sluiter J K E., Te Velde-Keyzer C A., de Borst M H., van Praagh G D., Greuter M J W., Luurtsema G., Boersma H H., Pol R A., Hillebrands J L., van Dijk P R., Hoogenberg K., Mulder D J. & Slart R H J A., 2023. Severely increased albuminuria in patients with type 2 diabetes mellitus is associated with increased subclinical atherosclerosis in femoral arteries with Na [^{18}F]F activity as a proxy - The DETERMINE study. *Atherosclerosis*. 117199. Available at: https://doi.org/10.1016/j.atherosclerosis.2023.117199.

Renick P J., Mulgaonkar A., Co C M., Wu C Y., Zhou N., Velazquez A., Pennington J., Sherwood A., Dong H., Castellino L., Öz O K., Tang L. & Sun X., 2021. Imaging of Actively Proliferating Bacterial Infections by Targeting the Bacterial Metabolic Footprint with d-[5-11C]-Glutamine. *ACS Infect Dis.* 7(2), p. 347-361. Available at: https://doi.org/10.1021/acsinfecdis.0c00617.

Richards P., Parker H E., Adriaenssens A E., Hodgson J M., Cork S C., Trapp S., Gribble F M. & Reimann F., 2014. Identification and characterisation of glucagon-like peptide-1 receptor expressing cells using a new transgenic mouse model. *Diabetes*. 63(4), p. 1224–1233. Available at: https://doi.org/10.2337/db13-1440.

Ridker P M. & Rane M., 2021. Interleukin-6 Signaling and Anti-Interleukin-6 Therapeutics in Cardiovascular Disease. *Circ Res.* 128(11), p. 1728-1746. Available at: https://doi.org/10.1161/CIRCRESAHA.121.319077.

Rinne P., Hellberg S., Kiugel M., Virta J., Li X.G., Käkelä M., Helariutta K., Luoto P., Liljenbäck H., Hakovirta H., Gardberg M., Airaksinen A J., Knuuti J., Saraste A. & Roivainen A., 2016. Comparison of Somatostatin Receptor 2-Targeting PET Tracers in the Detection of Mouse Atherosclerotic Plaques. *Mol Imaging Biol.* 18(1), p. 99-108. Available at: https://doi.org/10.1007/s11307-015-0873-1.

Roche-Molina M., Sanz-Rosa D., Cruz F M., García-Prieto J., López S., Abia R., Muriana F J G., Fuster V., Ibáñez B. & Bernal J A., 2015. Induction of sustained hypercholesterolemia by single adeno-associated virus-mediated gene transfer of mutant hPCSK9. *Arterioscler Thromb Vasc Biol.* 35(1), p. 50-59. Available at: https://doi.org/10.1161/ATVBAHA.114.303617.

Roque M., Fallon J T., Badimon J J., Zhang W X., Taubman M B. & Reis E D., 2000. Mouse model of femoral artery denudation injury associated with the rapid accumulation of adhesion molecules on the luminal surface and recruitment of neutrophils. *Arterioscler Thromb Vasc Biol*. 20(2), p. 335-342. Available at: https://doi: 10.1161/01.atv.20.2.335.

Ross T L., Honer M., Lam P Y H., Mindt T L., Groehn V., Schibli R., Schubiger P A. & Ametamey S M., 2008. Fluorine-18 click radiosynthesis and preclinical evaluation of a new 18F-labeled folic acid derivative. *Bioconjug Chem.* 19(12), p. 2462-2470. Available at: https://doi.org/10.1021/bc800356r.

Rudd J H F., Warburton E A., Fryer T D., Jones H A., Clark J C., Antoun N., Johnström P., Davenport A P., Kirkpatrick P J., Arch B N., Pickard J D. & Weissberg P L., 2002. Imaging atherosclerotic plaque inflammation with [18F]-fluorodeoxyglucose positron emission tomography. *Circulation.* 105(23), p. 2708-2711. Available at: https://doi.org/10.1161/01.cir.0000020548.60110.76.

Rudd J H F., Myers K S., Bansilal S., Machac J., Woodward M., Fuster V., Farkouh M E. & Fayad Z A., 2009. Relationships among regional arterial inflammation, calcification, risk factors, and biomarkers: a prospective fluorodeoxyglucose positron-emission tomography/computed tomography imaging study. *Circ Cardiovasc Imaging.* 2(2), p. 107-115. Available at: https://doi.org/10.1161/CIRCIMAGING.108.811752.

Rumberger J A., Simons D B., Fitzpatrick L A., Sheedy P F. & Schwartz R S., 1995. Coronary artery calcium area by electron-beam computed tomography and coronary atherosclerotic plaque area. A histopathologic correlative study. *Circulation*. 92(8), p. 2157-2162. Available at: https://doi.org/10.1161/01.cir.92.8.2157.

Ruotsalainen A K., Lappalainen J P., Heiskanen E., Merentie M., Sihvola V., Näpänkangas J., Lottonen-Raikaslehto L., Kansanen E., Adinolfi S., Kaarniranta K., Ylä-Herttuala S., Jauhiainen M., Pirinen E. & Levonen A L., 2019. Nuclear factor E2-related factor 2 deficiency impairs atherosclerotic lesion development but promotes features of plaque instability in hypercholesterolaemic mice. *Cardiovasc Res*.115(1), p. 243-254. Available at: https://doi.org/10.1093/cvr/cvy143.

Rösen P., Nawroth P P., King G., Möller W., Tritschler H J. & Packer L., 2001. The role of oxidative stress in the onset and progression of diabetes and its complications: a summary of a Congress Series sponsored by UNESCO-MCBN, the American Diabetes Association and the German Diabetes Society. *Diabetes Metab Res Rev.*17(3), p. 189-212. Available at: https://doi.org/10.1002/dmrr.196.

Sage A P., Tsiantoulas D., Binder C J. & Mallat Z., 2019. The role of B cells in atherosclerosis. *Nat Rev Cardiol*. 16(3), p. 180-196. Available at: https://doi.org/10.1038/s41569-018-0106-9.

Saigusa R., Winkels H. & Ley K., 2020. T cell subsets and functions in atherosclerosis. *Nat Rev Cardiol*. 17(7), p. 387-401. Available at: https://doi.org/10.1038/s41569-020-0352-5.

Sakai A., Kume N., Nishi E., Tanoue K., Miyasaka M. & Kita T., 1997. P-selectin and vascular cell adhesion molecule-1 are focally expressed in aortas of hypercholesterolemic rabbits before intimal accumulation of macrophages and T lymphocytes. *Arterioscler Thromb Vasc Biol.* 17(2), p. 310-316. Available at: https://doi.org/10.1161/01.atv.17.2.310.

Salim H M., Fukuda D., Higashikuni Y., Tanaka K., Hirata Y., Yagi S., Soeki T., Shimabukuro M. & Sata M., 2016. Dipeptidyl peptidase-4 inhibitor, linagliptin, ameliorates endothelial dysfunction and atherogenesis in normoglycemic apolipoprotein-E deficient mice. *Vascul Pharmacol.* 79, p. 16-23. Available at: https://doi.org/ 10.1016/j.vph.2015.08.011.

Sandoval R M., Kennedy M D., Low P S. & Molitoris B A., 2004. Uptake and trafficking of fluorescent conjugates of folic acid in intact kidney determined using intravital two-photon microscopy. *Am J Physiol Cell Physiol.* 287(2), p. C517-526. Available at: https://doi.org/10.1152/ajpcell.00006.2004.

Santos F O., Correia B R O., Marinho T S., Barbosa-da-Silva S., Mandarim-de-Lacerda C A. & Souza-Mello V., 2020. Anti-steatotic linagliptin pleiotropic effects encompasses suppression of de novo lipogenesis and ER stress in high-fat-fed mice. *Mol Cell Endocrinol.* 509:110804. Available at: https://doi.org/10.1016/j.mce.2020.110804.

Sata M., Maejima Y., Adachi F., Fukino K., Saiura A., Sugiura S., Aoyagi T., Imai Y., Kurihara H., Kimura K., Omata M., Makuuchi M., Hirata Y. & Nagai R., 2000. A mouse model of vascular injury that induces rapid onset of medial cell apoptosis followed by reproducible neointimal hyperplasia. *J Mol Cell Cardiol*. 32(11), p. 2097-2104. Available at: https://doi.org/10.1006/jmcc.2000.1238.

Saxena R., Nassiri M., Yin X M. & Morral N., 2022. Insights from a high-fat diet fed mouse model with a humanized liver. *PLoS One*. 17(5): e0268260. Available at: https://doi.org/10.1371/journal.pone.0268260.

Scarf A M. & Kassiou M., 2011. The translocator protein. *J Nucl Med.* 52(5), p. 677-680. Available at: https://doi.org/10.2967/jnumed.110.086629.

Schmidt A M., Yan S D., Brett J., Mora R., Nowygrod R. & Stern D., 1993. Regulation of human mononuclear phagocyte migration by cell surface-binding proteins for advanced glycation end products. *J Clin Invest*. 91(5), p. 2155-2168. Available at: https://doi.org/10.1172/JCI116442.

Schmidt A M. & Stern D., 2000. Atherosclerosis and diabetes: the RAGE connection. *Curr Atheroscler Rep.* 2(5), p. 430-436. Available at: https://doi.org/10.1007/s11883-000-0082-4.

Schulte M L., Hight M R., Ayers G D., Liu Q., Shyr Y., Washington M K. & Manning H C., 2017. Non-Invasive Glutamine PET Reflects Pharmacological Inhibition of BRAFV600E In Vivo. *Mol Imaging Biol.* 19(3), p. 421-428. Available at: https://doi.org/10.1007/s11307-016-1008-z.

Sharma A., Virmani T., Sharma A., Chhabra V., Kumar G., Pathak K. & Alhalmi A., 2022. Potential Effect of DPP-4 Inhibitors Towards Hepatic Diseases and Associated Glucose Intolerance. *Diabetes Metab Syndr Obes*. 15, p. 1845-1864. Available at: https://doi.org/10.2147/DMSO.S369712.

Shen J., Hilgenbrink A R., Xia W., Feng Y., Dimitrov D S., Lockwood M B., Amato R J. & Low P S., 2014. Folate receptor-β constitutes a marker for human proinflammatory monocytes. *J Leukoc Biol.* 96(4), p. 563-570. Available at: https://doi.org/10.1189/jlb.2AB0713-372R.

Selhub J. & Franklin W A., 1984. The folate-binding protein of rat kidney. Purification, properties, and cellular distribution. *J Biol Chem.* 259(10), p. 6601-6606.

Selvaraju R K., Velikyan I., Johansson L., Wu Z., Todorov I., Shively J., Kandeel F., Korsgren O. & Eriksson O., 2013. In vivo imaging of the glucagonlike peptide 1 receptor in the pancreas with 68Ga-labeled DO3A-exendin-4. *J Nucl Med.* 54(8), p. 1458-1463. Available at: https://doi.org/10.2967/jnumed.112.114066.

Senders M L., Hernot S., Carlucci G., van de Voort J C., Fay F., Calcagno C., Tang J., Alaarg A., Zhao Y., Ishino S., Palmisano A., Boeykens G., Meerwaldt A E., Sanchez-Gaytan B L., Baxter S.,

Zendman L., Lobatto M E., Karakatsanis N A., Robson P M., Broisat A., Raes G., Lewis J S., Tsimikas S., Reiner T., Fayad Z A., Devoogdt N., Mulder W J M. & Pérez-Medina C., 2019. Nanobody-Facilitated Multiparametric PET/MRI Phenotyping of Atherosclerosis. *JACC Cardiovasc Imaging.* 12(10), p. 2015-2026. Available at: https://doi.org/10.1016/j.jcmg.2018.07.027

Severino P., D'Amato A., Pucci M., Infusino F., Adamo F., Birtolo L I., Netti L., Montefusco G., Chimenti C., Lavalle C., Maestrini V., Mancone M., Chilian W M. & Fedele F., 2020. Ischemic Heart Disease Pathophysiology Paradigms Overview: From Plaque Activation to Microvascular Dysfunction. *Int J Mol Sci.* 21(21):8118. Available at: https://doi.org/10.3390/ijms21218118.

Silvola J M U., Saraste A., Laitinen I., Savisto N., Laine J O., Heinonen S E., Ylä-Herttuala S., Saukko P., Nuutila P., Roivainen A. & Knuuti J., 2011. Effects of age, diet, and type 2 diabetes on the development and FDG uptake of atherosclerotic plaques. *JACC Cardiovasc Imaging*. 4(12), p. 1294-1301. Available at:https://doi.org/10.1016/j.jcmg.2011.07.009.

Sluimer J C., Kolodgie F D., Bijnens A P P J J., Maxfield K., Pacheco E., Kutys B., Duimel H., Frederik P M., van Hinsbergh V W M., Virmani R. & Daemen M J A P., 2009. Thin-walled microvessels in human coronary atherosclerotic plaques show incomplete endothelial junctions- relevance of compromised structural integrity for intraplaque microvascular leakage. *J Am Coll Cardiol,* 53(17), p. 1517-1527. Available at: https://doi.org/10.1016/j.jacc.2008.12.056.

Spiegelstein O., Eudy J D. & Finnell R H., 2000. Identification of two putative novel folate receptor genes in humans and mouse. *Gene*. 258(1-2), p. 117-125. Available at: https://doi.org/10.1016/s0378-1119(00)00418-2.

Sriranjan R S., Tarkin J M., Evans N R., Le E P V., Chowdhury M M. & Rudd J H F., 2021. Atherosclerosis imaging using PET: Insights and applications. *Br J Pharmacol*. 178(11), p. 2186-2203. Available at: https://doi.org/10.1111/bph.14868.

Stalker T J., 2020. Mouse laser injury models: variations on a theme. *Platelets*. 31(4), p. 423-431. Available at: https://doi.org/10.1080/09537104.2020.1748589.

Stein M., Keshav S., Harris N. & Gordon S., 1992. Interleukin 4 potently enhances murine macrophage mannose receptor activity: a marker of alternative immunologic macrophage activation. *J Exp Med*. 176(1), p. 287-292. Available at: https://doi.org/10.1084/jem.176.1.287.

Ståhle M., Kytö V., Kiugel M., Liljenbäck H., Metsälä O., Käkelä M., Li.X-G., Oikonen V., Saukko P., Nuutila P., Knuuti J., Roivainen A. & Saraste A., 2020. Glucagon-like peptide-1 receptor expression after myocardial infarction: Imaging study using ^{68}Ga-NODAGA-exendin-4 positron emission tomography. *J Nucl Cardiol.* 27(6), p. 2386-2397. Available at: https://doi.org/10.1007/s12350-018-01547-1.

Su S., Zhang C., Zhang F., Li H., Yang X. & Tang X., 2016. The association between leptin receptor gene polymorphisms and type 2 diabetes mellitus: A systematic review and meta-analysis. *Diabetes Res Clin Pract*. 121, p. 49-58. Available at: https://doi.org/10.1016/j.diabres.2016.08.008.

Subramanian M. & Tabas I., 2014. Dendritic cells in atherosclerosis. *Semin Immunopathol*. 36(1), p. 93-102. Available at: https://doi.org/10.1007/s00281-013-0400-x.

Sun Z., Li L., Zhang L., Yan J., Shao C., Bao Z., Liu J., Li Y., Zhou M., Hou L., Jing L., Pang Q., Geng Y., Mao X., Gu W. & Wang Z., 2020. Macrophage galectin-3 enhances intimal translocation of vascular calcification in diabetes mellitus. *Am J Physiol Heart Circ Physiol.* 318(5), p. H1068-H1079. Available at: https://doi.org/10.1152/ajpheart.00690.2019.

Søndergaard E., Lauritzen E S., Lauritsen K M., Åkerblom A., Nuutila P., Oldgren J. & Gormsen L C., 2022. SGLT2 inhibition reduces myocardial oxygen consumption. *Metabol Open.* 23:15:100207. Available at: https://doi.org/10.1016/j.metop.2022.100207.

Ta N N., Schuyler C A., Li Y., Lopes-Virella M F. & Huang Y., 2011. DPP-4 (CD26) inhibitor alogliptin inhibits atherosclerosis in diabetic apolipoprotein E-deficient mice. *J Cardiovasc Pharmacol*. 58(2), p. 157-166. Available at: https://doi.org/10.1097/FJC.0b013e31821e5626.

Tabas I. & Bornfeldt K E., 2016. Macrophage Phenotype and Function in Different Stages of *Atherosclerosis. Circ Res*. 118(4), p. 653–667. Available at: https://doi.org/10.1161/CIRCRESAHA.115.306256.

Tahara N., Mukherjee J., de Haas H J., Petrov A D., Tawakol A., Haider N., Tahara A., Constantinescu C C., Zhou J., Boersma H H., Imaizumi T., Nakano M., Finn A., Fayad Z., Virmani R., Fuster V., Bosca L. & Narula J., 2014. 2-deoxy-2-[18F]fluoro-D-mannose positron emission tomography imaging in atherosclerosis. *Nat Med.* 20(2), p. 215-219. Available at: https://doi.org/10.1038/nm.3437

Takai S., Sakonjo H. & Jin D., 2014. Significance of vascular dipeptidyl peptidase-4 inhibition on vascular protection in Zucker diabetic fatty rats. *J Pharmacol Sci.* 125(4), p. 386-393. Available at: https://doi.org/10.1254/jphs.14052fp.

Tan Q., Akindehin S E., Orsso C E., Waldner R C., DiMarchi R D., Müller T D. & Haqq A M., 2020. Recent Advances in Incretin-Based Pharmacotherapies for the Treatment of Obesity and Diabetes. *Front Endocrinol (Lausanne).* 13:838410. Available at: https://doi.org/10.3389/fendo.2022.838410.

Tarkin J M., Dweck M R., Evans N R., Takx R A P., Brown A J., Tawakol A., Fayad Z A. & Rudd J H F., 2016. *Imaging Atherosclerosis. Circ Res*. 118(4), p. 750-769. Available at: https://doi.org/10.1161/CIRCRESAHA.115.306247.

Tarkin J M., Joshi F R., Evans N R., Chowdhury M M., Figg N L., Shah A V., Starks L T., Martin-Garrido A., Manavaki R., Yu E., Kuc R E., Grassi L., Kreuzhuber R., Kostadima M A., Frontini M., Kirkpatrick P J., Coughlin P A., Gopalan D., Fryer T D., Buscombe J R., Groves A M., Ouwehand W H., Bennett M R., Warburton E A., Davenport A P. & Rudd J H F., 2017. Detection of Atherosclerotic Inflammation by ^{68}Ga-DOTATATE PET Compared to [^{18}F]FDG PET Imaging. *J Am Coll Cardiol.* 69(14), p. 1774-1791. Available at: https://doi.org/10.1016/j.jacc.2017.01.060.

Tavakoli S., Downs K., Short J D., Nguyen H N., Lai Y., Jerabek P A., Goins B., Toczek J., Sadeghi M M. & Asmis R., 2017. Characterization of Macrophage Polarization States Using Combined Measurement of 2-Deoxyglucose and Glutamine Accumulation: Implications for Imaging of Atherosclerosis. *Arterioscler Thromb Vasc Biol*. 37(10), p. 1840-1848. Available at: https://doi.org/10.1161/ATVBAHA.117.308848.

Tawakol A., Fayad Z A., Mogg R., Alon A., Klimas M T., Dansky H., Subramanian S S., Abdelbaky A., Rudd J H F., Farkouh M E., Nunes I O., Beals C R. & Shankar S S., 2013. Intensification of statin therapy results in a rapid reduction in atherosclerotic inflammation: results of a multicenter fluorodeoxyglucose-positron emission tomography/computed tomography feasibility study. *J Am Coll Cardiol*. 62(10), p. 909-917. Available at: https://doi.org/10.1016/j.jacc.2013.04.066.

Tedgui A. & Mallat Z., 2006. Cytokines in atherosclerosis: pathogenic and regulatory pathways. *Physiol Rev.* 86(2), p. 515-581. Available at: https://doi.org/10.1152/physrev.00024.2005.

Toner Y C., Ghotbi A A., Naidu S., Sakurai K., van Leent M M T., Jordan S., Ordikhani F., Amadori L., Sofias A M., Fisher E L., Maier A., Sullivan N., Munitz J., Senders M L., Mason C., Reiner T., Soultanidis G., Tarkin J M., Rudd J H F., Giannarelli C., Ochando J., Pérez-Medina C., Kjaer A., Mulder W J M., Fayad Z A. & Calcagno C., 2022. Systematically evaluating DOTATATE and FDG as PET immuno-imaging tracers of cardiovascular inflammation. *Sci Rep*. 12(1):6185. Available at: https://doi.org/10.1038/s41598-022-09590-2.

Tripolt N J., Aberer F., Riedl R., Url J., Dimsity G., Meinitzer A., Stojakovic T., Aziz F., Hödl R., Brachtl G., Strunk D., Brodmann M., Hafner F. & Sourij H., 2018. Effects of linagliptin on endothelial function and postprandial lipids in coronary artery disease patients with early diabetes: a randomized, placebo-controlled, double-blind trial. *Cardiovasc Diabetol*. 17(1):71. Available at: https://doi.org/10.1186/s12933-018-0716-x.

Tse K., Tse H., Sidney J., Sette A. & Ley K., 2013. T cells in atherosclerosis. *Int Immunol.* 25(11), p. 615-622. Available at: https://doi.org/10.1093/intimm/dxt043.

Tsukada T., Rosenfeld M., Ross R. & Gown A M., 1986. Immunocytochemical analysis of cellular components in atherosclerotic lesions. Use of monoclonal antibodies with the Watanabe and fat-fed rabbit. *Arteriosclerosis.* 6(6), p. 601-613. Available at: https://doi.org/10.1161/01.atv.6.6.601.

Turkington T G., 2001. Introduction to PET instrumentation. *J Nucl Med Technol.* 29(1), p. 4-11.

Uemura S., Matsushita H., Li W., Glassford A J., Asagami T., Lee K H., Harrison D G. & Tsao P S., 2001. Diabetes mellitus enhances vascular matrix metalloproteinase activity: role of oxidative stress. *Circ Res*. 88(12), p. 1291-1298. Available at: https://doi.org/10.1161/hh1201.092042.

Ussher J R. & Drucker D J., 2023. Glucagon-like peptide 1 receptor agonists: cardiovascular benefits and mechanisms of action. *Nat Rev Cardiol.* 20(7), p. 463-474. Available at: https://doi.org/10.1038/s41569-023-00849-3.

van den Ameele J., Hong Y., Manavaki R., Kouli A., Biggs H., MacIntyre Z., Horvath R., Yu-Wai-Man P., Reid E., Williams-Gray C H., Bullmore E., Aigbirhio F., Fryer T. & Chinnery P., 2021. [11C]PK11195-PET Brain Imaging of the Mitochondrial Translocator Protein in Mitochondrial Disease. *Neurology*. 96(22), p. e2761-e2773. Available at: https://doi.org/10.1212/WNL.0000000000012033.

van den Maagdenberg A M., Hofker M H., Krimpenfort P J., de Bruijn I., van Vlijmen B., van der Boom H., Havekes L M. & Frants R R., 1993. Transgenic mice carrying the apolipoprotein E3-Leiden gene exhibit hyperlipoproteinemia. *J Biol Chem* 268(14), p. 10540-10545.

Van der Donckt C., Van Herck J F., Schrijvers D M., Vanhoutte G., Verhoye M., Blockx I., Van Der Linden A., Bauters D., Lijnen H R., Sluimer J C., Roth L., Van Hove C E., Fransen P., Knaapen M W., Hervent A-S., De Keulenaer G W., Bult H., Martinet W., Herman A G. & De Meyer G R Y., 2015. Elastin fragmentation in atherosclerotic mice leads to intraplaque neovascularization, plaque rupture, myocardial infarction, stroke, and sudden death. *Eur Heart J.* 36(17), p. 1049-1058. Available at: https://doi.org/10.1093/eurheartj/ehu041.

van der Valk F M., Bekkering S., Kroon J., Yeang C., den Bossche J V., van Buul J D., Ravandi A., Nederveen A J., Verberne H J., Scipione C., Nieuwdorp M., Joosten L A B., Netea M G., Koschinsky M L., Witztum J L., Tsimikas S., Riksen N P. & Stroes E S G., 2016. Oxidized Phospholipids on Lipoprotein(a) Elicit Arterial Wall Inflammation and an Inflammatory Monocyte Response in Humans. *Circulation.* 134(8), p. 611-624. Available at: https://doi.org/10.1161/CIRCULATIONAHA.116.020838.

van der Zande H J P., Nitsche D., Schlautmann L., Guigas B. & Burgdorf S., 2019. The Mannose Receptor: From Endocytic Receptor and Biomarker to Regulator of (Meta)Inflammation. *Front Immunol.* 14;12:765034. Available at: https://doi.org/10.3389/fimmu.2021.765034.

Van Herck J F., De Meyer G R Y., Martinet W., Van Hove C E., Foubert K., Theunis M H., Apers S., Bult H., Vrints C J. & Herman A G., 2009. Impaired fibrillin-1 function promotes features of plaque instability in apolipoprotein E-deficient mice. *Circulation*. 120(24), p. 2478-2487. Available at: https://doi.org/10.1161/CIRCULATIONAHA.109.872663.

Varasteh Z., Hyafil F., Anizan N., Diallo D., Aid-Launais R., Mohanta S., Li Y., Braeuer M., Steiger K., Vigne J., Qin Z., Nekolla S G., Fabre J E., Döring Y., Le Guludec D., Habenicht A., Vera D R. & Schwaiger M., 2019. Targeting mannose receptor expression on macrophages in atherosclerotic plaques of apolipoprotein E-knockout mice using 68Ga-NOTA-anti-MMR nanobody: non-invasive imaging of atherosclerotic plaques. *EJNMMI Res*. 9(1):5. Available at: https://doi.org/10.1186/s13550-019-0474-0.

Veillard N R., Kwak B., Pelli G., Mulhaupt F., James R W., Proudfoot A E. & Mach F., 2004. Antagonism of RANTES receptors reduces atherosclerotic plaque formation in mice. *Circ Res.* 94(2), p. 253-261. Available at: https://doi.org/10.1161/01.RES.0000109793.17591.4E.

Véniant M M., Zlot C H., Walzem R L., Pierotti V., Driscoll R., Dichek D., Herz J. & Young S G., 1998. Lipoprotein clearance mechanisms in LDL receptor-deficient "Apo-B48-only" and "Apo-B100-only" mice. *J Clin Invest*. 102(8), p. 1559-1568. Available at: https://doi.org/10.1172/JCI4164.

Venneti S., Dunphy M P., Zhang H., Pitter K L., Zanzonico P., Campos C., Carlin S D., La Rocca G., Lyashchenko S., Ploessl K., Rohle D., Omuro A M., Cross J R., Brennan C W., Weber W A., Holland E C., Mellinghoff I K., Kung H F., Lewis J S. & Thompson C B., 2015. Glutamine-based PET imaging facilitates enhanced metabolic evaluation of gliomas in vivo. *Sci Transl Med.* 7(274):274ra17. Available at: https://doi.org/10.1126/scitranslmed.aaa1009.

Verma S., Al-Omran M., Leiter L A., Mazer C D., Rasmussen S., Saevereid H A., Sejersten Ripa M. & Bonaca M P., 2022. Cardiovascular efficacy of liraglutide and semaglutide in individuals with diabetes and peripheral artery disease. *Diabetes Obes Metab.* 24(7), p. 1288-1299. Available at: https://doi.org/10.1111/dom.14700.

Verweij N J F., Yaqub M., Bruijnen S T G., Pieplenbosch S., Ter Wee M M., Jansen G., Chen Q., Low P S., Windhorst A D., Lammertsma A A., Hoekstra O S., Voskuyl A E. & van der Laken C J., 2020. First in man study of [^{18}F]fluoro-PEG-folate PET: a novel macrophage imaging technique to visualize rheumatoid arthritis. *Sci Rep.* 10(1):1047. Available at: https://doi.org/10.1038/s41598-020-57841-x.

Vinik A I., Erbas T., Park T S., Nolan R. & Pittenger G L., 2001. Platelet dysfunction in type 2 diabetes. *Diabetes Care.* 24(8), p. 1476-1485. Available at: https://doi.org/10.2337/diacare.24.8.1476.

Vinué Á., Navarro J., Herrero-Cervera A., García-Cubas M., Andrés-Blasco I., Martínez-Hervás S., Real J T., Ascaso J F. & González-Navarro H., 2017. The GLP-1 analogue lixisenatide decreases atherosclerosis in insulin-resistant mice by modulating macrophage phenotype. *Diabetologia.* 60(9), p. 1801-1812. Available at: https://doi.org/10.1007/s00125-017-4330-3.

Virmani R., Kolodgie F D., Burke A P., Farb A. & Schwartz S M., 2000. Lessons from sudden coronary death: a comprehensive morphological classification scheme for atherosclerotic lesions. *Arterioscler Thromb Vasc Biol.* 20(5), p. 1262-1275. Available at: https://doi.org/10.1161/01.atv.20.5.1262.

Virmani R., Burke A P., Kolodgie F D. & Farb A., 2003. Pathology of the thin-cap fibroatheroma: a type of vulnerable plaque. *J Interv Cardiol*, 16(3), p. 267-272. Available at: https://doi.org/10.1034/j.1600-0854.2003.8042.x.

von Hundelshausen P., Weber K S., Huo Y., Proudfoot A E., Nelson P J., Ley K. & Weber C., 2001. RANTES deposition by platelets triggers monocyte arrest on inflamed and atherosclerotic endothelium. *Circulation*. 103(13), p. 1772-1777. Available at: https://doi.org/10.1161/01.cir.103.13.1772.

Wang H., Li Y., Zhang X., Xu Z., Zhou J. & Shang W., 2020. DPP-4 Inhibitor Linagliptin Ameliorates Oxidized LDL-Induced THP-1 Macrophage Foam Cell Formation and Inflammation. *Drug Des Devel Ther*. 14, p. 3929-3940. Available at: https://doi.org/10.2147/DDDT.S249846.

Warmink K., Siebelt M., Low P S., Riemers F M., Wang B., Plomp S G M., Tryfonidou M A., van Weeren P R., Weinans H. & Korthagen N M., 2022. Folate Receptor Expression by Human Monocyte-Derived Macrophage Subtypes and Effects of Corticosteroids. *Cartilage*. 13(1):19476035221081469. Available at: https://doi.org/10.1177/19476035221081469.

Weber C., Zernecke A. & Libby P., 2008. The multifaceted contributions of leukocyte subsets to atherosclerosis: lessons from mouse models. *Nat Rev Immunol*. 8(10), p. 802-815. Available at: https://doi.org/10.1038/nri2415.

Wei Y., Liang M., Xiong L., Su N., Gao X. & Jiang Z., 2021. PD-L1 induces macrophage polarization toward the M2 phenotype via Erk/Akt/mTOR. *Exp Cell Res.* 402(2):112575. Available at: https://doi.org/10.1016/j.yexcr.2021.112575.

Wenning C., Kloth C., Kuhlmann M T., Jacobs A H., Schober O., Hermann S. & Schäfers M A., 2014. Serial F-18-FDG PET/CT distinguishes inflamed from stable plaque phenotypes in shear-stress induced murine atherosclerosis. *Atherosclerosis*. 234(2), p. 276-282. Available at: https://doi.org/10.1016/j.atherosclerosis.2014.03.008.

Westerterp M., van der Hoogt C C., de Haan W., Offerman E H., Dallinga-Thie G M., Jukema J W., Havekes L M. & Rensen P C N., 2006. Cholesteryl ester transfer protein decreases high-density lipoprotein and severely aggravates atherosclerosis in APOE*3-Leiden mice. *Arterioscler Thromb*

Vasc Biol. 26(11), p. 2552-2559. Available at: https://doi.org/10.1161/01.ATV.0000243925.65265.3c.

Wild D., Christ E., Caplin M E., Kurzawinski T R., Forrer F., Brändle M., Seufert J., Weber W A., Bomanji J., Perren A., Ell P J. & Reubi J C., 2011. Glucagon-like peptide-1 versus somatostatin receptor targeting reveals 2 distinct forms of malignant insulinomas. *J Nucl Med. 52*(7), p. 1073-1078. Available at: https://doi.org/10.2967/jnumed.110.085142.

Winkel L C., Groen H C., van Thiel B S., Müller C., van der Steen A F., Wentzel J J., de Jong M. & Van der Heiden K., 2014. Folate receptor–targeted single-photon emission computed tomography/computed tomography to detect activated macrophages in atherosclerosis: can it distinguish vulnerable from stable atherosclerotic plaques? *Mol Imaging.* 13. Available at: https://doi.org/10.2310/7290.2013.00061.

Witting P K., Pettersson K., Ostlund-Lindqvist A M., Westerlund C., Eriksson A W. & Stocker R., 1999. Inhibition by a coantioxidant of aortic lipoprotein lipid peroxidation and atherosclerosis in apolipoprotein E and low density lipoprotein receptor gene double knockout mice. *FASEB J.* 13(6), p. 667-675. Available at: https://doi.org/10.1096/fasebj.13.6.667.

Wiviott S D., Raz I., Bonaca M P., Mosenzon O., Kato E T., Cahn A., Silverman M G., Zelniker T A., Kuder J F., Murphy S A., Bhatt D L., Leiter L A., McGuire D K., Wilding J P H., Ruff C T., Gause-Nilsson I A M., Fredriksson M., Johansson P A., Langkilde A-M., Sabatine M S.; DECLARE–TIMI 58 Investigators, 2019. Dapagliflozin and Cardiovascular Outcomes in Type 2 Diabetes. *N Engl J Med.* 380(4), p. 347-357. Available at: https://doi.org/10.1056/NEJMoa1812389.

Wu J., He S., Song Z., Chen S., Lin X., Sun H., Zhou P., Peng Q., Du S., Zheng S. & Liu X., 2023. Macrophage polarization states in atherosclerosis. *Front Immunol*. 14:1185587. Available at: https://doi.org/10.3389/fimmu.2023.1185587.

Wu M Y., Li C J., Hou M F. & Chu P Y., 2017. New Insights into the Role of Inflammation in the Pathogenesis of Atherosclerosis. *Int J Mol Sci*. 18(10):2034. Available at: https://doi.org/10.3390/ijms18102034.

Xie Y., Chen H., Qu P., Qiao X., Guo L. & Liu L., 2022. Novel insight on the role of Macrophages in atherosclerosis: Focus on polarization, apoptosis and efferocytosis. *Int Immunopharmacol*. 113(Pt A):109260. Available at: https://doi.org/10.1016/j.intimp.2022.109260.

Yan D., Jauhiainen M., Hildebrand R B., van Dijk K W., Van Berkel T J C., Ehnholm C., Van Eck M. & Olkkonen V M., 2007. Expression of human OSBP-related protein 1L in macrophages enhances atherosclerotic lesion development in LDL receptor-deficient mice. *Arterioscler Thromb Vasc Biol.* 27(7), p. 1618-1624. Available at: https://doi.org/10.1161/ATVBAHA.107.144121.

Yan S F., Ramasamy R. & Schmidt A M., 2009. Receptor for AGE (RAGE) and its ligands-cast into leading roles in diabetes and the inflammatory response. *J Mol Med (Berl).* 87(3), p. 235-247. Available at: https://doi.org/10.1007/s00109-009-0439-2.

Yang L., Chen L., Li D., Xu H., Chen J., Min X., He M., Wu T., Zhong J., Yang H. & Chen J., 2021. Effect of GLP-1/GLP-1R on the Polarization of Macrophages in the Occurrence and Development of Atherosclerosis. *Mediators Inflamm.* 5568159. Available at: https://doi.org/10.1155/2021/5568159

Yang M M., Wang J., Fan J J., Ng T K., Sun D J., Guo X., Teng Y. & Li Y B., 2016. Variations in the Obesity Gene "LEPR" Contribute to Risk of Type 2 Diabetes Mellitus: Evidence from a Meta-Analysis. *J Diabetes Res.* 2016:5412084. Available at: https://doi.org/10.1155/2016/5412084.

Yang J., Zhang L., Yu C., Yang X-F. & Wang H., 2014. Monocyte and macrophage differentiation: circulation inflammatory monocyte as biomarker for inflammatory diseases. *Biomark Res*. 2:(1):1. Available at: https://doi.org/10.1186/2050-7771-2-1.

Ye Z., Zhong L., Zhu S., Wang Y., Zheng J., Wang S., Zhang J. & Huang R., 2019. The P-selectin and PSGL-1 axis accelerates atherosclerosis via activation of dendritic cells by the TLR4 signaling pathway. *Cell Death Dis*. 1;10(7):507. Available at: https://doi.org/10.1038/s41419-019-1736-5.

Ying W., Meiyan S., Wen C., Kaizu X., Meifang W. & Liming L., 2023. Liraglutide ameliorates oxidized LDL-induced endothelial dysfunction by GLP-1R-dependent downregulation of LOX-1-

mediated oxidative stress and inflammation. *Redox Rep*. 28(1):2218684. Available at: https://doi.org/10.1080/13510002.2023.2218684.

Zeng Q., Zou D., Wei Y., Ouyang Y., Lao Z. & Guo R., 2022. Association of vitamin D receptor gene rs739837 polymorphism with type 2 diabetes and gestational diabetes mellitus susceptibility: a systematic review and meta-analysis. *Eur J Med Res.* 27(1):65. Available at: https://doi.org/10.1186/s40001-022-00688-x.

Zhang X., Fan S., Zhang L. & Shi Y., 2020. Glucagon-like peptide-1 receptor undergoes importin-α-dependent nuclear localization in rat aortic smooth muscle cells. *FEBS Lett.* 594(10), p. 1506-1516. Available at: https://doi.org/10.1002/1873-3468.13751.

Zhao D., Cui H., Shao Z. & Cao L., 2023. Abdominal obesity, chronic inflammation and the risk of non-alcoholic fatty liver disease. *Ann Hepatol.* 28(4): 100726. Available at: https://doi.org/10.1016/j.aohep.2022.100726.

Zhao Y., Qu H., Wang Y., Xiao W., Zhang Y. & Shi D., 2020. Small rodent models of atherosclerosis. *Biomed Pharmacother.* 129:110426. Available at: https://doi.org/10.1016/j.biopha.2020.110426.

Zhuge F., Ni Y., Nagashimada M., Nagata N., Xu L., Mukaida N., Kaneko S. & Ota T., 2016. DPP-4 Inhibition by Linagliptin Attenuates Obesity-Related Inflammation and Insulin Resistance by Regulating M1/M2 Macrophage Polarization. *Diabetes*. 65(10), p. 2966-2979. Available at: https://doi.org/10.2337/db16-0317

Zhou R., Pantel A R., Li S., Lieberman B P., Ploessl K., Choi H., Blankemeyer E., Lee H., Kung H F., Mach R H. & Mankoff D A., 2017. [^{18}F](2 S,4 R)4-Fluoroglutamine PET Detects Glutamine Pool Size Changes in Triple-Negative Breast Cancer in Response to Glutaminase Inhibition. *Cancer Res.* 77(6), p. 1476-1484. Available at: https://doi.org/10.1158/0008-5472.CAN-16-1945.

Zinman B., Wanner C., Lachin J M., Fitchett D., Bluhmki E., Hantel S., Mattheus M., Devins T., Johansen O E., Woerle H J., Broedl U C., Inzucchi S E; EMPA-REG OUTCOME Investigators, 2015. Empagliflozin, Cardiovascular Outcomes, and Mortality in Type 2 Diabetes. *N Engl J Med.* 373(22), p. 2117-2128. Available at: https://doi.org/10.1056/NEJMoa1504720.

Örd T., Lönnberg T., Nurminen V., Ravindran A., Niskanen H., Kiema M., Õunap K., Maria M., Moreau P R., Mishra P P., Palani S., Virta J., Liljenbäck H., Aavik E., Roivainen A., Ylä-Herttuala S., Laakkonen J P., Lehtimäki T. & Kaikkonen M U., 2023. Dissecting the polygenic basis of atherosclerosis via disease-associated cell state signatures. *Am J Hum Genet*. 110(5), p. 722-740. Available at: https//doi.org/10.1016/j.ajhg.2023.03.013.

TURUN
YLIOPISTO
UNIVERSITY
OF TURKU

Painosalama, Turku, Finland 2024

ISBN 978-951-29-9783-1 (PRINT)
ISBN 978-951-29-9784-8 (PDF)
ISSN 0355-9483 (Print)
ISSN 2343-3213 (Online)